UPPSALA
UNIVERSITET

On Discontinuous Galerkin Multiscale Methods

DANIEL ELFVERSON

UPPSALA UNIVERSITY
Department of Information Technology

On Discontinuous Galerkin Multiscale Methods

Daniel Elfverson

daniel.elfverson@it.uu.se

June 2013

Division of Scientific Computing
Department of Information Technology
Uppsala University
Box 337
SE-751 05 Uppsala
Sweden

http://www.it.uu.se/

Dissertation for the degree of Licentiate of Technology in Scientific Computing

Abstract

In this thesis a new multiscale method, the discontinuous Galerkin multiscale method, is proposed. The method uses localized fine scale computations to correct a global coarse scale equation and thereby takes the fine scale features into account. We show a priori error bounds for convection dominated convection-diffusion-reaction problems with variable coefficients. We present an posteriori error bound in the case of no convection or reaction and an adaptive algorithm which tunes the method parameters automatically. We also present extensive numerical experiments which verify our analytical findings.

List of papers

This thesis is based on the following papers.

I D. Elfverson and A. Målqvist. *Finite Element Multiscale Methods for Possion's Equation with Rapidly Varying Heterogeneous Coefficients.* In Proc. 10th World Congress on Computational Mechanics, p 10, International Association for Computational Mechanics, Barcelona, Spain, 2012.

II D. Elfverson, G. H. Georgoulis and A. Målqvist. *An Adaptive Discontinuous Galerkin Multiscale Method for Elliptic Problems.* To appear in Multiscale Modeling and Simulation (MMS).

III D. Elfverson, G. H. Georgoulis and A. Målqvist. *Convergence of a Discontinuous Galerkin Multiscale Method.* In review in SIAM Journal on Numerical Analysis (SINUM), available as preprint arXiv:1211.5524, 2012.

IV D. Elfverson and A. Målqvist. *Discontinuous Galerkin Multiscale Methods for Convection Dominated Problems.* Technical Report 2013-011, Department of Information Technology, Uppsala University, 2013.

Contents

Chapter 1

Introduction

Computer simulations of problems which involve features on multiple scales, normally referred to as multiscale problems, is one of the greatest challenges in scientific computing today. Examples include the simulation of flow in a porous medium and composite materials. To obtain a numerical solution within an acceptable tolerance, the data in the problem needs to be resolved. Resolving the data using standard numerical methods can be very computationally demanding or even impossible for many multiscale problem.

To be able to cope with the computational issues in multiscale problems, many different methods have been developed during the last twenty years, often referred to as multiscale methods (Chapter 3). A common feature for these methods is that the problem is split into a coarse and fine scale, where fine scale sub-problems are solved (in parallel) on localized patches of the computational domain. The solutions to the sub-problems are then used to modify the coarse scale equation such that the fine scale behavior is taken into account.

Main contributions

The main contributions of this thesis are the following:

- The development of a new multiscale method, the "Discontinuous Galerkin multiscale method", using the framework for the variational multiscale method and the discontinuous Galerkin method for Poisson's equation with variable coefficients. See Paper I, II, and III.

- A priori error bounds with respect to the coarse mesh size, independent of the variation in data and without any assumption on scale separation or periodicity. See Paper III.

- Development of an adaptive algorithm, using a posteriori error bounds, to tune the method parameters in order to get efficient and reliable approximations. See Paper II.

- The development of a multiscale method for convection dominated problems together with a proof of convergence under mild assumptions on the magnitude of the convection term. See Paper IV.

Future work

There are many aspects in multiscale methods which still are relatively new and open for research. A few examples which would be interesting to investigate further are:

- Construction of an adaptive algorithm which balances the error caused by the uncertainty in the data and the discretization error, which are two important error sources for multiscale problems.

- Implement the methods on parallel machines to allow 3D simulations.

- Consider non-linear convection dominated problems with applications in two-phase flow, where systems of a coupled convection dominated transport equations and elliptic pressure equations arise.

Chapter 2

Setting end discretization

In this chapter the model problem and discrete setting, which the multiscale method is based on, are discussed. For simplicity we only consider the Poisson's equation with variable coefficients. For a discussion on convection-diffusion-reaction problems, we refer to Paper IV.

2.1 Model problem

We seek a (weak) solution u to,

$$
\begin{aligned}
-\nabla \cdot A\nabla u &= f \quad \text{in } \Omega, \\
u &= 0 \quad \text{on } \partial\Omega,
\end{aligned}
\tag{2.1}
$$

where A is given data describing the properties of the medium, f is an external forcing, and Ω is a domain with boundary $\partial\Omega$. For (2.1) to be characterised as a multiscale problem A varies on several different scales. This equation models diffusion processes and appears frequently in many different areas of science.

2.2 The finite element method

The finite element method, see e.g. [4] for an overview, approximates the weak (or variational) form of (2.1). The finite element method has a strong mathematical foundation which gives efficient tools for showing both a priori and a posteriori error bounds. Let $\mathcal{V}$ be an infinite dimensional space of sufficiently smooth functions, e.g., the Sobolev space $\mathcal{V} = \{v \in H^1(\Omega) \mid v|_{\partial\Omega} = 0\}$). The variational formulation is obtained by multiplying (2.1) with a test

function v and integrating over the domain Ω. The weak formulation reads: find $u \in \mathcal{V}$ such that,

$$a(u,v) := \int_\Omega A\nabla u \cdot \nabla v \, dx = \int_\Omega fv \, dx =: F(v) \quad \text{for all } v \in \mathcal{V}. \qquad (2.2)$$

Since there typically is no analytical solution to (2.2), we seek a solution in a finite dimensional subset $\mathcal{V}_H^c \subset \mathcal{V}$, which can be the space of continuous piecewise polynomials on a given the mesh $\mathcal{T}_H$. The finite element approximation reads: find $u_H \in \mathcal{V}_H^c$ such that

$$a(u_H,v) = F(v), \quad \text{for all } v \in \mathcal{V}_H^c. \qquad (2.3)$$

For the solution u_H to give a good approximation, the mesh $\mathcal{T}_H$ needs to resolve the variation in A. For many real life problems this assumption is very computational demanding to fulfill.

2.3 Discontinuous Galerkin methods

An interesting alternative to standard (conforming) finite element methods is the discontinuous Galerkin (dG) method. In dG methods there is no continuity constraint imposed on the approximation spaces. Instead the continuity is imposed weakly, i.e., the dG method allows for jumps in the numerical solution between different elements in the mesh. However, these jumps tends to zero as the mesh size decreases.

The first dG method was introduced in [26] for numerical approximations of first order hyperbolic problems. Error bounds are shown, in e.g. [21] and [19]. DG methods for elliptic problems, so called interior penalty methods, arise from an observation in [24], that essential boundary condition can be imposed weakly. In interior penalty methods the inter element continuity is imposed weakly. Some early work are [28, 6, 2]. See also [13, 5, 27] for a literature review for dG methods.

The approximation space for the dG method, $\mathcal{V}_H$, is the space of piecewise discontinuous polynomials, i.e, dG methods uses a non-conforming ansatz $\mathcal{V}_H \not\subset \mathcal{V}$. The dG method has a higher number of degrees of freedom than standard continuous Galerkin methods, but has the advantages that non-conforming meshes can be used and that it does not suffer from stability issues for first order or convection dominated PDEs. Also, the dG method is perfectly suited for hp-adaptivity, where both the mesh size and the order of the polynomials can vary over the domain, see e.g. [16]. Since the dG method seek the solution in a space which consists of piecewise polynomials

without any continuity constraints, a modified bilinear form has to be used. In the bilinear form the continuity is imposed weakly, i.e., there is a penalty which forces the jump in the approximate solution to decrease when the mesh-size decreases. Let $\mathcal{T}_H$ be a given mesh and $\mathcal{E}_H$ be the set of edges of the elements in $\mathcal{T}_H$. For two elements T^+ and T^- sharing a common edge, $e := T^+ \cap T^-$, the jump and averages on e are defined as

$$\{v\} = \frac{1}{2}(v|_{T^+} + v|_{T^-}) \quad \text{and} \quad [v] = v|_{T^+} - v|_{T^-} \tag{2.4}$$

in the interior and as $\{v\} = [v] = v_T$ on the boundary. Defining ν_e to be the unit normal pointing from T^+ to T^-, $H : \Omega \to \mathbb{R}$ to be the mesh-size defined element-wise as $H|_T = \text{diam}(T)$, and σ_e to be a edge-wise constant depending on A. The bilinear form for the dG method is defined as

$$a_H(u, v) = \sum_{T \in \mathcal{T}_H} \int_T A\nabla u \cdot \nabla v \, dx$$
$$- \sum_{e \in \mathcal{E}_H} \int_e \left(\nu_e \cdot \{A\nabla u\}[v] + \nu_e \cdot \{A\nabla v\}[u] - \frac{\sigma_e}{h}[u][v] \right) ds. \tag{2.5}$$

where σ_e is chosen large enough to makes the bilinear form coercive in the standard dG energy norm, which is defined as

$$|||v||| = \left(\sum_{T \in \mathcal{T}_H} \|A^{1/2}\nabla v\|^2_{L^2(T)} + \sum_{E \in \mathcal{E}_H} \frac{\sigma_e}{h} \|[v]\|^2_{L^2(e)} \right)^{1/2}. \tag{2.6}$$

The dG method reads: find $u_H \in \mathcal{V}_H$ such that

$$a_H(u_H, v) = F(v), \quad \text{for all } v \in \mathcal{V}_H. \tag{2.7}$$

Discontinuous Galerkin methods as well as conforming finite element methods perform badly when the smallest length scale of the medium is not resolved. However, dG methods has the advantage in treating discontinuous coefficients, convection dominated problems, mass conservation, and flexibility of the underling mesh, all which are crucial issues in many multiscale problems including e.g. porous media flow.

Chapter 3

Multiscale method

In the last two decades there have been a lot of research on multiscale methods. Some important contributions are the Multiscale Finite Element Method (MsFEM) introduced in [15, 14] (see also [11, 10]), the heterogeneous multiscale method (HMM), introduced in [7] (see also [8, 9]), and the variational multiscale method (VMS) introduced in [17, 18] (see also [20, 22, 23]). Common for all these approaches is that local sub-problem are solved on fine scale patches which locally resolve the variations in the data, and that the solutions to the sub-problems are used to modify a coarse scale space or equation.

It is known that standard (one mesh) finite element methods perform badly when the mesh does not resolve the variations in the coefficients describing the medium, see e.g. [3]. In this thesis we propose a multiscale method, using the framework from dG and VMS, which converges to a fine scale reference solution, independent of the variations in A or regularity of the underlying solution.

3.1   Multiscale decomposition

To make a multiscale decomposition, we need a coarse mesh $\mathcal{T}_H$, and a fine mesh $\mathcal{T}_h$ constructed by (possible adaptive) refinements of $\mathcal{T}_H$. We let $\mathcal{V}_H$ and $\mathcal{V}_h$ be the discontinuous Galerkin approximation spaces on $\mathcal{T}_H$ and $\mathcal{T}_h$, respectively. We assume that the fine mesh $\mathcal{T}_h$ resolves the smallest length scale of the data, A. The reference dG solution is given by: find $u_h \in \mathcal{V}_h$ such that

$$a_h(u_h, v) = F(v) \quad \text{for all } v \in \mathcal{V}_h. \tag{3.1}$$

We assume u_h to be a sufficiently good approximation to u. The space $\mathcal{V}_h$ is split into a coarse and a fine scale contribution. To this end, let $\Pi_H : L^2(\Omega) \to \mathcal{V}_H$ be the element-wise L^2-projection onto the coarse space $\mathcal{V}_H$ and note the we can express the coarse space as $\mathcal{V}_H = \Pi_H \mathcal{V}_h$. The fine space is defined by

$$\mathcal{V}^f = (1 - \Pi_H)\mathcal{V}_h = \{v \in \mathcal{V}_h \mid \Pi_H v = 0\}. \tag{3.2}$$

Any function $v_h \in \mathcal{V}_h$ can be decomposed into a coarse contribution, $v_H \in \mathcal{V}_H$, and fine scale remainder, $v^f \in \mathcal{V}^f$, i.e., $v_h = v_H + v^f$. Choosing $\mathcal{V}_H$ as the coarse space the fine scale remainder v^f is large and oscillatory and does not decay until $\mathcal{T}_H$ resolves the variations in the data. In the next section we construct a (corrected) coarse space which takes the fine scale features into account.

3.2 Discontinuous Galerkin multiscale method

The aim of our proposed discontinuous Galerkin multiscale method is to construct a corrected basis which takes the fine scale features of the data into account, i.e., the corrected basis has both a coarse and fine scale contribution. The coarse contribution comes from the coarse discontinuous Galerkin approximation space spanned by the element-wise Lagrange basis, i.e., $\mathcal{V}_H = \text{span}\{\lambda_{T,j} \mid T \in \mathcal{T}_H, j = 1, \ldots, r\}$ where r is the number of basis functions on each element T. For each of the basis functions, $\{\lambda_{T,j} \mid T \in \mathcal{T}_H, j = 1, \ldots, r\}$, we will compute a corrector as follows: find $\phi_{T,j} \in \mathcal{V}^f$ such that

$$a_h(\phi_{T,j}, v) = a_h(\lambda_{T,j}, v) \quad \text{for all } v \in \mathcal{V}^f. \tag{3.3}$$

It is not feasible in real computations to solve (3.3) for each coarse basis function since it evolves a variational problem on the entire domain. Instead, since the correctors, $\phi_{T,j}$, decay exponentially away from the support of $\lambda_{T,j}$ the computations of the corrector function will be done on small patches of the domain. To this end, let $\omega_T \subset \Omega$ be a patch centered at element T and define $\mathcal{V}^f(\omega_T) = \{v \in \mathcal{V}^f \mid v|_{\Omega \setminus \omega_T} = 0\}$. The localized corrector functions are calculated as follows: for all $T \in \mathcal{T}_H$, $j = 1, \ldots, r$, find $\phi_{T,j} \in \mathcal{V}^f(\omega_T)$ such that

$$a_h(\phi_{T,j}, v) = a_h(\lambda_{T,j}, v) \quad \text{for all } v \in \mathcal{V}^f(\omega_T). \tag{3.4}$$

The corrected coarse space is defined $\mathcal{V}_H^{ms} := \{\lambda_{T,j} - \phi_{T,j} \mid T \in \mathcal{T}_H, j = 1, \ldots, r\}$, and the discontinuous Galerkin multiscale method reads: find

$u_H^{ms} \in \mathcal{V}_H^{ms}$ such that

$$a_h(u_H^{ms}, v) = F(v) \quad \text{for all } v \in \mathcal{V}_H^{ms}. \qquad (3.5)$$

We have the following a priori error bound

$$|||u - u_H^{ms}||| \leq |||u - u_h||| + CH, \qquad (3.6)$$

choosing the patch size to $\mathcal{O}(H \log(H^{-1}))$, where H is the mesh size. For a more elaborate discussion, see Paper III for Poisson's equation with variable coefficients, and Paper IV for convection dominated problems.

3.3 Adaptive discontinuous Galerkin multiscale method

For porous media flow problems the permeability in the ground can vary with several orders of magnitudes over the entire domain. Which motivates the use of an adaptive multiscale method to tune the method parameters in order to obtain an efficient and reliable solution. For adaptive multiscale methods, see e.g [20, 25, 12, 1]. In Paper II an adaptive discontinuous Galerkin multiscale method is presented. It is a slight variation to the discontinuous Galerkin multiscale method presented in Section 3.2 (Paper III) in the sense that a fine scale corrector for the right hand side is present. Given a uniform or possibly an adaptive coarse mesh $\mathcal{T}_H$, the adaptive discontinuous Galerkin multiscale method balances the error caused by truncation of the patches and the fine scale discretization error. The a posteriori error bound takes the form

$$|||u - u_H^{ms}||| \leq C_1 \left(\sum_{S \in \mathcal{T}_h} \rho_S^2(u_H^{ms}) \right)^{1/2} + C_2 \left(\sum_{T \in \mathcal{T}_H} \rho_{\omega_T}^2(u_H^{ms}) \right)^{1/2}, \quad (3.7)$$

where ρ_S^2 is an error indicator which measure the effect of the local fine scale mesh size, and $\rho_{\omega_T}^2$ is an error indicator measuring the effect of the truncated patches. Because of the general nonconforming meshes allowed using dG, it is easy to construct a global reference grid for the localized fine scale computations. This takes advantage of the cancellation of error between different fine scale patches and also formulates the dG multiscale method into the convergence framework presented in Paper III. A more elaborate discussion can be found in Paper II.

Chapter 4

Summary of papers

4.1 Paper I

D. Elfverson and A. Målqvist. *Finite Element Multiscale Methods for Possion's Equation with Rapidly Varying Heterogeneous Coefficients.* In Proc. 10th World Congress on Computational Mechanics, p 10, International Association for Computational Mechanics, Barcelona, Spain, 2012.

An abstract framework for constructing finite element multiscale methods based on the VMS is presented. Using this framework we propose and compare two different multiscale methods, one based on the continuous Galerkin finite element method and one on the discontinuous Galerkin finite element method. The continuous Galerkin multiscale method uses local Dirichlet problems and the discontinuous Galerkin multiscale method uses local Neumann problems, for the localized fine scale problems.

4.2 Paper II

D. Elfverson, G. H. Georgoulis and A. Målqvist. *An Adaptive Discontinuous Galerkin Multiscale Method for Elliptic Problems.* To appear in Multiscale Modeling and Simulation (MMS).

We present an adaptive discontinuous Galerkin multiscale method driven by an energy norm a posteriori error bound. The a posteriori error bound is used within an adaptive algorithm to tune the critical parameters, i.e., the refinement level and the size of the different patches on which the fine scale constituent problems are solved. We solve local Dirichlet problem instead for Neumann problem (Paper I) for the localized fine scale problems.

4.3 Paper III

D. Elfverson, G. H. Georgoulis, A. Målqvist, and D. Peterseim. *Convergence of a Discontinuous Galerkin Multiscale Method.* In review in SIAM Journal on Numerical Analysis (SINUM), available as preprint arXiv:1211.5524, 2012.

A convergence result for a discontinuous Galerkin multiscale method for a second order elliptic problem is presented. The method differs from the one proposed in Paper II in the sense that right hand side correction term is not present. We prove that the error, due to truncation of corrected basis, decreases exponentially with the size of the patches. The same corrected basis as in Paper II is used. We also discuss a way to further localize the corrected basis to element-wise support leading to a slight increase of the dimension of the space. Improved convergence rate can be achieved depending on the piecewise regularity of the forcing function. Linear convergence in energy norm and quadratic convergence in L^2-norm is obtained independently of the forcing function.

4.4 Paper IV

D. Elfverson and A. Målqvist. *Discontinuous Galerkin Multiscale Methods for Convection Dominated Problems.* Technical Report 2013-011, Department of Information Technology, Uppsala University, 2013.

In this paper we extend the discontinuous Galerkin multiscale method in Paper III to convection dominated problems. The advantages of the multiscale method and the discontinuous Galerkin method allows us to better cope with multiscale features and boundary layers in the solution. We prove decay of the corrected basis functions as well as an a priori error bound for the multiscale method.

Acknowledgements

Bibliography

[1] A. Abdulle and A. Nonnenmacher. A posteriori error analysis of the heterogeneous multiscale method for homogenization problems. *C. R. Math. Acad. Sci. Paris*, 347:1081–1086, 2009.

[2] D. N. Arnold. An interior penalty finite element method with discontinuous elements. *SIAM J. Numer. Anal.*, 19:742–760, 1982.

[3] I. Babuška and J. E. Osborn. Can a finite element method perform arbitrarily badly? *Math. Comp.*, 69:443–462, 2000.

[4] S. C. Brenner and L. R. Scott. *The mathematical theory of finite element methods*, volume 15 of *Texts in Applied Mathematics*. Springer, New York, third edition, 2008.

[5] D. A. Di Pietro and A. Ern. *Mathematical aspects of discontinuous Galerkin methods*, volume 69 of *Mathématiques & Applications (Berlin) [Mathematics & Applications]*. Springer, Heidelberg, 2012.

[6] J. Douglas and T. Dupont. Interior penalty procedures for elliptic and parabolic Galerkin methods. In *Computing methods in applied sciences (Second Internat. Sympos., Versailles, 1975)*, pages 207–216. Lecture Notes in Phys., Vol. 58. Springer, Berlin, 1976.

[7] W. E and B. Engquist. The heterogeneous multiscale methods. *Commun. Math. Sci.*, 1:87–132, 2003.

[8] W. E and B. Engquist. Multiscale modeling and computation. *Notices Amer. Math. Soc.*, 1:1062–1070, 2003.

[9] W. E and B. Engquist. The heterogeneous multi-scale method for homogenization problems. In *Multiscale methods in science and engineering*, volume 44 of *Lect. Notes Comput. Sci. Eng.*, pages 89–110. Springer, Berlin, 2005.

[10] Y. Efendiev and T. Y. Hou. *Multiscale finite element methods*, volume 4 of *Surveys and Tutorials in the Applied Mathematical Sciences*. Springer, New York, 2009. Theory and applications.

[11] Y. R. Efendiev, T. Y. Hou, and X.-H. Wu. Convergence of a nonconforming multiscale finite element method. *SIAM J. Numer. Anal.*, 37:888–910, 2000.

[12] P. Henning and M. Ohlberger. The heterogeneous multiscale finite element method for elliptic homogenization problems in perforated domains. *Numer. Math.*, 113:601–629, 2009.

[13] J. S. Hesthaven and T. Warburton. *Nodal discontinuous Galerkin methods*, volume 54 of *Texts in Applied Mathematics*. Springer, New York, 2008.

[14] T.. Hou, X.-H. Wu, and Z. Cai. Convergence of a multiscale finite element method for elliptic problems with rapidly oscillating coefficients. *Math. Comp.*, 68:913–943, July 1999.

[15] T. Y. Hou and X.-H. Wu. A multiscale finite element method for elliptic problems in composite materials and porous media. *J. Comput. Phys.*, 134:169–189, 1997.

[16] P. Houston and E. Süli. *hp*-adaptive discontinuous Galerkin finite element methods for first-order hyperbolic problems. *SIAM J. Sci. Comput.*, 23:1226–1252, 2001.

[17] T. Hughes. Multiscale phenomena: Green's functions, the Dirichlet-to-Neumann formulation, subgrid scale models, bubbles and the origins of stabilized methods. *Computer Methods in Applied Mechanics and Engineering*, 127:387–401, 1995.

[18] T. Hughes, G. Feijóo, L. Mazzei, and J.-B. Quincy. The variational multiscale method—a paradigm for computational mechanics. *Comput. Methods Appl. Mech. Engrg.*, 166:3–24, 1998.

[19] C. Johnson and J. Pitkäranta. An analysis of the discontinuous Galerkin method for a scalar hyperbolic equation. *Math. Comp.*, 46:1–26, 1986.

[20] M. G. Larson and A. Målqvist. Adaptive variational multiscale methods based on a posteriori error estimation: energy norm estimates for elliptic problems. *Comput. Methods Appl. Mech. Engrg.*, 196:2313–2324, 2007.

[21] P. Lesaint and P.-A. Raviart. On a finite element method for solving the neutron transport equation. In *Mathematical aspects of finite elements in partial differential equations (Proc. Sympos., Math. Res. Center, Univ. Wisconsin, Madison, Wis., 1974)*, pages 89–123. Publication No. 33. Math. Res. Center, Univ. of Wisconsin-Madison, Academic Press, New York, 1974.

[22] A. Målqvist. Multiscale methods for elliptic problems. *Multiscale Modeling & Simulation*, 9:1064–1086, 2011.

[23] A. Målqvist and D. Peterseim. Localization of elliptic multiscale problems. *Submitted for publication in Math. Comp., in revision, available as preprint arXiv:1110.0692*, 2011.

[24] J. Nitsche. Über ein Variationsprinzip zur Lösung von Dirichlet-Problemen bei Verwendung von Teilräumen, die keinen Randbedingungen unterworfen sind. *Abh. Math. Sem. Univ. Hamburg*, 36:9–15, 1971.

[25] M. Ohlberger. A posteriori error estimates for the heterogeneous multiscale finite element method for elliptic homogenization problems. *Multiscale Model. Simul.*, 4:88–114 (electronic), 2005.

[26] W. H. Reed and T. R. Hill. Triangular mesh methods for the neutron transport equation. Technical report, Los Alamos Scientific Laboratory, 1973.

[27] B. Rivière. *Discontinuous Galerkin methods for solving elliptic and parabolic equations*, volume 35 of *Frontiers in Applied Mathematics*. Society for Industrial and Applied Mathematics (SIAM), Philadelphia, PA, 2008. Theory and implementation.

[28] M. Wheeler. An elliptic collocation-finite element method with interior penalties. *SIAM J. Numer. Anal.*, 15(1):152–161, 1978.

Paper I

FINITE ELEMENT MULTISCALE METHODS FOR POISSON'S EQUATION WITH RAPIDLY VARYING HETEROGENEOUS COEFFICIENTS

D. Elfverson[1], A. Målqvist[1]

[1] Department of Scientific Computing, Uppsala University (daniel.elfverson@it.uu.se)

Abstract. *An abstract framework for constructing finite element multiscale methods is presented. Using this framework we propose and compare two different multiscale methods, one based on the continuous Galerkin finite element method and one on the discontinuous Galerkin finite element method. In these multiscale methods the solution is split into coarse and fine scale contributions. The fine scale contribution is obtained by solving localized constituent problems on patches and is used to obtain a modified coarse scale equation. The localized constituent problems are completely parallelizable i.e, no communication between the different problems are needed. The modified coarse scale equation has considerably less degrees of freedom than the original problem. Numerical experiments are presented where the effect of the patch size of the local constituent problems as well as the convergence of the multiscale methods are investigated and compared for the proposed multiscale methods. We conclude that for a given accuracy and a fixed number of patches, smaller patches can be used for the discontinuous Galerkin multiscale method compared to the continuous Galerkin multiscale method.*

Keywords: *finite element methods, discontinuous Galerkin, multiscale methods*

1. INTRODUCTION

There are numerous applications which involves solutions that varies over several different scales, for example flow in porous media such as oil reservoir simulations and CO_2 storage. These, so called multiscale problems, are often impossible to solve with standard single mesh methods since the finest scale needs to be resolved to get a reliable result, see e.g. [5].

To resolve this problem several multiscale methods have been developed during the last two decades e.g., the Multiscale Finite Element Method (MsFEM) by Hou and Wu [9] and the Variational Multiscale Method (VMS) by Hughes [10]. See also [8,7,12] and references therein for recent development and exposition. Using the framework of the Variational Multiscale Methods Larson and Målqvist introduced the Adaptive Variational Multiscale method [11]. This method has further been developed in [12], where the framework for constructing multiscale methods used in this paper is presented and further discussed.

Lately, there have been a lot of interest in discontinuous Galerkin multiscale methods. Discontinuous Galerkin (DG) methods appeared in the 1970s; see [3,6] for some early work for elliptic problem and [4,14,15] for a literature review. A desired property with DG methods is that they admits good conservation properties of the state variable and are ideally suited for application to complex and irregular meshes. Conservation is a crucial property for multiscale problems. Recently proposed multiscale discontinuous Galerkin methods include e.g., [1] based on the MsFEM, and [2] based on the Heterogeneous Multiscale Method.

In this paper a continuous Galerkin multiscale method and a discontinuous Galerkin multiscale method for solving Poisson's equation with rapidly variable heterogeneous coefficients are studied. The continuous Galerkin version was first presented in [11], while the DG version is new. In the proposed multiscale method the solution is split into coarse and fine scale contributions. The fine scale contribution is obtained by solving localized constituent problems on patches and is used to obtain a modified coarse scale equation. Both a symmetric and a non-symmetric version of the modified coarse scale equation are presented. Numerical experiments are presented, where the size needed for the constituent problems to get a sufficient approximation as well as the convergence of the different multiscale methods, are investigated. We conclude that for a given accuracy and a fixed number of patches, smaller patches can be used for the discontinuous Galerkin multiscale compared to the continuous Galerkin multiscale method. On the coarse scale the discontinuous Galerkin multiscale method is approximating the L^2-projection, rather than the nodal values, which is the case for continuous Galerkin multiscale method. The property of approximating the L^2-projection is preferable in a multiscale setting. Also, DG has better conservation properties than CG.

The precise setting of the paper is the following. We consider the following model problem:

$$\begin{aligned} -\nabla \cdot \alpha \nabla u &= f \quad u \in \Omega, \\ \mathbf{n} \cdot \nabla u &= 0 \quad u \in \partial\Omega, \end{aligned} \tag{1}$$

where $\Omega \subset \mathbb{R}^d$ for $d = 1, 2, 3$, is a polygonal domain and $\alpha \in L^\infty(\Omega)$, such that $\alpha > \beta > 0$, $\beta \in \mathbb{R}$ has multiscale structure. Equation (1) has a unique solution $u \in H^1(\Omega)$ up to a constant for each $f \in L^2(\Omega)$ provided that $\int_\Omega f \, dx = 0$ is satisfied. Defining the L^2-scalar product as $(\cdot, \cdot)_{L^2(\omega)}$ on a domain $\omega \subseteq \Omega$, the weak formulation of (1) reads: find $u \in \mathcal{V} = H^1$ such that

$$(\alpha \nabla u, \nabla v)_{L^2(\Omega)} = (f, v)_{L^2(\Omega)}, \quad \forall v \in \mathcal{V}. \tag{2}$$

The rest of the paper is organized as follows. In Section 2, we present the different finite element methods needed to construct the multiscale methods. In Section 3 an abstract framework for constructing multiscale methods as well as the specific multiscale methods used in the numerical examples are proposed. Section 4, is devoted to some implementation details. Finally, in Section 5 numerical experiment are presented.

2. FINITE ELEMENT METHODS

Let $\mathcal{K} = \{K\}$ be a shape-regular mesh and let Γ denote the set of all edges (or faces in 3D) of the mesh $\mathcal{K}$. The set Γ is the union of two disjoint subsets $\Gamma = \Gamma^I \cap \Gamma^B$, where Γ^I is the union of the interior edges and Γ^B the union of the boundary edges. Given an interior

edge $e = \partial K^+ \cap \partial K^- \subset \Gamma^I$ for $K^+, K^- \in \mathcal{K}$, denote K^+ the element with the higher index and n as the outward unit normal of K^+ on e. Defining $v^+ := v|_{\partial K^+}$ and $v^- := v|_{\partial K^-}$, we set the average and jump operator as,

$$\{v\} = \frac{1}{2}(v^+ + v^-), \quad [v] = v^+ - v^-, \tag{3}$$

for $e \in \Gamma^I$ and

$$\{v\} = v^+, \quad [v] = v^+, \tag{4}$$

for $e \in \Gamma^B$. Also, for a non negative integer p, we denote by $\mathcal{P}_p(K)$, the set of all polynomials on $\mathcal{K}$ of total degree at most p.

2.1. Continuous Galerkin method

In the continuous Galerkin (CG) finite element discretization we are using a conforming approximation of the test space i.e., $\mathcal{V}_h = \{v \in \mathcal{V} : v|_K \in \mathcal{P}_p(K), \forall K \in \mathcal{K}\} \subset \mathcal{V}$. Given a bilinear form $\mathcal{B}_{cg} : \mathcal{V} \times \mathcal{V} \to \mathbf{R}$ and a linear functional $\mathcal{F}_{cg} : \mathcal{V} \to \mathbf{R}$, the continuous Galerkin method reads: find $u_h \in \mathcal{V}_h$ such that

$$\mathcal{B}_{cg}(u_h, v) := (\alpha \nabla u_h, \nabla v)_{L^2(\Omega)} = (f, v)_{L^2(\Omega)} =: \mathcal{F}_{cg}(v), \quad \forall v \in \mathcal{V}_h. \tag{5}$$

2.2. Discontinuous Galerkin method

In the discontinuous Galerkin method discretization we use a non-conforming approximation i.e., $S_h = \{v \in L^2(\Omega) : v|_K \in \mathcal{P}_r(K), \mathcal{K} \in \mathcal{K}\} \not\subset \mathcal{V}$. The discontinuous Galerkin method reads: find $u_h \in S_h$ such that

$$\mathcal{B}_{dg}(u_h, v) = \mathcal{F}_{dg}(v), \quad \forall v \in S_h, \tag{6}$$

where the bilinear form $\mathcal{B}_{dg} : S_h \times S_h \to \mathbb{R}$ and the linear functional $\mathcal{F}_{dg} : S_h \to \mathbb{R}$ are given by

$$\mathcal{B}_{dg}(v, z) := \sum_{K \in \mathcal{K}} (\alpha \nabla v, \nabla z)_{L^2(K)} - \sum_{e \in \Gamma^I} \left((n \cdot \{\alpha \nabla v\}, [z])_{L^2(e)} \right. \tag{7}$$
$$\left. + (n \cdot \{\alpha \nabla z\}, [v])_{L^2(e)} - \frac{\sigma_e}{h_e}([v], [z])_{L^2(e)} \right),$$
$$\mathcal{F}_{dg}(v) := (f, v)_{L^2(\Omega)}, \tag{8}$$

respectively; here $h_e := \operatorname{diam}(e)$, and $\sigma_e \in \mathbb{R}$ is a positive constant, depending on the variable α, large enough to make the bilinear form (7) coercive with respect to the natural energy norm. We refer, e.g., to [14,4] and references therein for details on the analysis of DG methods for elliptic problems.

3. ABSTRACT MULTISCALE METHOD

In the VMS framework, the fine scale finite element space, $\mathcal{W}_h$, is decoupled into coarse and fine scale contributions $\mathcal{W}_h = \mathcal{W}_c \oplus \mathcal{W}_f$, where $\mathcal{W}_c$ is associated with a coarse

mesh $\mathcal{K}_c$. The split between the coarse and the fine scales is determined by an inclusion operator $\mathcal{I}_c : \mathcal{W}_h \to \mathcal{W}_c$. The coarse and fine scale contributions are defined as, $\mathcal{W}_c := \mathcal{I}_c \mathcal{W}_h$ and $\mathcal{W}_f := (I - \mathcal{I}_c)\mathcal{W} = \{v \in \mathcal{W} : \mathcal{I}_c v = 0\}$. There are several different chooses of $\mathcal{I}_c$ e.g. the L^2-projection onto $\mathcal{W}_c$ or the nodal interpolant onto the coarse mesh. Let $\mathcal{B} : \mathcal{W} \times \mathcal{W} \to \mathbb{R}$ be a bilinear form, we can then define a multiscale map $\mathcal{T} : \mathcal{W}_c \to \mathcal{W}_f$ from the coarse to the fine scale as

$$\mathcal{B}(\mathcal{T}v_c, v_f) = -\mathcal{B}(v_c, v_f) \quad \forall v_c \in \mathcal{W}_c \text{ and } \forall v_f \in \mathcal{W}_f. \tag{9}$$

The reference solution and the test function can be decomposed into a coarse and fine-scale contribution; $u_h = u_c + \mathcal{T}u_c + u_f$, $v = v_c + v_f$ where $u_c, v_c \in \mathcal{W}_c$ and $(\mathcal{T}u_c + u_f), v_f \in \mathcal{W}_f$. The multiscale problem reads: find $u_c \in \mathcal{W}_c$ and $v_f \in \mathcal{W}_f$ such that

$$\mathcal{B}(u_c + \mathcal{T}u_c + u_f, v_c + v_f) = \mathcal{F}(v_c + v_f), \quad \forall v_c \in \mathcal{W}_c \text{ and } \forall v_f \in \mathcal{W}_f. \tag{10}$$

The fine scale component u_f can be computed by letting $v_c = 0$ in (10) and using the multiscale map (9). We arrive to the problem: find $u_f \in \mathcal{W}_f$ such that

$$\mathcal{B}(u_f, v_f) = \mathcal{F}(v_f), \quad \forall v_f \in \mathcal{W}_f. \tag{11}$$

The coarse scale solution is obtained by letting $v_f = 0$ in (10): find $u_c \in \mathcal{W}_c$ such that

$$\mathcal{B}(u_c + \mathcal{T}u_c, v_c) = \mathcal{F}(v_c) - \mathcal{B}(u_f, v_c), \quad \forall v_c \in \mathcal{W}_c. \tag{12}$$

In (12), $\mathcal{T}u_c$ and u_f are unknown and obtained by solving (9) and (11). Note that $\mathcal{B}(u_c + \mathcal{T}u_c, \mathcal{T}v_c) = 0$ and $\mathcal{B}(u_f, \mathcal{T}v_c) = \mathcal{F}(\mathcal{T}v_c)$. Then a symmetric formulation of the coarse scale problem is obtained by considering

$$\mathcal{B}(u_c + \mathcal{T}u_c, v_c + \mathcal{T}v_c) = \mathcal{F}(v_c + \mathcal{T}v_c) - \mathcal{B}(u_f, v_c + \mathcal{T}v_c), \quad \forall v_c \in \mathcal{W}_c. \tag{13}$$

The linear systems (12) and (13) has $\dim(\mathcal{W}_c)$ unknowns, but (9) and (11) are equally hard to solve as the original problem and need to be approximated.

3.1. Localization of the multiscale method

Let $\mathcal{N}$ be the index set of all nodes, $\{x_i\}$, in the mesh $\mathcal{K}_c$. Further, given that the coarse space is spanned by basis functions $\mathcal{W}_c = \mathrm{span}\{\phi_j\}$, let $\mathcal{M}_i$ be the index set of all ϕ_j such that $\phi_j(x_i) = 1$, in the continuous setting $\mathcal{M}_i = \{i\}$ and in the discontinuous case $\mathcal{M}_i$ have several entries. For each basis function ϕ_j we solve: find $\mathcal{T}\phi_j \in \mathcal{W}_f$ such that

$$\mathcal{B}(\mathcal{T}\phi_j, v_f) = -\mathcal{B}(\phi_j, v_f), \quad \forall v_c \in \mathcal{W}_f, \tag{14}$$

where $\phi_j + \mathcal{T}\phi_j$ can be viewed as a modified basis function. Because the fast decay of $\phi_j + \mathcal{T}\phi_j$ away from $\mathrm{supp}(\phi_j)$, see [13] for the conforming case, we can solve (9) on small overlapping patches $\omega_i \subset \Omega$ for each basis function ϕ_j where $j \in \mathcal{M}_i$. Defining $\mathcal{W}_f(\omega_i)$ to be $\mathcal{W}_f$ restricted to the patch ω_i, (9) is transformed to: for each $i \in \mathcal{N}$ and $j \in \mathcal{M}_i$ find $\tilde{\mathcal{T}}\phi_j \in \mathcal{W}_f(\omega_i)$ such that

$$\mathcal{B}(\tilde{\mathcal{T}}\phi_j, v_f) = -\mathcal{B}(\phi_j, v_f), \quad \forall v_f \in \mathcal{W}_f(\omega_i) \tag{15}$$

The term (11) can be handled in i similar fashion by splitting the right hand into local contributions using a partition of unity. The size of the patches is determined by adding a superscript L, ω_i^L, as in Definition 1.

Definition 1 *Let $\{\phi_j : j = 1, \ldots, dim(\mathcal{W}_c)\}$ be the Lagrange basis (continuous or discontinuous) of $\mathcal{W}_c$. The sum $\Phi_i := \sum_{j \in \mathcal{M}_i} \phi_j$ constructs a standard continuous Lagrangian basis function. We say that ω_i^1 is an 1-layer patch, if $\omega_i^1 = supp(\Phi_i)$. Further, we say that ω_i^L is an L-layer patch if*

$$\omega_i^L = \cup_{\{i:supp(\Phi_i) \cap \omega_i^{L-1}\} \neq \emptyset} supp(\Phi_i), \quad L = 2, 3, \ldots. \tag{16}$$

Finally, the set $\omega_i^L \backslash \omega_i^{L-1}$ will be referred to as an L-ring. This is illustrated in Figure 2.
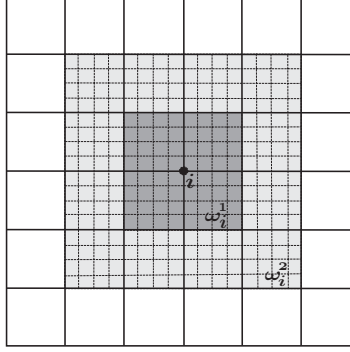

Figure 1. Example of a 1 layer patch ω_i^1 and 2 layer patch ω_i^2 around node i.

3.2. Continuous Galerkin multiscale method

The split between the coarse and fine scale spaces, $\mathcal{V}_h = \mathcal{V}_c \oplus \mathcal{V}_f$, is realized by choosing the inclusion operator to be the nodal interpolant; $\mathcal{I}_c = \Pi_c$. To keep the conformity of the method the fine scale problem is solved on patches using Dirichlet boundary condition. The multiscale problem reads: for all $i \in \mathcal{N}$ find $\tilde{\mathcal{T}}\phi_i, U_{f,i} \in \mathcal{V}_f(\omega_i^L)$ such that

$$\begin{aligned} \mathcal{B}_{cg}(\tilde{\mathcal{T}}\phi_j, v) &= -\mathcal{B}_{cg}(\phi_j, v), \quad \forall v_f \in \mathcal{V}_f(\omega_i^L), \\ \mathcal{B}_{cg}(U_{f,i}, v) &= \mathcal{F}_{cg}(\phi_i v), \quad \forall v_f \in \mathcal{V}_f(\omega_i^L). \end{aligned} \tag{17}$$

The modified coarse scale equations is then formulated as: find $U_c \in \mathcal{V}_c$ such that

$$\mathcal{B}_{cg}(U_c + \tilde{\mathcal{T}}U_c, v_c) = \mathcal{F}_{cg}(v_c) - \mathcal{B}_{cg}(U_f, v_c), \quad \forall v_c \in \mathcal{V}_c, \tag{18}$$

for the non-symmetric formulation and as

$$\mathcal{B}_{cg}(U_c + \tilde{\mathcal{T}}U_c, v_c + \tilde{\mathcal{T}}v_c) = \mathcal{F}_{cg}(v_c + \tilde{\mathcal{T}}v_c) - \mathcal{B}_{cg}(U_f, v_c + \tilde{\mathcal{T}}v_c), \quad \forall v_c \in \mathcal{V}_c, \tag{19}$$

for the symmetric formulation. The solution to the multiscale problem is $U = U_c + \tilde{\mathcal{T}}U_c + U_f$ where $U_f = \sum_{i \in \mathcal{N}} U_{f,i}$.

3.3. Discontinuous Galerkin multiscale method

Exploiting the discontinuous nature of S_h the split between the coarse and fine spaces, $S_h = S_c \oplus S_f$, is realized by choosing the inclusion operator to be the element wise L^2-projection onto S_c; $\mathcal{I}_c = \mathcal{P}_c$. This is more natural in a multiscale setting since the coarse scale solution approximate the average on each coarse element rather than the nodal values. The discontinuous nature of S_h also allows for using Neumann boundary conditions on the fine scale problems. With $\mathcal{V}_c = \text{span}\{\phi_j\}$, we need to solve the fine scale problem: for all $i \in \mathcal{N}$ and $j \in \mathcal{M}_i$ where $\Phi_i = \sum_{j \in \mathcal{M}_i} \phi_j$ find $\tilde{\mathcal{T}}\phi_j, U_i^f \in S_f(\omega_i^L)$ such that

$$
\begin{aligned}
\mathcal{B}_{dg}(\tilde{\mathcal{T}}\phi_j, v) &= -\mathcal{B}_{dg}(\phi_j, v), \quad \forall v_f \in S_f(\omega_i^L), \\
\mathcal{B}_{dg}(U_i^f, v) &= \mathcal{F}_{dg}(\Phi_i v), \quad \forall v_f \in S_f(\omega_i^L).
\end{aligned}
\tag{20}
$$

The modified coarse scale equations are formulated as: find $U_c \in S_c$ such that

$$
\mathcal{B}_{dg}(U_c + \tilde{\mathcal{T}}U_c, v_c) = \mathcal{F}_{dg}(v_c) - \mathcal{B}_{dg}(U_f, v_c), \quad \forall v_c \in S_c,
\tag{21}
$$

for the non-symmetric formulation or

$$
\mathcal{B}_{dg}(U_c + \tilde{\mathcal{T}}U_c, v_c + \tilde{\mathcal{T}}v_c) = \mathcal{F}_{dg}(v_c + \tilde{\mathcal{T}}v_c) - \mathcal{B}_{dg}(U_f, v_c + \tilde{\mathcal{T}}v_c), \quad \forall v_c \in S_c,
\tag{22}
$$

for the symmetric formulation. The solution to the multiscale problem is $U = U_c + \tilde{\mathcal{T}}U_c + U_f$ where $U_f = \sum_{i \in \mathcal{N}} U_{f,i}$.

4. IMPLEMENTATION

In the proposed multiscale method, the fine scale problem is perfectly parallelizable i.e., no communication between different fine scale problems are required. Algorithm 1 shows how the multiscale methods can be implemented. Note that the outer for-loop is perfectly parallel. An schematic overview is given in Figure 2 where the lines between the boxes represent communication. Also, note that the assembly of the coarse stiffness matrix and load vector is also done in parallel, in the fine scale problems. The extra constraints on the fine scale problems are realized using Lagrange multipliers

---
Algorithm 1 Multiscale Method

 1: Initialize the coarse mesh with mesh size H.
 2: Let the fine mesh size be $h = H/2^n$ and the size of the patches L.
 3: **for** $i \in \mathcal{N}$ **do**
 4:      Determine the patch ω_i^L.
 5:      **for** $j \in \mathcal{M}_i$ **do**
 6:          Compute the fine scale contribution for the modified basis functions $\tilde{\mathcal{T}}\phi_j$.
 7:      **end for**
 8:      Compute the right hand side correction U_i^f.
 9: **end for**
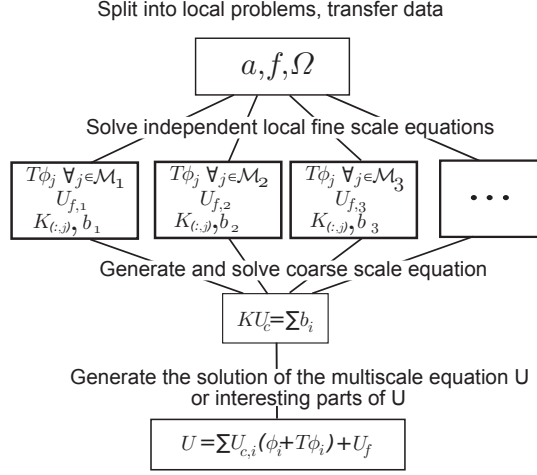10: Solve the modified coarse scale problem to obtain U_c.

Figure 2. Implementation scheme of the discontinuous Galerkin multiscale method.

5. NUMERICAL EXPERIMENTS

5.1. Decay of modified basis functions

Consider the domain ω_i^L, for $L = 1, \ldots, N$. On ω_i^N for $N = 8$, let $\mathcal{K}_c$ be a coarse mesh consisting of 16×16 elements and $\mathcal{K}_f$ be a fine mesh consisting of 128×128 elements. Let $\tilde{\mathcal{T}}^L \phi_j \in \mathcal{W}_f(\omega_i^L)$ be the solution of

$$\mathcal{B}(\tilde{\mathcal{T}}^L \phi_j, v) = -\mathcal{B}(\phi_j, v), \quad \forall v \in \mathcal{W}_f(\omega_i^L), \tag{23}$$

computed on ω_i^L and extended by 0 in $\Omega \setminus \omega_i^L$, where $\phi_j \in \mathcal{M}_i$, is a basis function on the coarse scale. Three types of permeabilities, called *Ones*, *Period*, and *SPE*, are used. For *One*, $a = 1$, for *Period*, $\alpha = 1$ or $\alpha = 0.1$ with a period of $1/64$ in x-direction, and *SPE*, data is taken from the 31st layer permeability data in the tenth SPE comparative solution project[1] and illustrated in Figure 3. The aspect ration is $a_{max}/a_{min} = 5.9823 \cdot 10^5$. The decay of the coarse modified basis function $\phi_j + \tilde{\mathcal{T}}^L \phi_j$ is illustrated by computing $\tilde{\mathcal{T}}^L \phi_j$ for $L = 1, \ldots, N - 1$ using $\tilde{\mathcal{T}}^N \phi_j$ as a reference solution. The space $\mathcal{W}_f$ and the bilinear form $\mathcal{B}(\cdot, \cdot)$, are defined as $\mathcal{V}_f$ and $\mathcal{B}_{cg}(\cdot, \cdot)$ for the continuous Galerkin multiscale method, and as S_f and $\mathcal{B}_{dg}(\cdot, \cdot)$ for the discontinuous Galerkin multiscale method. Exponential decay, in the broken energy norm

$$|||v|||^2 = \sum_{K \in \mathcal{K}_f} \|\sqrt{\alpha} \nabla v\|_{L^2(K)}^2, \tag{24}$$

for $L = 1, \ldots, N$ when $N = 4$, is observed in Figure 4. The fast decay motivates us to solve the constituent problems on patches $\omega_i^L \subset \Omega$ using a small number of L-rings. This, in turn, means less computational work and a smaller overlap between the localized problems. The DG method converges faster than CG to to the reference solution in the relative broken energy

---

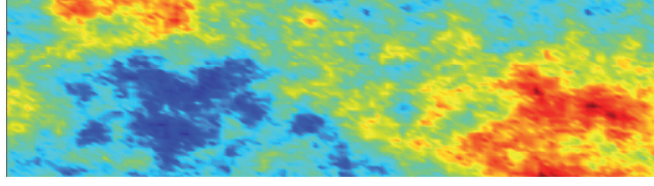[1]Tenth SPE comparative solution project http://www.spe.org/web/csp/

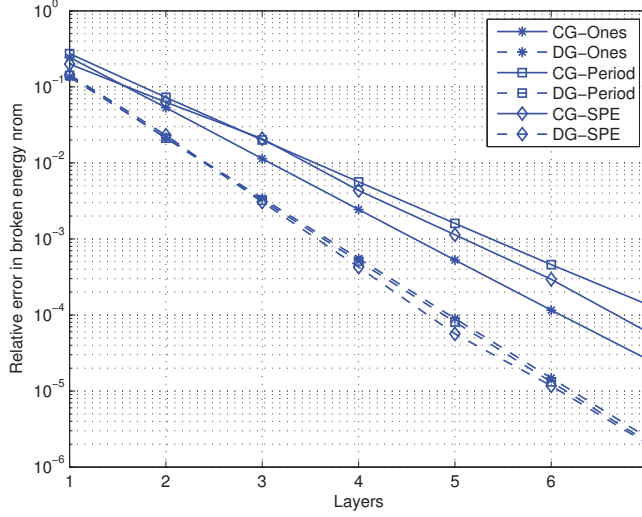Figure 3. Permeability structure for *SPE* (c) in log scale.

Figure 4. Convergence in the relative energy norm (24) when $L = 1, 2, 3$ in equation (23) for different permeability using continuous Galerkin (solid line) and discontinuous Galerkin (dashed line).

norm (24). Hence, smaller patches are needed for solving the local problems using DG than CG to achieve the same accuracy.

5.2. Comparison of the continuous and discontinuous Galerkin multiscale methods

Consider the model problem (1) on the unit square $\Omega = (0, 1) \times (0, 1)$. Let $\mathcal{K}$ be a reference mesh with $MN \times MN$ elements, and $\mathcal{K}_c$ a coarse mesh of $N \times N$ elements i.e., each coarse elements is further subdivided into $M \times M$ elements. In the numerical experiment $N = 16$ and $M = 8$. Let, $f(x, y) = -1$ for $\{0 < x, y < 1/128\}$, $f(x, y) = 1$ for $\{127/128 < x, y < 1\}$, and $f = 0$ otherwise, be the forcing function. The same permeabilities, *Ones*, *Rand* and *SPE*, as in Section 5.1 are used. In the numerical experiments all patches, ω_i^L, are of the same size, L, and for each iteration L is increased by one. The continuous Galerkin multiscale method and the discontinuous Galerkin multiscale method are compared, see Figure 5. We conclude:
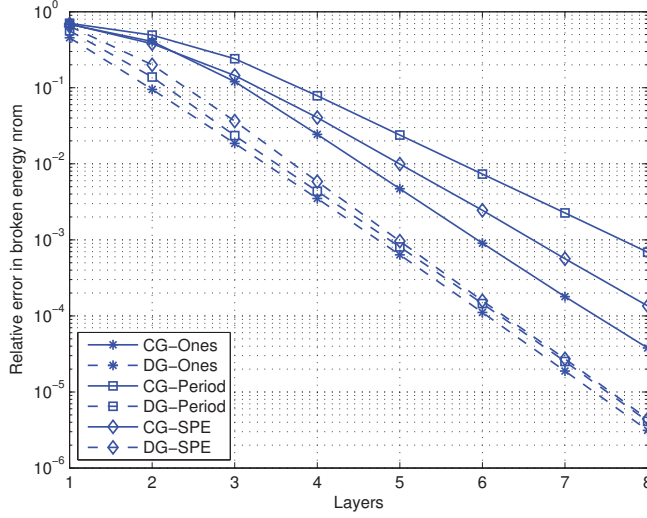
Figure 5. Convergence in the broken relative energy norm (24) when $L = 1, 2, \ldots, 8$ for different permeability using continuous Galerkin multiscale method (solid line) and discontinuous Galerkin multiscale method (dashed line).

- To obtain a given accuracy, in the relative broken energy norm (24), the discontinuous Galerkin multiscale method requires approximately one layer less than the continuous Galerkin multiscale method. For a comparison of the degrees of freedom required for the fine scale problems, see Table 1.

- This is a bit unfair comparison since the reference solution is the DG respectively CG solution computed on the fine scale. DG has a more enriched test and trial space and may give a better approximation than CG because of the discontinuous permeability coefficients.

- On the coarse scale the discontinuous Galerkin multiscale method is approximating the L^2-projection rather than the nodal values, which is the case for continuous Galerkin multiscale method. This is preferable in a multiscale setting.

- The DG method has better conservation properties which is an important property in many multiscale applications.

Table 1. Degree of freedom for the fine scale problems

layers	CGMM	DGMM
1	$(2n+1)^d$	$(4n)^d$
2	$(4n+1)^d$	$(8n)^d$
3	$(6n+1)^d$	$(12n)^d$
4	$(8n+1)^d$	$(16n)^d$

6. REFERENCES

[1]   J. Aarnes, B.-0. Hemsund, "Multiscale discontinuous Galerkin methods for elliptic problems with multiple scale". *Letc. notes in Comput. Sci. Eng.* vol 44, Springer, Heidelberg, Berlin, 2005.

[2]   A. Abdulle, "Discontinuous Galerkin finite element heterogeneous multiscale method for elliptic problems with multiple scale". *Math. Comp.* 81, 687-713, 2012.

[3]   D. N. Arnold, "An interior penalty finite element method with discontinuous elements". *SIAM J. Numer. Anal.* 19, 742-760, 1982.

[4]   D. N. Arnold, F. Brezzi, B. Cockburn, L. Marini "Unified analysis of discontinuous Galerkin methods for elliptic problems". *SIAM J. Numer. Anal.* 39, 1749-1779, 2001.

[5]   A. Babuška, J. E. Osborn, "Can a finite element method perform arbitrarily bad?". *Math. Comp.* 69(230), 443-462, 2000.

[6]   G. A. Baker, "Finite element methods for elliptic equations using nonconforming elements". *Math. Comp* 31, 45-59, 1977.

[7]   W. E, "Principles of multiscale modeling". *Math. Model. and Methods* Cambridge university press, 2011.

[8]   Y. Efendiev, T. Y. Hou, "Multiscale finite element methods: Theory and Applications". *Surveys and Tut. in Appl. Math. Sci.*, vol 4, Springer, New York,2009

[9]   T. Y. Hou, X.-H. Wu, "A multiscale finite element method for elliptic problems in composite materials and porous media". *J. of Comput. Phys.* 134, 169-189, 1997

[10]   T. Hughes, "Multiscale phenomena: Green's functions, the Dirichlet-to-Neumann formulation, subgrid scale models, bubbles and the origins of stabilized methods". *Comput. Methods Appl. Mech. Engrg.* 166(1-2), 3-24, 1998.

[11]   M. G. Larson, A. Målqvist, "Adaptive variational multiscale methods based on a posteriori error estimation: Energy norm estimates for elliptic problems". *Comput. Mehtods Appl. Mech. Engrg. s* 196(21-24), 2313-2324, 2007.

[12]   A. Målqvist, "Multiscale methods for elliptic problems". *Multiscale Model. and Simul.* 9, 1064-1086, 2011.

[13]   A. Målqvist, D. Peterseim "Localization of elliptic multiscale problems". *arXiv:1110.0692.* Submitted, 2011.

[14]   D. A. Di Pietro, A. Ern, "Mathematical aspect of discontinuous Galerkin methods". *Mathématiques et Apllications* vol 19, Springer, 2012.

[15]   B. Rivière, "Discontinuous Galerkin methods for solving elliptic and parabolic equations: Theory and Implementation". *Soc. for Industrial and Applied Math.*, Philadelphia, PA, USA. 2008

Paper II

AN ADAPTIVE DISCONTINUOUS GALERKIN
MULTISCALE METHOD FOR ELLIPTIC PROBLEMS

DANIEL ELFVERSON[†§], EMMANUIL H. GEORGOULIS[‡], AND AXEL MÅLQVIST[†¶]

Abstract. An adaptive discontinuous Galerkin multiscale method driven by an energy norm a posteriori error bound is proposed. The method is based on splitting the problem into a coarse and a fine scale. Localized fine scale constituent problems are solved on patches of the domain and are used to obtain a modified coarse scale equation. The coarse scale equation has considerably less degrees of freedom than the original problem. The a posteriori error bound is used within an adaptive algorithm to tune the critical parameters, i.e., the refinement level and the size of the different patches on which the fine scale constituent problems are solved. The fine scale computations are completely parallelizable, since no communication between different processors is required for solving the constituent fine scale problems. The convergence of the method, the performance of the adaptive strategy and the computational effort involved are investigated through a series of numerical experiments.

Key words. multiscale, discontinuous Galerkin, a posteriori error bound

AMS subject classifications. 65N30, 65N15

1. Introduction. Problems involving features on several different scales, usually termed multiscale problems, can be found in many branches of the engineering sciences. Examples include the modelling of flow in a porous medium and of composite materials. Multiscale problems involving partial differential equations are often impossible to simulate with an acceptable accuracy using standard (single mesh) numerical methods. A different approach, usually coming under the general term of multiscale methods, consists of considering coarse and fine scale contributions to the solution, with the fine scale contributions approximated on localized patches. The fine scale contributions are then used to upscale the problem in order to obtain an approximation to the global multiscale solution.

1.1. Previous work. Numerous multiscale methods have been developed during the last three decades, see e.g. [8, 7] for early works, or [16, 29, 15] and references therein for exposition and recent developments. An important development is the Multiscale Finite Element Method (MsFEM) by Hou and Wu [21], which was further developed in [12], with the introduction of oversampling to reduce resonance effects. Another approach is the, so-called, Variational Multiscale method (VMS) of Hughes and co-workers [22, 23]. The idea in VMS is to decompose the solution space into coarse and fine scale contributions. A modified coarse scale problem is then solved (using a finite element approach), so that the fine scale contribution is taken into account. To maintain the conformity of the resulting modified finite element space, homogeneous Dirichlet boundary conditions are imposed on each fine-problem patch boundary. The Adaptive variational multiscale method (AVMS) using the VMS framework, introduced by Larson and Målqvist [27], makes use of multiscale-type a posteriori error bound to adapt the coarse and fine scale mesh sizes as well as the fine-problem patch-sizes automatically. A priori error analysis can be found in [30].

An interesting alternative to conforming finite element methods is the class of discontinuous Galerkin (DG) methods, whereby the approximation spaces are element-wise discontinuous; the continuity of the underlying exact solutions is imposed weakly. DG methods appeared in the 1970s and in the early 1980s [32, 28, 9, 5, 24] and have recently received renewed interest; we refer to the volumes [13, 14, 20, 33] and the references therein for a literature review. DG methods admit good conservation properties of the state variable and, due to the lack of inter-element continuity requirements are ideally suited for application to complex and/or irregular meshes. Also, there has been work to better cope with the case of high contrast diffusion; see e.g. [19] where a DG method based on weighted average is proposed and analysed. Discontinuous Galerkin methods for solving multiscale problems have been discussed using the framework of the MsFEM [1] and of the Heterogeneous Multiscale Method (HMM) [2]; see also [37, 36, 35, 34]. An a priori error analysis for the class of discontinuous Galerkin multiscale method studied in this paper can be found in [17].

1.2. New contributions. In this work, we propose an *Adaptive Discontinuous Galerkin MultiScale method* (ADG-MS) using the framework of VMS. The underling DG method is based on weighted averages across the element interfaces. The adaptivity is driven by energy norm a posteriori error bounds. The multiscale method is based on solving localized problems on patches, which are then upscaled to solve a coarse scale equation. The lack of any inter-element continuity requirements of the approximate solution, allows for very general meshes which is very common in multiscale applications, i.e., meshes that contains several types of elements and/or hanging nodes. The split between the coarse and fine sale is realized using the elemetwise L^2-projection onto the coarse mesh. This is more natural in a multiscale setting than, e.g., using the nodal interpolant as in [27]. It is also much easier and efficient to construct an L^2 orthogonal split using DG as opposed to conforming multiscale methods. The ADG-MS inherits a local conservation property from DG on the coarse scale, which is crucial in many applications such as porous media flow. The fine scale problems can be solved independently with localized right hand sides, and it is known that the solutions decay exponentially [17], which allows for small patches. In this case the ADG-MS converges to the reference solution, thereby taking full advantage of cancellation between patches; this is not the case for the original AVMS [27] since hanging nodes are not allowed. In the a posteriori error bound, the error is bounded in terms of the size of the different fine-scale patches and on both the fine-scale and the coarse-scale mesh sizes. An adaptive algorithm to tune all these parameters automatically is proposed. The numerical experiments show good performance of the algorithm for a number of benchmark problems.

1.3. Outline. The rest of this work is structured as follows. Section 2 is devoted to setting up the model problem, the basic DG discretization and some notation. A general framework for multiscale problems along with the discontinuous Galerkin multiscale method is derived in Section 3, and the a posteriori error bound is derived in Section 4. The implementation of the method and the adaptive algorithm are discussed in Section 5. In Section 6, a number of numerical experiments are presented, and finally some conclusions are drawn in Section 7.

2. Preliminaries. In this section we define some notations and the underling DG method is presented.

2.1. Notation. Let $\omega \subseteq \mathbb{R}^d$, $d = 2, 3$ be an open polygonal domain. Denote the $L^2(\omega)$-inner product by $(\cdot, \cdot)_{L^2(\omega)}$, and the corresponding norm by $\| \cdot \|_{L^2(\omega)}$. Also, let

$H^1(\omega)$ be the Sobolev space with norm $\| \cdot \|_{H^1(\omega)} := (\| \cdot \|_{L^2(\omega)}^2 + \|\nabla \cdot \|_{L^2(\omega)}^2)^{1/2}$ and $H^s(\omega)$ the standard Hilbertian Sobolev space of index $s \in \mathbb{R}$. We shall also make use of the space $L^\infty(\omega)$ consisting of almost everywhere bounded functions, with norm $\| \cdot \|_{L^\infty(\omega)} := \text{ess sup}_\omega |\cdot|$; see, e.g., [3] for details. Finally, the d-dimensional Lebesgue measure will be denoted by $\mu_d(\cdot)$.

2.2. The Model problem. Let $\Omega \subset \mathbb{R}^d$ be an open polygonal domain with Lipschitz boundary $\partial\Omega$, $d = 2, 3$, and consider the elliptic boundary value problem find $u \in \{v \in H^1(\Omega) : v|_{\partial\Omega} = 0\}$ fulfilling

$$-\nabla \cdot A\nabla u = f \qquad u \in \Omega, \tag{2.1}$$

$$u = 0 \qquad u \in \partial\Omega, \tag{2.2}$$

with $f \in L^2(\Omega)$ and $A \in L^\infty(\Omega, \mathbb{R}^{d,d}_{\text{sym}})$ such that A has uniform spectral bounds, bounded below by $\alpha > 0 \in \mathbb{R}$ almost everywhere.

2.3. Discretization and subdivision. The domain Ω is subdivided into a partition $\mathcal{K} = \{K\}$ of shape-regular and closed elements K with boundaries ∂K, i.e. $\bar{\Omega} = \cup_{K \in \mathcal{K}} \bar{K}$. On the partition $\mathcal{K}$, let $h : \cup_{K \in \mathcal{K}} K \to \mathbb{R}$ be a mesh-function defined element-wise by $h|_K := \text{diam}(K)$, $K \in \mathcal{K}$. The partition is allowed to be irregular (i.e,. hanging nodes are allowed) and it is locally quasi-uniform in the sense that the ratio of the mesh function h for neighboring elements is uniformly bounded from above and below. Let Γ^B be the set of all boundary edges and Γ^I be the set of all interior edges (or faces when $d = 3$) such that $\Gamma = \Gamma^B \cap \Gamma^I$ is the set of all edges in the partition $\mathcal{K}$. Associated with the diffusion tensor, we consider the element-wise constant functions $A^0, A_0 : \cup_{K \in \mathcal{K}} K \to \mathbb{R}$ defined by the biggest and smallest eigenvalue of A, respectively, on each element K. For $K_i, K_j \in \mathcal{K}$, with $\mu_{d-1}(\partial K_i \cap \partial K_j) > 0$, let K_i, K_j be denoted by K^+ and K^-, where K^+ is the element with the higher index. On interior element interfaces $e \in \Gamma^I$ we shall make use of the shorthand notation $v^+ := v|_{K^+}$, $v^- := v|_{K^-}$; on boundary edges we set $v^+ := v|_K$. We also define the weighted mean value by

$$\{v\}_w := w_{K^+(e)}v^+ + w_{K^+(e)}v^-, \tag{2.3}$$

where

$$w_{K^+(e)} := \frac{A^0|_{K^-}}{A^0|_{K^+} + A^0|_{K^-}}, \qquad w_{K^-(e)} := \frac{A^0|_{K^+}}{A^0|_{K^+} + A^0|_{K^-}}, \tag{2.4}$$

for each $e \in \Gamma^I$ and

$$w_{K^+(e)} = 1, \qquad w_{K^+(e)} = 0, \tag{2.5}$$

for $e \in \Gamma^B$. Further, the jump across element interfaces is defined by

$$[v] := v^+ - v^- \text{ for } e \in \Gamma^I, \qquad \text{and} \qquad [v] := v^+ \text{ for } e \in \Gamma^B, \tag{2.6}$$

and the harmonic mean value γ_e by

$$\gamma_e := \frac{2A^0|_{K^+} \cdot A^0|_{K^-}}{A^0|_{K^+} + A^0|_{K^-}}. \tag{2.7}$$

Also, n will denote the outward unit normal to ∂K^+ when $\mu_{d-1}(\partial K^+ \cap \partial K^-) > 0$. When $\mu_{d-1}(\partial K \cap \partial\Omega) > 0$, n will be the outward unit normal to $\partial\Omega$.

2.4. The Discontinuous Galerkin method. For a nonnegative integer r, we denote by $\mathcal{P}_r(\hat{K})$, the set of all polynomials on $\hat{K}$ of total degree at most r, if $\hat{K}$ if the reference d-simplex or, of degree at most r in each variable, if $\hat{K}$ the reference d-hypercube.

Consider the space $\mathcal{V} := \mathcal{V}_h + H^{1+\epsilon}(\Omega)$ with $\epsilon > 0$ but arbitrary small, and let the discontinuous finite element space be given by

$$\mathcal{V}_h := \{v \in L^2(\Omega) : v \circ F_K|_K \in \mathcal{P}_r(\hat{K}), \ \hat{K} \in \mathcal{K}\}, \tag{2.8}$$

where $F_K : \hat{K} \to K$ is the respective elemental map for $K \in \mathcal{K}$, which is allowed to be non-affine, provided its Jacobian remains non-singular and uniformly bounded from above and below with respect to all meshes.

The discontinuous Galerkin method then reads: find $u_h \in \mathcal{V}_h$ such that

$$a(u_h, v) = \ell(v), \quad \forall v \in \mathcal{V}_h, \tag{2.9}$$

where the bilinear form $a(\cdot, \cdot) : \mathcal{V} \times \mathcal{V} \to \mathbb{R}$ and the linear form $\ell(\cdot) : \mathcal{V} \to \mathbb{R}$ are given by

$$a(v, z) := \sum_{K \in \mathcal{K}} (A\nabla v, \nabla z)_{L^2(K)} - \sum_{e \in \Gamma} \Big((n \cdot \{A\Pi\nabla v\}_w, [z])_{L^2(e)} \tag{2.10}$$
$$+ (n \cdot \{A\Pi\nabla z\}_w, [v])_{L^2(e)} - \frac{\sigma_e \gamma_e}{h_e}([v], [z])_{L^2(e)} \Big),$$
$$\ell(v) := (f, v)_{L^2(\Omega)}, \tag{2.11}$$

respectively. Here $\Pi : (L^2(\Omega))^d \to (\mathcal{V}_h)^d$ denotes the orthogonal L^2-projection operator onto $(\mathcal{V}_h)^d$, $h_e := \mathrm{diam}(e)$, and $\sigma_e \in \mathbb{R}$ is a positive constant. The bilinear form (2.11) is coercive with respect to the natural energy norm,

$$|||v||| = \left(\sum_{K \in \mathcal{K}} \|A^{1/2}\nabla v\|_{L^2(K)}^2 + \sum_{e \in \Gamma} \frac{\sigma_e \gamma_e}{h_e} \|[v]\|_{L^2(e)}^2 \right)^{1/2} \tag{2.12}$$

if σ_e is chosen to be large enough. We refer, e.g., to [14, 6] and references therein for details on the analysis of DG methods for elliptic problems. Discontinuous Galerkin methods with weighted averages were introduced in [10, 19].

REMARK 2.1. *For all $v \in \mathcal{V}_h$, we have $\Pi\nabla v = \nabla v$, therefore the bilinear form (2.10) with $v, z \in \mathcal{V}_h$ is reduced to the more familiar form*

$$a(v, z) = \sum_{K \in \mathcal{K}} (A\nabla v, \nabla z)_{L^2(K)} - \sum_{e \in \Gamma} \Big((n \cdot \{A\nabla v\}_w, [z])_{L^2(e)} \tag{2.13}$$
$$+ (n \cdot \{A\nabla z\}_w, [v])_{L^2(e)} - \frac{\sigma_e \gamma_e}{h_e}([v], [z])_{L^2(e)} \Big).$$

3. The Multiscale method. In the VMS framework, the finite element solution space $\mathcal{V}_h$ is decoupled into coarse and fine scale contributions, viz., $\mathcal{V}_h = \mathcal{V}_H \oplus \mathcal{V}_f$, with $\mathcal{V}_H \subset \mathcal{V}_h$. To this end, let $\Pi_H : L^2(\Omega) \to \mathcal{V}_H$ be the (ortogonal) L^2-projection onto the coarse mesh. The split between the coarse and fine scales is then determined by, $\mathcal{V}_H := \Pi_H \mathcal{V}_h$ and $\mathcal{V}_f := (I - \Pi_H)\mathcal{V}_h = \{v \in \mathcal{V}_h : \Pi_H v = 0\}$ where I is the identity operator.

The multiscale map $\mathcal{T} : \mathcal{V}_H \to \mathcal{V}_f$ from the coarse to the fine scale is defined as

$$a(\mathcal{T}v_H, v_f) = -a(v_H, v_f) \quad \forall v_H \in \mathcal{V}_H \text{ and } \forall v_f \in \mathcal{V}_f. \tag{3.1}$$

The next step is to decompose u_h and v in (2.9) into coarse and fine scale components. In particular, we have

$$u_h = u_H + \mathcal{T}u_H + u_f, \tag{3.2}$$

and $v = v_H + v_f$, with $u_H, v_H \in \mathcal{V}_H$ and $\mathcal{T}u_H, v_f \in \mathcal{V}_f$, for some $u_f \in \mathcal{V}_f$. Equation (2.9) is equivalent to the problem: find $u_H \in \mathcal{V}_H$ and $v_f \in \mathcal{V}_f$ such that

$$a(u_H + \mathcal{T}u_H + u_f, v_H + v_f) = \ell(v_H + v_f), \quad \forall v_H \in \mathcal{V}_H \text{ and } \forall v_f \in \mathcal{V}_f. \tag{3.3}$$

The fine scale component u_f can be computed by letting $v_H = 0$ in (3.3) and using the multiscale map (3.1). We obtain the fine scale problem driven by the right hand side data f: find $u_f \in \mathcal{V}_f$ such that

$$a(u_f, v_f) = \ell(v_f), \quad \forall v_f \in \mathcal{V}_f. \tag{3.4}$$

The coarse scale solution is obtained by letting $v_f = 0$ in (3.3): find $u_H \in \mathcal{V}_H$ such that

$$a(u_H + \mathcal{T}u_H, v_H) = \ell(v_H) - a(u_f, v_H), \quad \forall v_H \in \mathcal{V}_H. \tag{3.5}$$

In (3.5), $\mathcal{T}v_H$ and u_f are unknown and obtained by solving (3.1) and (3.4). Note that the linear system (3.5) has $\dim(\mathcal{V}_H)$ unknowns.

3.1. Localization and Discretization. The bilinear form is characterized by more local behavior in $\mathcal{V}_f$ than in $\mathcal{V}_h$ [30, 17]. This motivates us to solve the fine scale equations on (localized) overlapping patches, instead of the whole domain Ω. The patches are chosen large enough to ensure sufficiently accurate computations of $\mathcal{T}v_H$ and u_f. The computations of the fine scale components of the solution can be done in parallel with localized right hand sides. To define the coarse space $\mathcal{V}_H$, we begin by fixing a coarse mesh $\mathcal{K}_H$. Then, $\mathcal{V}_H$ is defined as,

$$\mathcal{V}_H := \{v \in L^2(\Omega) : v \circ F_K|_K \in \mathcal{P}_r(\hat{K}), \ \hat{K} \in \mathcal{K}_H\}. \tag{3.6}$$

DEFINITION 3.1. *For all $K \in \mathcal{K}_H$, define element patches of size L patch as*

$$\begin{aligned} \omega_K^1 &= int(K) \\ \omega_K^L &= int(\cup\{K' \in \mathcal{K}_H \mid K' \cap \bar{\omega}_K^L\}), \quad L = 2, 3, \dots. \end{aligned} \tag{3.7}$$

The patch ω_K^L will be refered to as a L-layer patch. This is illustrated in Figure 3.1.

On each L-layer patch, we let $\mathcal{K}(\omega_K^L)$ be a restiction of $\mathcal{K}$ to ω_K^L, such that $\cup_{K \in \mathcal{K}(\omega_K^L)} = \bar{\omega}_K^L$. Also let $\Gamma^I(\omega_K^L)$ and $\Gamma^B(\omega_K^L)$ be the interior respectively boundary edges on $\mathcal{K}(\omega_K^L)$. Moreover, we assume that $\mathcal{K}_H|_{\omega_K^L}$ and $\mathcal{K}(\omega_K^L)$ are nested, that is, every coarse element $K_H \in \mathcal{K}_H|_{\omega_K^L}$ coincides with a union of fine elements $K \in \mathcal{K}(\omega_K^L)$. Also, the fine test spaces $\mathcal{V}_f(\omega_K^L)$, are defined by

$$\mathcal{V}_f(\omega_K^L) := \{v \in \mathcal{V}_f : v|_{\Omega \setminus \omega_K^L} = 0\}. \tag{3.8}$$

Finally, let the indicator function be $\chi_K = 1$ on element K and 0 otherwise and $\mathcal{M}_K$ be the index set of all basis functions $\phi_j \in \mathcal{V}_H$ that have support on K i.e., $\chi_K = \sum_{j \in \mathcal{M}_K} \phi_j$.
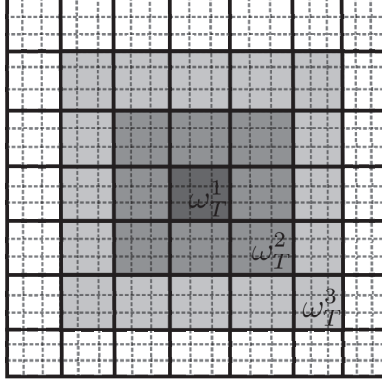
FIGURE 3.1. *Example of a one ω_K^1, two ω_K^2, and three ω_K^3 layer patches around element T in a quadrilateral mesh.*

3.2. The Discontinuous Galerkin Multiscale method. For each $K \in \mathcal{K}_H$ the following local problems need to be solved: find $\tilde{\mathcal{T}}\phi_j \in \mathcal{V}_f(\omega_K^L)$, $\forall j \in \mathcal{M}_K$ and $U_{f,K} \in \mathcal{V}_f(\omega_K^L)$ such that

$$a(\tilde{\mathcal{T}}\phi_j, v_f) = -a(\phi_j, v_f), \quad \forall v_f \in \mathcal{V}_f(\omega_K^L), \tag{3.9}$$

$$a(U_{f,K}, v_f) = \ell(\chi_K v_f), \quad \forall v_f \in \mathcal{V}_f(\omega_K^L). \tag{3.10}$$

The modified coarse scale problem is formulated as: find $U_H \in \mathcal{V}_H$ such that

$$a(U_H + \tilde{\mathcal{T}}U_H, v_H) = \ell(v_H) - a(U_f, v_H), \quad \forall v_H \in \mathcal{V}_H, \tag{3.11}$$

where $U_f := \sum_{K \in \mathcal{K}_H} U_{f,K}$. The approximate solution to the multiscale problem is given by

$$U = U_H + \tilde{\mathcal{T}}U_H + U_f. \tag{3.12}$$

The above procedure will be referred to as the *discontinuous Galerkin multiscale method*.

We note that the approximation U is *not* equal to u_h in general, since the domains of the fine scale problems are truncated. However, as discussed above, it is expected that U is a good approximation to u_h, due to the decaying nature of the fine scale solutions away from the respective patch. For the approximation U to converge to the exact solution u of (2.1) in the limit, both the support of the local problems should be gradually extended to the whole computational domain and the fine scale meshsize h should converge to 0. The multiscale method proposed here differs from the one proposed in [17], in that a right hand side correction is present. Using the formulation without the presence a right hand side correction, the multiscale solution converges to a some H-perturbation of the exact solution u, uniformly with respect to the diffusion coefficient structure.

REMARK 3.2. *Note that for a non-uniform mesh $\mathcal{K}$ (and/or $\mathcal{K}_H$), the convergence results presented in [17] still hold if the corrected basis functions are computed on patches of a common reference mesh $\mathcal{K}$. On the other hand if the adaptive algorithm is used so that the overlap between different corrected basis functions are*

computed on different meshes (cf., e.g., [27]), less cancellation of the error will occur and convergence can no longer be guaranteed by the argument in [17].

3.3. Local conservation property. The DG methods are known to have good local conservation properties in that the normal fluxes are conservative. The ADG-MS inherits this property on the coarse scale. To see this, we introduce the normal fluxes on element $K_H \in \mathcal{K}_H$ as

$$\hat{\sigma}(U) := (\{n \cdot A\nabla U\}_w - \sigma_e \gamma_e h_e^{-1}[U])[\chi_{K_H}], \quad e \in \partial K_H, \tag{3.13}$$

where $U = U_H + \tilde{\mathcal{T}}U_H + U_f$, $\chi_{K_H} = 1$ on element K_H and $\chi_{K_H} = 0$ otherwice ($[\chi_{K_H}]$ is either 1 or -1), and each interface e is a face of a fine scale element $K \in \mathcal{K}$, i.e., the number of edges can exceed the number of faces for each element K_H. By setting $w \in \mathcal{V}_H$ to be $w = \chi_{K_H}$ in (2.10), (2.11), and by using the discrete normal fluxes defined in (3.13), we arrive to the discrete element-wise conservation law

$$(f, 1)_{L^2(K_H)} + (\hat{\sigma}(U), 1)_{L^2(\partial K_H)} = 0, \tag{3.14}$$

for all $K_H \in \mathcal{K}_H$.

4. A Posteriori Error Bound in Energy Norm. Let the constant $0 \le C < \infty$ be any generic constant neither depending on H, h, L, nor A; let $a \lesssim b$ abbreviates the inequality $a \le Cb$. The following approximation results will be used frequently throughout this section. Let π be the orthogonal L^2-projection operator onto element-wise constant functions. Then π satisfies the following approximation properties: for an element K, we have

$$\|v - \pi v\|_{L^2(K)} \lesssim \frac{h_K}{\sqrt{A_0}} \|A^{1/2}\nabla v\|_{L^2(K)}, \quad \forall v \in H^1(K), \tag{4.1}$$

$$\|v - \pi v\|_{L^2(\partial K)} \lesssim \sqrt{\frac{h_K}{A_0}} \|A^{1/2}\nabla v\|_{L^2(K)} \quad \forall v \in H^1(K). \tag{4.2}$$

LEMMA 4.1. *Let $\mathcal{I}_h^c : \mathcal{V}_h \to \mathcal{V}_h \cap H^1(\Omega)$ be a averaging interpolation operator defined pointwise as*

$$\mathcal{I}_h^c v_h(\tilde{x}) = \frac{1}{|\mathcal{K}_{\tilde{x}}|} \sum_{K \in \mathcal{K}_{\tilde{x}}} v_h(\tilde{x})|_K, \tag{4.3}$$

where $\mathcal{K}_{\tilde{x}}$ is the set of elements in $\mathcal{K}$ for which $\tilde{x}$ belong, with the cardinal $|\mathcal{K}_{\tilde{x}}|$. Then,

$$\|v_h - \mathcal{I}_h^c v_h\|_{L^2(K)}^2 \lesssim \|\sqrt{h_e}[v_h]\|_{L^2(\partial K)}^2, \tag{4.4}$$

$$\|A^{1/2}\nabla(v_h - \mathcal{I}_h^c v_h)\|_{L^2(K)}^2 \lesssim A^0 \|\frac{1}{\sqrt{h_e}}[v_h]\|_{L^2(\partial K)}^2. \tag{4.5}$$

holds for all $v_h \in \mathcal{V}_h$ and $K \in \mathcal{K}$.

The proof, omitted here, follows closely that of [25]. Lemma 4.1 can also be extended to irregular meshes. There a hierarchical refinement of the mesh is performed to eliminate the hanging nodes; we refer to [26] for details. For irregular meshes the constant in the bounds of Lemma 4.1 also depends on the number of hanging nodes on each face.

REMARK 4.2. *The result in Lemma 4.1 can be sharpened if the diffusion tensor is isotropic and a locally quasi-monotone [31] distribution is assumed to hold. Then $A^0|_K$ can be replaced by the harmonic mean value γ_e on face e; see [11].*

First we derive a posteriori error bound for the underling (one scale) DG method.

THEOREM 4.3. *Let* u, u_h *be given by* (2.1)-(2.2) *and* (2.9), *respectively. Let also* $\mathcal{I}_h^c u_h \in \mathcal{V}_h \cap H^1(\Omega)$ *be given by* (4.3). *Moreover, let* $\mathcal{E} := \mathcal{E}_c + \mathcal{E}_d$ *where* $\mathcal{E}_c := u - \mathcal{I}_h^c u_h$ *and* $\mathcal{E}_d := \mathcal{I}_h^c u_h - u_h$. *Then*

$$|||\mathcal{E}||| \lesssim \big(\sum_{K \in \mathcal{K}} \varrho_K^2\big)^{1/2} + \big(\sum_{K \in \mathcal{K}} \zeta_K^2\big)^{1/2}, \tag{4.6}$$

where

$$\varrho_K = \frac{h_K}{\sqrt{A_0}}||(1 - \Pi)(f + \nabla \cdot A\nabla u_h)||_{L^2(K)}, \tag{4.7}$$

$$+ \sqrt{\frac{h_K}{A_0}}\Big(||(1 - w_{K(e)})n \cdot [A\nabla u_h]||_{L^2(\partial K \setminus \Gamma^B)} + ||\frac{\sigma_e \gamma_e}{h_e}[u_h]||_{L^2(\partial K)}\Big),$$

$$\zeta_K^2 = ||A^{1/2}\nabla(u_h - \mathcal{I}_h^c u_h)||_{L^2(K)}^2 + ||\sqrt{\frac{\sigma_e \gamma_e}{h_e}}[u_h]||_{L^2(\partial K)}^2. \tag{4.8}$$

REMARK 4.4. *Using* $\mathcal{I}_h^c u_h$ *as the conforming part of* u_h, *we arrive to an a posteriori bound whereby* $\mathcal{I}_h^c u_h$ *can either be evaluated directly, or bounded using Lemma 4.1. Another possible choice is a weighted averaging interpolation operator with the weights depending on the diffusion tensor* [4].

REMARK 4.5. *Concerning the lower efficiency bounds, the term* (4.7) *is robust with respect to the diffusion tensor; see* [18]. *But to prove that* (4.8) *is robust with respect to the diffusion tensor, to the authors' knowledge, the diffusion tensor has to be isotropic and satisfy a locally quasi-monotone property* [31, 11].

Proof. Note that

$$|||\mathcal{E}||| \leq |||\mathcal{E}_c||| + |||\mathcal{E}_d|||, \tag{4.9}$$

where the first part can be bounded by

$$|||\mathcal{E}_c|||^2 \lesssim a(\mathcal{E}_c, \mathcal{E}_c) = a(\mathcal{E}, \mathcal{E}_c) - a(\mathcal{E}_d, \mathcal{E}_c) \lesssim a(\mathcal{E}, \mathcal{E}_c) + |||\mathcal{E}_d||| \, |||\mathcal{E}_c|||. \tag{4.10}$$

Let π_h be the L^2-orthogonal projection onto the element-wise constant functions and define $\eta := \mathcal{E}_c - \pi_h \mathcal{E}_c$. We then have

$$a(\mathcal{E}, \mathcal{E}_c) = a(u, \mathcal{E}_c) - a(u_h, \mathcal{E}_c) = \ell(\mathcal{E}_c) - a(u_h, \mathcal{E}_c) = \ell(\eta) - a(u_h, \eta), \tag{4.11}$$

which implies

$$|||\mathcal{E}_c|||^2 = a(\mathcal{E}_c, \mathcal{E}_c) = \big(\ell(\eta) - a(u_h, \eta)\big) - a(\mathcal{E}_d, \mathcal{E}_c). \tag{4.12}$$

Upon integration by parts and using the identity $[vw] = \{v\}_w[w] + \{w\}_{\bar{w}}[v]$ where $\bar{w}$ is the skew-weighted average given by

$$\{v\}_{\bar{w}} := w_{K^-(e)}v^+ + w_{K^+(e)}v^-, \tag{4.13}$$

the first term on the right-hand side of (4.12) yields

$$\ell(\eta) - a(u_h, \eta)$$
$$= \sum_{K \in \mathcal{K}} (f + \nabla \cdot A\nabla u_h, \eta)_{L^2(K)} + \sum_{e \in \Gamma} \Big(- (n \cdot [A\nabla u_h], \{\eta\}_{\bar{w}})_{L^2(e \setminus \Gamma^B)} \tag{4.14}$$
$$+ (n \cdot \{A\Pi\nabla\eta\}_w, [u_h])_{L^2(e)} - \sigma\gamma_e h_e^{-1}([u_h], [\eta])_{L^2(e)}\Big).$$

The first term on the right-hand side of (4.14) can be bounded as follows,

$$\sum_{K \in \mathcal{K}} (f + \nabla \cdot A \nabla u_h, \eta)_{L^2(K)} \lesssim \sum_{K \in \mathcal{K}} \frac{h_K}{\sqrt{A_0}} ||(1 - \Pi)(f + \nabla \cdot A \nabla u_h)||_{L^2(K)} ||A^{1/2} \nabla \mathcal{E}_c||_{L^2(K)},$$

using (4.1). The second term on the right-hand side of (4.14) gives

$$\sum_{e \in \Gamma \setminus \Gamma^B} (n \cdot [A \nabla u_h], \{\eta\}_{\bar{w}})_{L^2(e)} \tag{4.15}$$

$$\lesssim \sum_{K \in \mathcal{K}} \sqrt{\frac{h_K}{A_0}} ||(1 - w_{K(e)}) n \cdot [A \nabla u_h]||_{L^2(\partial K \setminus \Gamma^B)} ||A^{1/2} \nabla \mathcal{E}_c||_{L^2(K)},$$

using (4.2). For the third term on the right-hand side of (4.14), noting that $\nabla \eta = \nabla \mathcal{E}_c$, we deduces

$$\sum_{e \in \Gamma} (n \cdot \{A \Pi \nabla \mathcal{E}_c\}_w, [\mathcal{E}_d])_{L^2(e)} \lesssim \sum_{K \in \mathcal{K}} \frac{1}{\sqrt{h_K A_0}} ||\gamma_e [\mathcal{E}_d]||_{L^2(\partial K)} ||A^{1/2} \nabla \mathcal{E}_c||_{L^2(K)},$$

using an inverse estimate and the L^2-stability of Π. For the last term on the right-hand side of (4.14), we have

$$\sum_{e \in \Gamma} \frac{\sigma_e \gamma_e}{h_e} ([u_h], [\eta])_{L^2(e)} \lesssim \sum_{K \in \mathcal{K}} \sqrt{\frac{h_K}{A_0}} ||\frac{\sigma_e \gamma_e}{h_e} [u_h]||_{L^2(\partial K \setminus \Gamma^B)} ||A^{1/2} \nabla \mathcal{E}_c||_{L^2(K)}.$$

The last term on the right-hand side of (4.12) is bounded using the continuity if the bilinear form. Combining all the above bounds and using Lemma 4.1 to bound the nonconforming part, the result follows. □

A posteriori error estimate for the ADG-MS is given below.

THEOREM 4.6. *Let u, U be defined in (2.1)-(2.2) and (3.12), respectively and set $\mathcal{I}_h^c U \in H^1(\Omega)$. Set $\mathcal{E} := \mathcal{E}_c + \mathcal{E}_d$ where $\mathcal{E}_c := u - \mathcal{I}_h^c U$ and $\mathcal{E}_d := \mathcal{I}_h^c U - U$. Define $U_{K_H} := \sum_{j \in \mathcal{M}_{K_H}} U_j(\phi_j + \tilde{\mathcal{T}} \phi_j) + U_{f, K_H}$, where U_j are the nodal values calculated by (3.11) for all $\mathcal{K}_H$. Then, $\mathcal{E}$ satisfies the estimate*

$$|||\mathcal{E}||| \lesssim (\sum_{K \in \mathcal{K}} \varrho_K^2)^{1/2} + (\sum_{K \in \mathcal{K}} \zeta_K^2)^{1/2} + (\sum_{K_H \in \tilde{\mathcal{K}}_H} \rho_{\omega_{K_H}^L}^2)^{1/2}, \tag{4.16}$$

where

$$\rho_{\omega_{K_H}^L}^2 = \sum_{e \in \Gamma^B(\omega_{K_H}^L)} \left(\frac{H_{K_H^O}^2}{h_{K^O} A_0|_{K_H^O}} \right) \left(||n \cdot \{A \nabla U_i\}_w||_{L^2(e)} + \frac{\sigma_e \gamma_e}{h_e} ||[U_i]||_{L^2(e)} \right)^2, \tag{4.17}$$

measures the effect of the truncated patches, K^O, K_H^O are from outside of $\omega_{K_H}^L$, and

$$\varrho_K = \frac{h_K}{\sqrt{A_0}} ||(1 - \Pi)(f + \nabla \cdot A \nabla U)||_{L^2(K)}, \tag{4.18}$$

$$+ \sqrt{\frac{h_K}{A_0}} \left(||(1 - w_{K(e)}) n \cdot [A \nabla U]||_{L^2(\partial K)} + ||\frac{\sigma_e \gamma_e}{h_e} [U]||_{L^2(\partial K)} \right),$$

$$\zeta_K^2 = ||\sqrt{A} \nabla (U - \mathcal{I}_h^c U)||_{L^2(K)}^2 + ||\sqrt{\frac{\sigma_e \gamma_e}{h_e}} [U]||_{L^2(\partial K)}^2. \tag{4.19}$$

messuring the refinement level of the fine scale.

REMARK 4.7. *One possible adaptive strategy would be to refine the coarse mesh as much one can afford, using a standard a posteriori error bound (e.g., using Theorem 4.3), and then further improve the approximation using Theorem 4.6. Note that fine scale problems do not have to be solved everywhere.*

REMARK 4.8. *For the estimator $\rho_{\omega_{K_H}^L}$ to retain its optimality with respect to the mesh-sizes, one should assume that $H_{K_H}^2 \lesssim h_K$. We note that this is not an unreasonable requirement, for, otherwise, each fine scale problem would be more expensive to solve than the coarse scale problem.*

Proof. Using the same idea as in Theorem 4.3. We first, note that

$$|||\mathcal{E}_c|||^2 = a(\mathcal{E}_c, \mathcal{E}_c) = a(\mathcal{E}, \mathcal{E}_c) - a(\mathcal{E}_d, \mathcal{E}_c). \tag{4.20}$$

Then, using (2.9) and the fine scale equations (3.9)–(3.10), we have

$$a(\mathcal{E}, \mathcal{E}_c) = \ell(\mathcal{E}_c) - a(U, \mathcal{E}_c), \tag{4.21}$$
$$= \ell(\mathcal{E}_c - v_H) - a(U, \mathcal{E}_c - v_H), \tag{4.22}$$
$$= \ell(\mathcal{E}_c - v_H - v_f) - a(U, \mathcal{E}_c - v_H - v_f) + \ell(v_f) - a(U, v_f), \tag{4.23}$$

for any $v_H \in \mathcal{V}_H$ and $v_f \in \mathcal{V}_f$. Note that,

$$\ell(v_f) - a(U, v_f) = \sum_{K_H \in \tilde{\mathcal{K}}_H} \ell(\chi_{K_H} v_f) - a(U_{K_H}, v_f) \tag{4.24}$$

$$= \sum_{K_H \in \tilde{\mathcal{K}}_H} \sum_{e \in \Gamma^B(\omega_{K_H}^L)} \Big((n \cdot \{A\nabla U_i\}_w, [\xi_{K_H}^L v_f])_{L^2(e)} \tag{4.25}$$

$$+ (n \cdot \{A\nabla \xi_{K_H}^L v_f\}_w, [U_i])_{L^2(e)} - \frac{\sigma_e \gamma_e}{h_e}([U_i], [\xi_{K_H}^L v_f])_{L^2(e)} \Big),$$

where $\xi_{K_H}^L = 0$ on $\omega_{K_H}^L$ and $\xi_{K_H}^L = 1$ otherwise, that is, $v_f = \xi_{K_H}^L v_f + (1 - \xi_{K_H}^L)v_f$ where $(1 - \xi_{K_H}^L)v_f \in \mathcal{V}_f(\omega_{K_H}^L)$. Then, applying (4.25), we deduce

$$a(\mathcal{E}, \mathcal{E}_c) = \Big(\ell(\mathcal{E}_c - v_H - v_f) - a(U, \mathcal{E}_c - v_H - v_f) \Big) \tag{4.26}$$

$$+ \sum_{K_H \in \tilde{\mathcal{K}}_H} \sum_{e \in \Gamma^B(\omega_{K_H}^L)} \Big((n \cdot \{A\nabla U_i\}_w, [\xi_{K_H}^L v_f])_{L^2(e)}$$

$$+ (n \cdot \{A\nabla \xi_{K_H}^L v_f\}_w, [U_i])_{L^2(e)} - \frac{\sigma_e \gamma_e}{h_e}([U_i], [\xi_{K_H}^L v_f])_{L^2(e)} \Big)$$

$$=: I + II.$$

Term I can be estimated as in the proof of Theorem 4.3, upon selecting $v_H := \pi_H \mathcal{E}_c$ and $v_f = \pi_f(\mathcal{E}_c - \pi_H \mathcal{E}_c) = \pi_f \mathcal{E}_c$, where π_H and π_f are the element-wise constant L^2-orthogonal projections onto the coarse space $\mathcal{V}_H$ on the fine space $\mathcal{V}_f$, respectively. We note that, by construction, $\pi_f \pi_H v = 0$, for all $v \in \mathcal{V}_h$.

Since v_f is chosen to be piecewise constant the second term in II is equal to zero. For each $K \in \mathcal{K}$, and for each $e \in \Gamma^B(\omega_{K_H}^L)\backslash \Gamma^B$, we have

$$\Big| (n \cdot \{A\nabla U_i\}_w, [\xi_{K_H}^L v_f])_{L^2(e)} - \frac{\sigma_e \gamma_e}{h_e}([U_i], [\xi_{K_H}^L v_f])_{L^2(e)} \Big|$$
$$\lesssim \Big(\|n \cdot \{A\nabla U_i\}_w\|_{L^2(e)} + \frac{\sigma_e \gamma_e}{h_e}\|[U_i]\|_{L^2(e)} \Big)\|[\xi_{K_H}^L v_f]\|_{L^2(e)}, \tag{4.27}$$

using (4.28) and the Cauchy-Schwarz inequality, for $e \in \Gamma^B$, the first term in (4.27) disappears. Note that, $||[\xi_{K_H}^L v_f]||_{L^2(e)}$ is either $||[v_f^+]||_{L^2(e)}$ or $||[v_f^-]||_{L^2(e)}$ depending on $\xi_{K_H}^L$. To bound the term involving v_f, for simplicity let v_f be either v_f^+ or v_f^-, we note that:

$$||v_f||_{L^2(e)} \lesssim \frac{1}{\sqrt{h_K}}||v_f||_{L^2(K)} \lesssim \frac{1}{\sqrt{h_K}}||v_f||_{L^2(K_H)}$$

$$\lesssim \frac{1}{\sqrt{h_K}}||\mathscr{E}_c - \pi_H \mathscr{E}_c||_{L^2(K_H)} \quad \lesssim \frac{H_{K_H}}{\sqrt{h_K}}||\nabla \mathscr{E}_c||_{L^2(K_H)}$$

$$\lesssim \frac{H_{K_H}}{\sqrt{h_K}A_0}||\sqrt{A}\nabla \mathscr{E}_c||_{L^2(K)}, \tag{4.28}$$

using a trace inequality, and the L^2-stability of π_f, viz., $||\pi_f v||_{L^2(K_H)} \leq ||v||_{L^2(K_H)}$.

Combining the above and summing over all patches, using the discrete version of the Cauchy-Schwarz inequality, the proof is concluded. $\square$

5. Implementation and Adaptivity. The system of equations arising from the discretization of the modified coarse multiscale problem (3.11) is given by

$$KU = b - d, \tag{5.1}$$

where $K_{i,j} = a(\phi_j + \tilde{\mathcal{T}}\phi_j, \phi_i)$, $b_i = \ell(\phi_i)$, and $d_i = a(U_f, \phi_i)$. To assemble the right and left hand sides of (5.1), $\tilde{\mathcal{T}}\phi_i$ and $U_{f,i}$ need to be computed for all $i \in \mathcal{N}$. This can be done in parallel since no communication is required between the different fine scale problems. For each fine scale problem it is also possible to assemble $K_{i,j} = a(\phi_j + \tilde{\mathcal{T}}\phi_j, \phi_i)$, $b_i = \ell(\phi_i)$, and $d_i = \sum_{j \in \mathcal{N}} a(U_{f,j}, \phi_i)$ for a fixed i and for all j such that $\mu_d(\mathrm{supp}(\phi_j) \cap \bar{\omega}_K) > 0$. The constraints needed on the fine scale test spaces to solve $\tilde{\mathcal{T}}\phi_i$ and $U_{f,i}$ are $\mathcal{V}_f = \{v \in \mathcal{V}^h : \Pi_H v = 0\}$, which are implemented using Lagrange multipliers. The spaces $\mathcal{V}_f$ and $\mathcal{V}_H$ are orthogonal with respect to the L^2-inner product.

Let $\mathcal{V}_H = \mathrm{span}\{\phi_i\}$ and $\mathcal{V}_f = \mathrm{span}\{\varphi_i\}$. Then, the system of equations to be solved on the fine scale is given by

$$\begin{pmatrix} K & P^T \\ P & 0 \end{pmatrix} \xi = \begin{pmatrix} b \\ 0 \end{pmatrix}, \tag{5.2}$$

where

$$P = \begin{pmatrix} (\phi_1, \varphi_1) & (\phi_1, \varphi_2) & \dots & (\phi_1, \varphi_N) \\ (\phi_2, \varphi_1) & (\phi_2, \varphi_2) & \dots & (\phi_2, \varphi_N) \\ \vdots & \vdots & \ddots & \vdots \\ (\phi_M, \varphi_1) & (\phi_M, \varphi_2) & \dots & (\phi_M, \varphi_N) \end{pmatrix}, \tag{5.3}$$

with $K_{k,l} = a_i(\varphi_k, \varphi_l)$ and b either $b_k = l_i(\varphi_k)$ for (3.10) or $b_k = -a_i(\phi_i, \varphi_k)$ for (3.9).

Using the a posteriori error estimate above, it is possible to design an adaptive algorithm that automatically tunes the fine mesh size and the size of the patches. In the numerical experiments below, we have implemented Algorithm 1, which extends the patches in all directions and uses a uniform mesh refinement of the fine scale on each coarse element. A more elaborate algorithm which only extends in the direction where the error is large and uses adaptive mesh refinement would be a possible extension, since the a posteriori indicators above contain local contributions of each individual patch-boundary face and of each fine scale element residual.

Algorithm 1 Adaptive Discontinuous Galerkin Multiscale Method

---

1: Initialize the coarse mesh, $\mathcal{K}_H$ with mesh function H, and a fine mesh, $\mathcal{K}_h$ with meshfunction h, by using to uniform refinements of $\mathcal{K}_H$ i.e., h = H/4.
2: For all $\mathcal{K}_H$ let the size of the patches be $\omega^3_{K_H}$.
3: Set the mesh refinement level to X%.
4: **while** $(\sum_{K\in\mathcal{K}} \varrho^2_{h,K})^{1/2} + (\sum_{K\in\mathcal{K}} \zeta^2_{h,K})^{1/2} + (\sum_{K_H\in\mathcal{K}_H} \rho^2_{\omega^L_{K_H}})^{1/2} > TOL$ **do**
5:      **for** $K \in \tilde{\mathcal{K}}_H$ **do**
6:          Solve the fine scale problems (3.1) and (3.10).
7:          Compute the matrix and vector entries on the coarse scale (5.1).
8:      **end for**
9:      Solve the modified coarse scale problem (3.11).
10:     Mark the indicator with X% largest error in $\{\varrho^2_{h,K} + \zeta^2_{h,K}, \rho^2_{L,\omega_i}\}$.
11:     **for** $K_H \in K_H$ **do**
12:         **if** ρ^2_{L,ω_i} is marked **then**
13:             $\omega^L_{K_H} := \omega^{L+1}_{K_H}$
14:         **end if**
15:         **if** $\rho^2_{h,K} + \zeta^2_{h,K}$ is marked **then**
16:             $h|_{K_H} := h|_{K_H}/2$
17:         **end if**
18:   **end for**
19: **end while**

---

6. Numerical examples. We present some numerical experiments where the converge of the method as well as the performance of the adaptive algorithm is investigated.

6.1. Convergence. We consider the model problem (2.1)–(2.2) on the L-shaped domain constructed by removing the lower right quadrant in the unit square, with forcing function $f = 1$. We consider a coarse quadrilateral mesh of size $H = 2^{-4}$. Furthermore, each coarse element $K \in \mathcal{K}_H$ is further subdivided using two uniform refinements to construct the fine mesh. The error is measured in the relative energy norm, (2.12), where u_h is the DG solution on the fine mesh i.e., there is only a truncation error (due to the fine scale patch size) between the multiscale solution and the DG solution. The permeabilities *One* and *SPE*[1], illustrated in Figure 6.1, are used. In *One*, we have $A = 1$, and in *SPE* the data is taken from the tenth SPE comparative solution project and is projected into the fine mesh. Exponential decay is observed with respect to the number of layers for the different permeabilities *One* and *SPE*, until the patches covers the whole domain when $L = 8$; this is illustrated in Figure 6.2. As expected, when $L = 8$, only round off error between the multiscale solution and the reference solution is observed. Note that, by including the right-hand side fine scale correction, convergence of U to u_h itself is observed.

6.2. Adaptivity for a problem with analytic solution. Let us consider the model problem (2.1)–(2.2) on a unit square, using the permeability $A = 1$ and the forcing function $f = 4a^2(1 - ar^2)e^{-ar^2}$, for some $a > 0$. Using $a = 400$, the analytic solution can be approximated sufficiently well by the Gaussian pulse $u = ae^{-ar^2}$, centred in the middle of the domain. We consider a coarse quadrilateral mesh of size

---

[1]Data is taken from the tenth SPE comparative solution project http://www.spe.org/web/csp/
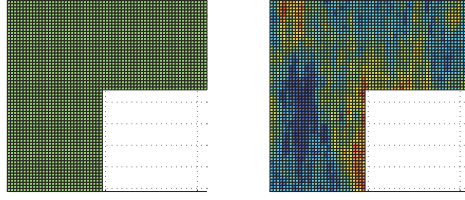
FIGURE 6.1. *Permeability structure of* One *and* SPE *in log scale on a L-shaped domain.*
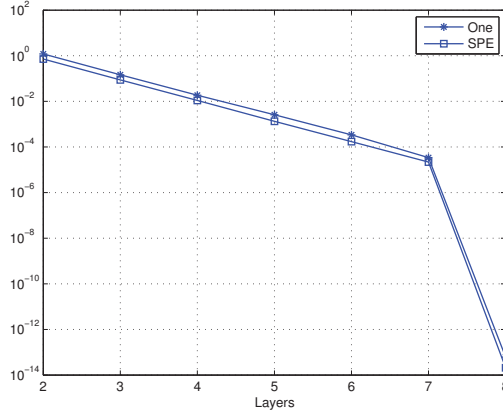
FIGURE 6.2. *Convergence in relative energy norm* (2.12), *on a L-shaped domain when the number of layers are increased using the different permeabilities* One *and* SPE.

$H = 2^{-4}$, and a fine mesh of size $h = 2^{-6}$. The adaptive algorithm (Algorithm 1) with 10% refinement level is used. The starting values for L and h used are $L = 3$ layers, and the fine scale mesh is uniformly refined two times. Figure 6.3 show the error and the error indicators decay after each iteration of the adaptive algorithm, while Figure 6.4 shows the locations where the adaptive algorithm has chosen to concentrate the computational effort, which indeed coincides with the position of the pulse.

6.3. Adaptivity on an L-shaped domain. Consider the model problem and the same data as in Section 6.1. The solution produced by the adaptive algorithm is compared to a reference solution computed with the standard (one scale) DG method on a uniform quadrilateral mesh with mesh-size $h = 2^{-9}$, see Figure 6.3. Consider a coarse mesh consisting of a uniform quadrilateral mesh of size $H = 2^{-4}$. The starting values in the adaptive algorithm (Algorithm 1) are $L = 3$ and the fine scale mesh is derived by two uniform refinements of the coarse mesh. In each iteration, a refinement level of 30% is used. Figure 6.3 shows the error decays after each iteration of the adaptive algorithm. Also, the adaptive algorithm chooses to increase the patches in the beginning since the error from the truncation is initially larger than the discretization error and after a few iterations it is starting to refine the fine scale mesh more and
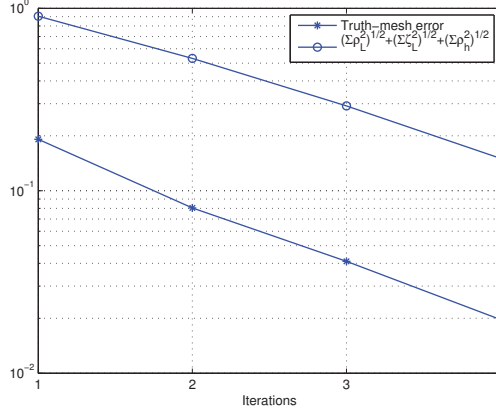
FIGURE 6.3. *Convergence in relative energy norm (2.12), using the adaptive algorithm on the unit square with Gaussian pulse in the middle.*
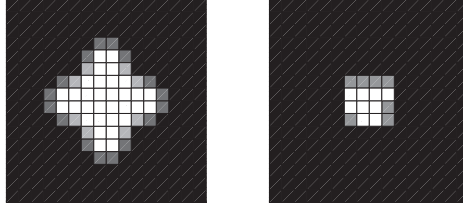

FIGURE 6.4. *The level of refinement and the size of the patches L illustrated in the left, resp. right plots, using the adaptive algorithm on a unit square with Gaussian pulse in the middle. White is where most refinements, resp. bigger L, are used and black is where least refinements, resp. smallest patches, are used.*

more. When the patch sizes are increased the error, due to truncation, decays exponentially independent of the regularity of the solution as shown theoretically in [17]. This is not true for the discretization error. This motivates the use of an adaptive algorithm which tune the error between the truncation and discretization. Figure 6.7 shows where the adaptive algorithm put most computational effort.

6.4. Adaptivity for a porous media flow problem. We consider the problem (2.1)–(2.2) on the unit square $\Omega = [0,1]^2$, with forcing function $f = -1$ in the lower left corner $\{0 \leq x, y \leq 1/128\}$, $f = 1$ in the upper right corner $\{127/128 \leq x, y \leq 1\}$, and $f = 0$ otherwise. The following permeabilities *SPE11* and *SPE21* are used and projected into a mesh with 64×64 elements; see Figure 6.8. The computational domain Ω is split into 32×32 coarse square elements $K_H \in \mathcal{K}_H$. The error is measured in the relative energy norm, with the reference solution u_h being the DG solution computed on a 512×512-element mesh. The adaptive algorithm (Algorithm 1) with refinment level 30% is used. In Iteration 1 the multiscale problem is solved using two
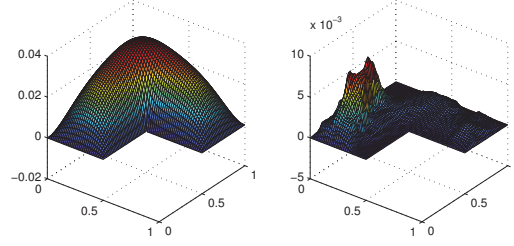
FIGURE 6.5. *Reference solution for the different permeabilities computed onto a mesh with size* $h = 2^{-9}$ *and projected onto a mesh with size* $h = 2^{-6}$.
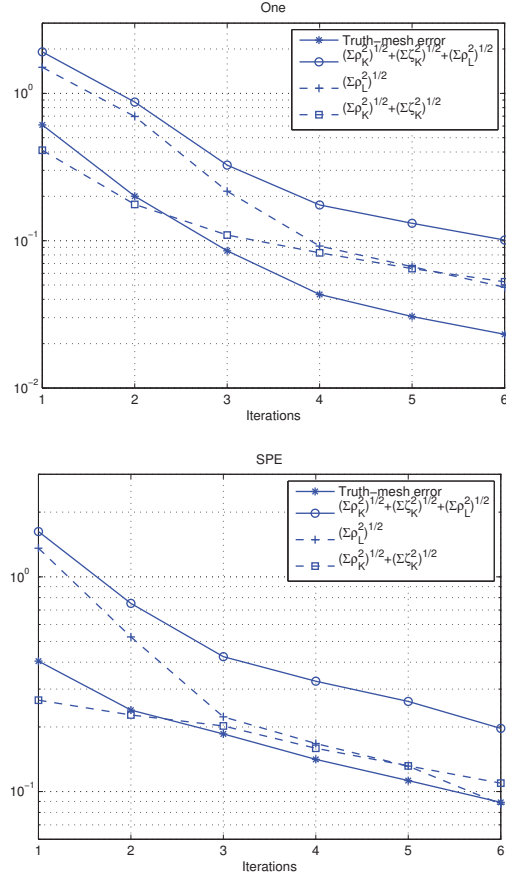

FIGURE 6.6. *The relative energy norm error for the multiscale solution using the adaptive algorithm;* ρ_L *denotes the truncation error indicator,* ϱ_K *and* ζ_K *are the discretization error indicators.*
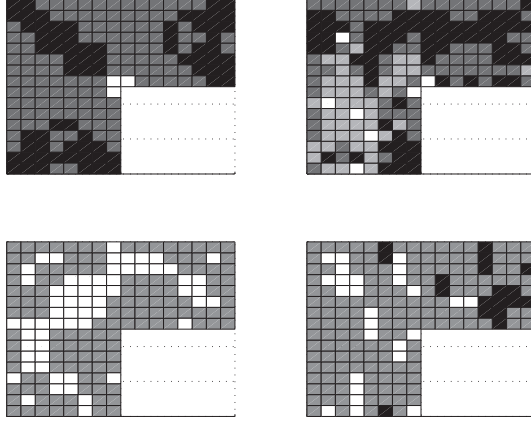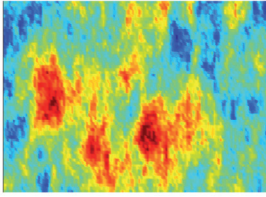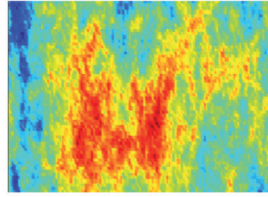
FIGURE 6.7. *The level of refinement and size of the patches illustrated in the upper resp. lower plots for the different permeability One (left) and SPE (right). White is where most refinements resp. larger patch are used and black is where least refinements resp. smallest patches are used.*

(a) SPE11, $\alpha_{max}/\alpha_{min} = 6.1765e - 5$.   (b) SPE21, $\alpha_{max}/\alpha_{min} = 5.0193e - 5$

FIGURE 6.8. *Permeabilities projection in log scale.*

refinements on each coarse element and each fine scale problem is solved with $L = 3$, and so on. Even though complicated permeabilities with $\alpha_{max}/\alpha_{min} \sim 10^5$ are used, the proposed adaptive algorithm is able to reduce relative error considerably; this is shown in Figure 6.9.

7. Concluding remarks. An adaptive multiscale method based on discontinuous Galerkin discretization has been proposed and assessed in practice. There are several different advantages for using the proposed multiscale method. The possibility to allow a global underling reference grid (using the DG framework including hanging nodes) is crucial. This does not only account for cancellation of the error between different fine scale problems in the a posteriori error bound, it also fits the method into the convergence framework presented in [17]. It admits a local conservation of the state variable, which is crucial in many applications e.g. porous media flow. The multiscale method and the adaptive algorithm admit naturally parallel implementation,
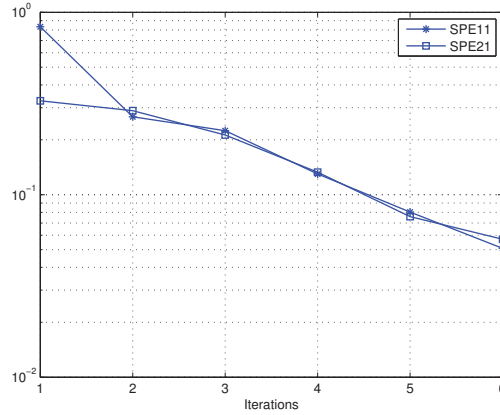
FIGURE 6.9. *Relative in error broken energy norm against the number of iterations using the adaptive algorithm for flow in porous media.*

which results in further savings in computational time.

An adaptive algorithm for which the coarse scale, the fine scale, and the size of the different patches are taken into account, based on an energy norm a posteriori bound has been proposed. Using the proposed multiscale method, together with the adaptive algorithm, leads to substantial computational savings, while maintaining a good performance when applied to challenging benchmark problems.

REFERENCES

[1] J. Aarnes and B.-O. Heimsund, *Multiscale discontinuous Galerkin methods for elliptic problems with multiple scales*, Lecture Notes in Computational Science and Engineering, vol. 44, Springer Berlin Heidelberg, 2005.

[2] A. Abdulle, *Discontinuous Galerkin finite element heterogeneous multiscale method for elliptic problems with multiple scales*, To appear http://dx.doi.org/10.1090/S0025-5718-2011-02527-5, 2011.

[3] R. A. Adams, *Sobolev spaces*, Academic Press, New York, 1975.

[4] M. Ainsworth, *Robust a posteriori error estimation for nonconforming finite element approximation*, SIAM Journal on Numerical Analysis **42** (2005), no. 6, pp. 2320–2341.

[5] D. N. Arnold, *An interior penalty finite element method with discontinuous elements*, SIAM J. Numer. Anal. **19** (1982), no. 4, 742–760.

[6] D. N. Arnold, F. Brezzi, B. Cockburn, and L. Marini, *Unified analysis of discontinuous Galerkin methods for elliptic problems*, SIAM J. Numer. Anal. **39** (2001), no. 5, 1749–1779.

[7] I. Babuška, G. Caloz, and J. E. Osborn, *Special finite element methods for a class of second order elliptic problems with rough coefficients*, SIAM J. Numer. Anal. **31** (1994), no. 4, 945–981.

[8] I. Babuška and J. E. Osborn, *Generalized finite element methods: their performance and their relation to mixed methods*, SIAM J. Numer. Anal. **20** (1983), no. 3, 510–536.

[9] G. A. Baker, *Finite element methods for elliptic equations using nonconforming elements*, Math. Comp. **31** (1977), no. 137, 45–59.

[10] E. Burman and P. Zunino, *A domain decomposition method based on weighted interior penalties for advection-diffusion-reaction problems*, SIAM J. Numer. Anal. **44** (2006), no. 4, 1612–1638 (electronic). MR 2257119 (2007m:65123)

[11] Z. Cai, X. Ye, and S. Zhang, *Discontinuous galerkin finite element methods for interface problems: A priori and a posteriori error estimations*, SIAM Journal on Numerical Analysis

49 (2011), no. 5, 1761–1787.

[12] J. Chu, Y. Efendiev, V. Ginting, and T. Y. Hou, *Flow based oversampling technique for multiscale finite element methods*, Advances in Water Resources **31** (2008), no. 4, 599–608.

[13] B. Cockburn, G. E. Karniadakis, and C-W. Shu (eds.), *Discontinuous Galerkin methods*, Lecture Notes in Computational Science and Engineering, vol. 11, Springer-Verlag, Berlin, 2000, Theory, computation and applications, Papers from the 1st International Symposium held in Newport, RI, May 24–26, 1999.

[14] D. A. Di Pietro and A. Ern, *Mathematical aspects of discontinuous galerkin methods*, Mathématiques et Applications, vol. 69, Springer, 2012.

[15] W. E, *Principles of multiscale modeling*, Mathematical Modeling and Methods, Cambridge University Press, 2011.

[16] Y. Efendiev and T. Y. Hou, *Multiscale finite element methods*, Surveys and Tutorials in the Applied Mathematical Sciences, vol. 4, Springer, New York, 2009, Theory and applications.

[17] D. Elfverson, E. H. Georgoulis, A. Målqvist, and D. Peterseim, *Convergence of a discontinuous Galerkin multiscale method*, Submitted for publication, available as preprint arXiv:1211.5524 (2012).

[18] A. Ern and A.F. Stephansen, *A posteriori energy-norm error estimates for advection-diffusion equations approximated by weighted interior penalty methods*, J. Comput. Math. **26** (2008), no. 4, 488–510.

[19] A. Ern, A.F. Stephansen, and P. Zunino, *A discontinuous Galerkin method with weighted averages for advection-diffusion equations with locally small and anisotropic diffusivity*, IMA Journal of Numerical Analysis **29** (2009), no. 2, 235–256.

[20] J. S. Hesthaven and T. Warburton, *Nodal discontinuous Galerkin methods*, Texts in Applied Mathematics, vol. 54, Springer, New York, 2008, Algorithms, analysis, and applications.

[21] T. Y. Hou, T. Y. Hou, and X.-H. Wu, *A multiscale finite element method for elliptic problems in composite materials and porous media*, Journal of Computational Physics **134** (1997), 169–189.

[22] T. Hughes, *Multiscale phenomena: Green's functions, the Dirichlet-to-Neumann formulation, subgrid scale models, bubbles and the origins of stabilized methods*, Computer Methods in Applied Mechanics and Engineering **127** (1995), no. 1-4, 387–401.

[23] T. Hughes, G. Feijóo, L. Mazzei, and J.-B. Quincy, *The variational multiscale method–a paradigm for computational mechanics*, Computer Methods in Applied Mechanics and Engineering **166** (1998), no. 1-2, 3 – 24.

[24] C. Johnson and J. Pitkäranta, *An analysis of the discontinuous Galerkin method for a scalar hyperbolic equation*, Math. Comp. **46** (1986), no. 173, 1–26.

[25] O. Karakashian and F. Pascal, *A posteriori error estimates for a discontinuous Galerkin approximation of second-order elliptic problems*, SIAM J. Numer. Anal. **41** (2003), 2374–2399.

[26] O. Karakashian and F. Pascal, *Adaptice discontinuous Galerkin approximation of secound-order elliptic problems*, In Proceedings of the European Congress on Computational Methods in Applied Sciences and Engineering ECCOMAS 2004. P. Neittaanmäki et al. eds. Jyväsklä, 24-28 July 2004.

[27] M. G. Larson and A. Målqvist, *Adaptive variational multiscale methods based on a posteriori error estimation: Energy norm estimates for elliptic problems*, Computer Methods in Applied Mechanics and Engineering **196** (2007), no. 21-24, 2313–2324.

[28] P. Lesaint and P.-A. Raviart, *On a finite element method for solving the neutron transport equation*, Mathematical aspects of finite elements in partial differential equations (Proc. Sympos., Math. Res. Center, Univ. Wisconsin, Madison, Wis., 1974), Math. Res. Center, Univ. of Wisconsin-Madison, Academic Press, New York, 1974, pp. 89–123. Publication No. 33.

[29] A. Malqvist, *Multiscale methods for elliptic problems*, Multiscale Modeling & Simulation **9** (2011), no. 3, 1064–1086.

[30] A. Målqvist and D. Peterseim, *Localization of elliptic multiscale problems*, Submitted for publication in Math. Comp., in revision, available as preprint arXiv:1110.0692 (2011).

[31] M. Petzoldt, *A posteriori error estimators for elliptic equations with discontinuous coefficients*, Advances in Computational Mathematics **16** (2002), 47–75.

[32] W. H. Reed and T. R. Hill, *Triangular mesh methods for the neutron transport equation.*, Tech. report, Los Alamos Scientific Laboratory, 1973.

[33] B. Rivière, *Discontinuous Galerkin methods for solving elliptic and parabolic equations*, Frontiers in Applied Mathematics, vol. 35, Society for Industrial and Applied Mathematics (SIAM), Philadelphia, PA, 2008, Theory and implementation.

[34] W. Wang, *Multiscale discontinuous Galerkin methods and applications*, ProQuest LLC, Ann Arbor, MI, 2008, Thesis (Ph.D.)–Brown University.

[35] W. Wang, J. Guzmán, and C.-W. Shu, *The multiscale discontinuous Galerkin method for solving a class of second order elliptic problems with rough coefficients*, Int. J. Numer. Anal. Model. **8** (2011), no. 1, 28–47.

[36] L. Yuan and C.-W. Shu, *Discontinuous Galerkin method based on non-polynomial approximation spaces*, J. Comput. Phys. **218** (2006), no. 1, 295–323.

[37] L. Yuan and C.-W. Shu, *Discontinuous Galerkin method for a class of elliptic multi-scale problems*, Internat. J. Numer. Methods Fluids **56** (2008), no. 8, 1017–1032.

Paper III

CONVERGENCE OF A
DISCONTINUOUS GALERKIN MULTISCALE METHOD

DANIEL ELFVERSON[†][¶], EMMANUIL H. GEORGOULIS[‡], AXEL MÅLQVIST[†][¶], AND DANIEL PETERSEIM[§][‖]

Abstract. A convergence result for a discontinuous Galerkin multiscale method for a second order elliptic problem is presented. We consider a heterogeneous and highly varying diffusion coefficient in $L^\infty(\Omega, \mathbb{R}^{d\times d}_{sym})$ with uniform spectral bounds and without any assumption on scale separation or periodicity. The multiscale method uses a corrected basis that is computed on patches/subdomains. The error, due to truncation of corrected basis, decreases exponentially with the size of the patches. Hence, to achieve an algebraic convergence rate of the multiscale solution on a uniform mesh with mesh size H to a reference solution, it is sufficient to choose the patch sizes as $\mathcal{O}(H|\log(H^{-1})|)$. We also discuss a way to further localize the corrected basis to element-wise support leading to a slight increase of the dimension of the space. Improved convergence rate can be achieved depending on the piecewise regularity of the forcing function. Linear convergence in energy norm and quadratic convergence in L^2-norm is obtained independently of the forcing function. A series of numerical experiments confirms the theoretical rates of convergence.

Key words. multiscale method, discontinuous Galerkin, a priori error estimate, convergence

AMS subject classifications. 65N12, 65N30

1. Introduction. This work considers the numerical solution of second order elliptic problems with heterogeneous and highly varying (non-periodic) diffusion coefficient. The heterogeneities and oscillations of the coefficient may appear on several non-separated scales. More specifically, let $\Omega \subset \mathbb{R}^d$ be a bounded Lipschitz domain with polygonal boundary Γ. The boundary Γ may be partitioned into some non-empty closed subset Γ_D (the Dirichlet boundary) and its complement $\Gamma_N := \Gamma \setminus \Gamma_D$ (the, possibly empty, Neumann boundary). We assume that the diffusion matrix $A \in L^\infty(\Omega, \mathbb{R}^{d\times d}_{\text{sym}})$ has uniform spectral bounds $0 < \alpha, \beta < \infty$, defined by

$$0 < \alpha := \operatorname*{ess\,inf}_{x\in\Omega} \inf_{v\in\mathbb{R}^d\setminus\{0\}} \frac{(A(x)v)\cdot v}{v\cdot v} \le \operatorname*{ess\,sup}_{x\in\Omega} \sup_{v\in\mathbb{R}^d\setminus\{0\}} \frac{(A(x)v)\cdot v}{v\cdot v} =: \beta < \infty. \qquad (1.1)$$

Given $f \in L^2(\Omega)$, we seek the weak solution of the boundary-value problem

$$-\nabla \cdot A\nabla u = f \quad \text{in } \Omega,$$
$$u = 0 \quad \text{on } \Gamma_D,$$
$$\nu \cdot A\nabla u = 0 \quad \text{on } \Gamma_N,$$

i.e., we seek $u \in H^1_D(\Omega) := \{v \in H^1(\Omega) \mid v|_{\Gamma_D} = 0 \text{ in the sense of traces}\}$, such that

$$a(u,v) := \int_\Omega A\nabla u \cdot \nabla v \, \mathrm{d}x = \int_\Omega fv \, \mathrm{d}x =: F(v) \quad \text{for all } v \in H^1_D(\Omega). \qquad (1.2)$$

Many methods have been developed in recent years to overcome the lack of performance of classical finite element methods in cases where A is rough, meaning that

---

[†]Information Technology, Uppsala University, Box 337, SE-751 05, Uppsala, Sweden.
[‡]Department of Mathematics, University of Leicester, Leicester, UK.
[§]Institut für Mathematik, Humboldt-Universität zu Berlin, Berlin, Germany.

A has discontinuities and/or high variation; we refer to [4, 2, 11, 9, 6] amongst others. Common to all the aforementioned approaches is the idea to solve the problems on small subdomains and to use the results to construct a better basis for some Galerkin method or to modify the coarse scale operator. However, apart from the one-dimensional setting, the performance of those methods correlates strongly with periodicity and scale separation of the diffusion coefficient.

Other approaches [5, 16, 3] perform well without any assumptions of periodicity or scale separation in the diffusion coefficient at the price of a high computational cost: in [5, 16] the support of the modified basis functions is large and in [3] the computation of the basis functions involves the solutions of local eigenvalue problems.

Only recently in [14], a variational multiscale method has been developed that allows for textbook convergence with respect to the mesh size H, $\|u - u_H\|_{H^1(\Omega)} \leq C_{f,\beta/\alpha} H$ with a constant $C_{f,\beta/\alpha}$ that depends on f and the global bounds of the diffusion coefficient but not its variations. This result is achieved by an operator-dependent modification of the classical nodal basis based on the solution of local problems on vertex patches of diameter $\mathcal{O}(H|\log(H^{-1})|)$. The method in [14] is an extension of the method presented in [13, 15].

In this work, we present a discontinuous Galerkin (dG) multiscale method with similar performance. The method is a slight variation of the method [8], in the sense that the boundary conditions for the local problems are now of Dirichlet type. The dG finite element method admits good conservation properties of the state variable, and also offers the use of very general meshes due to the lack of inter-element continuity requirements, e.g., meshes that contain several different types of elements and/or hanging nodes. Both those features are crucial in many applications. In the context of multiscale methods the discontinuous formulation allows for more flexibility in the construction of the basis function e.g., allowing more general boundary conditions [8]. Although the error analysis presented in this work is restricted to regular simplicial or quadrilateral/hexahedral meshes, we stress that all the results appear to be extendable for the case of irregular meshes (i.e., meshes containing hanging nodes). We refrained from presenting these extensions here for simplicity of the current presentation. Under these assumptions, we provide a complete a priori error analysis of this method including errors caused by the approximation of basis functions.

In this dG multiscale method and in previous related methods [14, 8], the accuracy is ensured by enlarging the support of basis functions appropriately. Hence, supports of basis functions overlap and the communication is no longer restricted to neighboring elements but is present also between elements at a certain distance. We will prove that resulting overhead is acceptable in the sense that it scales only logarithmically in the mesh size.

In order to retain the dG-typical structure of the stiffness matrix, we discuss the possibility of localizing the multiscale basis functions to single elements. Instead of having $\mathcal{O}(1)$ basis functions per element with $\mathcal{O}(H|\log(H^{-1})|)$ support, we would then have $\mathcal{O}(|\log(H^{-1})|)$ basis functions per element with element support. The element-wise application of a singular value decomposition easily prevents ill-conditioning of the element stiffness matrices, while simultaneously achieving further compression of the multiscale basis.

The outline of the paper is as follows. In Section 2, we recall the dG finite element method. Section 3 defines our multiscale method, which is then analyzed in Section 4. Section 5 presents numerical experiments confirming the theoretical developments.

Throughout this paper, standard notation on Lebesgue and Sobolev spaces is

employed. Let $0 \leq C < \infty$ be any generic constant that neither depends on the mesh size nor the diffusion matrix A; $a \lesssim b$ abbreviates an inequality $a \leq C b$ and $a \approx b$ abbreviates $a \lesssim b \lesssim a$. Also, let the constant $C_{\beta/\alpha}$ depend on the minimum and maximum bound bound (α and β) of the diffusion matrix A in (1.1).

2. Fine scale discretization.

2.1. Finite element meshes and spaces. Let $\mathcal{T}$ denote a subdivision of Ω into (closed) regular simplices or into quadrilaterals (for $d = 2$) or hexahedra (for $d = 3$), i.e., $\bar{\Omega} = \cup_{T \in \mathcal{T}} T$. We assume that $\mathcal{T}$ is regular in the sense that any two elements are either disjoint or share exactly one face or share exactly one edge or share exactly one vertex.

Let $\mathcal{E}$ denote the set of edges (or faces for $d = 3$) of $\mathcal{T}$; $\mathcal{E}(\Omega)$ denotes the set of interior edges, $\mathcal{E}(\Gamma)$, $\mathcal{E}(\Gamma_D)$ and $\mathcal{E}(\Gamma_N)$) refer to the set of edges on the boundary of Ω, on the Dirichlet and on the Neumann boundary, respectively. Let $\hat{T}$, denote the reference simplex or (hyper)cube and let $\mathcal{P}_p(\hat{T})$ and $\mathcal{Q}_p(\hat{T})$ denote the spaces of polynomials of degree less than or equal to p in all or on each variable, respectively. Then, we define the set of piecewise polynomials

$$P_p(\mathcal{T}) := \{v : \Omega \to \mathbb{R} \mid \forall T \in \mathcal{T}, v|_T \circ F_T \in \mathcal{R}_p(\hat{T})\},$$

with $\mathcal{R}_p \in \{\mathcal{P}_p, \mathcal{Q}_p\}$, where $F_T : \hat{T} \to T$, $T \in \mathcal{T}$ is a family of element maps. Let also $\Pi_p(\mathcal{T}) : L^2(\Omega) \to P_p(\mathcal{T})$ denote the L^2-projection onto $\mathcal{T}$-piecewise polynomial functions of order p. In particular, we have $(\Pi_0(\mathcal{T})f)|_T = |T|^{-1} \int_T f \, dx$, $T \in \mathcal{T}$ for all $f \in L^2(\Omega)$. Note that $v \in P_p(\mathcal{T})$ does not necessarily belong to $H^1(\Omega)$. The $\mathcal{T}$-piecewise gradient $\nabla_{\mathcal{T}} v$, with $(\nabla_{\mathcal{T}} v)|_T = \nabla(v|_T)$ for all $T \in \mathcal{T}$, is well-defined and $\nabla_{\mathcal{T}} v \in (P_{p-1}(\mathcal{T}))^d$.

For any interior edge/face $e \in \mathcal{E}(\Omega)$ there are two adjacent elements T^- and T^+ with $e = \partial T^- \cap \partial T^+$. We define ν to be the normal vector of e that points from T^- to T^+. For boundary edges/faces $e \in \mathcal{E}(\Gamma)$ let ν be the outward unit normal vector of Ω.

Define the jump of $v \in P_k(\mathcal{T})$ across $e \in \mathcal{E}(\Omega)$ by $[v] := v|_{T^-} - v|_{T^+}$ and define $[v] := v|_e$ for $e \in \mathcal{E}(\Gamma)$. The average of $v \in P_p(\mathcal{T})$ across $e \in \mathcal{E}(\Omega)$ is defined by $\{v\} := (v|_{T^-} + v|_{T^+})/2$ and for boundary edges $e \in \mathcal{E}(\Gamma)$ by $\{v\} := v|_e$.

In the remaining part of this work, we consider two different meshes: a coarse mesh $\mathcal{T}_H$ and a fine mesh $\mathcal{T}_h$, with respective definitions for the edges/faces $\mathcal{E}_H$ and $\mathcal{E}_h$. We denote the $\mathcal{T}_H$-piecewise gradient by $\nabla_H v := \nabla_{\mathcal{T}_H} v$ and, respectively, $\nabla_h v := \nabla_{\mathcal{T}_h} v$ for the $\mathcal{T}_h$-piecewise gradient . We assume that the fine mesh $\mathcal{T}_h$ is the result of one or more refinements of the coarse mesh $\mathcal{T}_H$. The subscripts h, H refer to the corresponding mesh sizes; in particular, we have $H \in P_0(\mathcal{T}_H)$ with $H|_T = \mathrm{diam}(T) =: H_T$ for all $T \in \mathcal{T}_H$, $H_e = \mathrm{diam}\, e$, for all $e \in \mathcal{E}_H$, $h \in P_0(\mathcal{T}_h)$, with $h|_T = \mathrm{diam}(T) =: h_T$ for all $T \in \mathcal{T}_h$, and $h_e = \mathrm{diam}\, e$ for all $e \in \mathcal{E}_h$. Obviously, $h \leq H$.

2.2. Discretization by the symmetric interior penalty method. We consider the symmetric interior penalty method (SIP) discontinuous Galerkin method [7, 1, 10]. We seek an approximation in the space $\mathcal{V}_h := P_1(\mathcal{T}_h)$. Given some positive penalty parameter $\sigma > 0$, we define the symmetric bilinear form $a_h : \mathcal{V}_h \times \mathcal{V}_h \to \mathbb{R}$ by

$$
\begin{aligned}
a_h(u, v) :=& (A\nabla_h u, \nabla_h v)_{L^2(\Omega)} - \sum_{e \in \mathcal{E}_h(\Omega) \cup \mathcal{E}_h(\Gamma_D)} \Big((\{\nu \cdot A\nabla u\}, [v])_{L^2(e)} \\
& + (\{\nu \cdot A\nabla v\}, [u])_{L^2(e)} - \frac{\sigma}{h_e}([u], [v])_{L^2(e)} \Big).
\end{aligned}
\tag{2.1}
$$

The jump-seminorm associated with the space $\mathcal{V}_h$, is defined by

$$| \bullet |_h^2 := \sum_{e \in \mathcal{E}_h(\Omega) \cup \mathcal{E}_h(\Gamma_D)} \frac{\sigma}{h_e} \|[\bullet]\|_{L^2(e)}^2, \tag{2.2}$$

while the energy norm in $\mathcal{V}_h$ is then given by

$$\||\bullet\||_h := (\|A^{1/2}\nabla_h \bullet\|_{L^2(\Omega)}^2 + |\bullet|_h^2)^{1/2}. \tag{2.3}$$

If the penalty parameter is chosen sufficiently large, the dG bilinear form (2.1) is coercive and bounded with respect to the energy norm (2.3). Hence, there exists a (unique) dG approximation $u_h \in \mathcal{V}_h$, satisfying

$$a_h(u_h, v) = F(v) \quad \text{for all } v \in \mathcal{V}_h. \tag{2.4}$$

We assume that (2.4) is computationally intractable for practical problems, so we shall never seek to solve for u_h directly. Instead, u_h will serve as a reference solution to compare our coarse grid multiscale dG approximation with. The underlying assumption is that the mesh $\mathcal{T}_h$ is chosen sufficiently fine so that u_h is sufficiently accurate. The aim of this work is to devise and analyse a multiscale dG discretization with coarse scale H, in such a way that the accuracy of u_h is preserved up to an $\mathcal{O}(H)$ perturbation independent of the variation of the coefficient A.

3. Discontinuous Galerkin multiscale method. As mentioned above, the choice of the reference mesh $\mathcal{T}_h$ is not directly related to the desired accuracy, but is instead strongly affected by the roughness and variation of the coefficient A. The corresponding coarse mesh $\mathcal{T}_H$, with mesh width function $H \geq h$, is assume to be completely independent of A. To encapsulate the fine scale information in the coarse mesh, we shall design coarse generalized finite element spaces based on $\mathcal{T}_H$.

3.1. Multiscale decompositions. We introduce a scale splitting for the space $\mathcal{V}_h$. To this end, let $\Pi_H := \Pi_1(\mathcal{T}_H)$ and define $\mathcal{V}_H := \Pi_H \mathcal{V}_h = P_1(\mathcal{T}_H)$ and

$$\mathcal{V}^{\mathrm{f}} := (1 - \Pi_H)\mathcal{V}_h = \{v \in \mathcal{V}_h \mid \Pi_H v = 0\}.$$

LEMMA 1 (L^2-orthogonal multiscale decomposition). *The decomposition*

$$\mathcal{V}_h = \mathcal{V}_H \oplus \mathcal{V}^{\mathrm{f}},$$

is orthogonal in $L^2(\Omega)$.

Proof. The proof is immediate, as any $v \in \mathcal{V}_h$ can be decomposed uniquely into a coarse finite element function $v_H := \Pi_H v \in \mathcal{V}_H$ and a (possibly highly oscillatory) remainder $v^{\mathrm{f}} := (1 - \Pi_H)v \in \mathcal{V}^{\mathrm{f}}$, with $\|v\|_{L^2(\Omega)}^2 = \|v_H\|_{L^2(\Omega)}^2 + \|v^{\mathrm{f}}\|_{L^2(\Omega)}^2$. $\square$

We now orthogonalize the above splitting with respect to the dG scalar product a_h; we keep the space of fine scale oscillations $\mathcal{V}^{\mathrm{f}}$ and simply replace $\mathcal{V}_H$ with the orthogonal complement of $\mathcal{V}^{\mathrm{f}}$ in $\mathcal{V}_h$. We define the fine scale projection $\mathfrak{F} : \mathcal{V}_h \to \mathcal{V}^{\mathrm{f}}$ by

$$a_h(\mathfrak{F}v, w) = a_h(v, w) \quad \text{for all } w \in \mathcal{V}^{\mathrm{f}}. \tag{3.1}$$

Using the fine scale projection, we can define the coarse scale approximation space by

$$\mathcal{V}_H^{ms} := (1 - \mathfrak{F})\mathcal{V}_H.$$

LEMMA 2 (a_h-orthogonal multiscale decomposition). *The decomposition*

$$\mathcal{V}_h = \mathcal{V}_H^{ms} \oplus \mathcal{V}^{\mathrm{f}},$$

is orthogonal with respect to a_h, i.e., any function v in $\mathcal{V}_h$ can be decomposed uniquely into some function $v_H^{ms} \in \mathcal{V}_H^{ms}$ plus $v^{\mathrm{f}} \in \mathcal{V}^{\mathrm{f}}$ with $|||v|||_h^2 \approx |||v_H^{ms}|||_h^2 + |||v^{\mathrm{f}}|||_h^2$. The functions $v_H^{ms} \in \mathcal{V}_H^{ms}$ and $v^{\mathrm{f}} \in \mathcal{V}^{\mathrm{f}}$ are the Galerkin projections of $v \in \mathcal{V}_h$ onto the subspaces $\mathcal{V}_H^{ms}$ and $\mathcal{V}^{\mathrm{f}}$, i.e.,

$$a_h(v_H^{ms}, w) = a_h(v, w) = F(w) \quad \text{for all } w \in \mathcal{V}_H^{ms},$$
$$a_h(v^{\mathrm{f}}, w) = a_h(v, w) = F(w) \quad \text{for all } w \in \mathcal{V}^{\mathrm{f}}.$$

The unique Galerkin approximation $u_H^{ms} \in \mathcal{V}_H^{ms}$ of $u \in \mathcal{V}$ solves

$$a_h(u_H^{ms}, v) = F(v) \quad \text{for all } v \in \mathcal{V}_H^{ms}. \tag{3.2}$$

We shall see in the error analysis (cf. Theorem 8) that the orthogonality yields error estimates for the Galerkin approximation $u_H^{ms} \in \mathcal{V}_H^{ms}$ of (3.2) that are independent of the regularity of the solution and of the diffusion coefficient A. However, the space $\mathcal{V}_H^{ms}$ is not suitable for practical computations as a local basis for this space is not easily available. Indeed, given a basis of $\mathcal{V}_H$, e.g., the element-wise Lagrange basis functions $\{\lambda_{T,j} \mid T \in \mathcal{T}_H, \ j = 1, \ldots, r\}$ where $r = (1 + d)$ for regular simplices or $r = 2^d$ for quadrilaterals/hexahedra. The space $\mathcal{V}_H^{ms}$ may be spanned by the corrected basis functions $(1 - \mathfrak{F})\lambda_{T,j}$, $T \in \mathcal{T}_H$, $j = 1, \ldots, r$. Although $\lambda_{T,j}$ has local support $\operatorname{supp} \lambda_{T,j} = T$, its corrected version $(1 - \mathfrak{F})\lambda_{T,j}$ may have global support in Ω, as (3.1) is a variational problem on the whole domain Ω. Fortunately, as we shall prove later, the corrector functions $\phi_{T,j}$ decay quickly away from T (cf. previous numerical results in [8] and a similar observation for the corresponding conforming version of the method [14]). This decay motivates the local approximation of the corrector functions, at the expense of introducing small perturbations in the method's accuracy.

3.2. Discontinuous Galerkin multiscale method. The localized approximations of the corrector functions are supported on element patches in the coarse mesh $\mathcal{T}_H$.

DEFINITION 3. *For all $T \in \mathcal{T}_H$, define element patches with size L as*

$$\omega_T^1 := int(T),$$
$$\omega_T^L := int(\cup\{T' \in \mathcal{T}_H \mid T' \cap \bar{\omega}_T^{L-1} \neq \emptyset\}), \quad k = 1, 2, \ldots.$$

We refer to Figure 3.2 for an illustration. We introduce a new discretization parameter $L > 0 \in \mathbb{N}$ and define localized corrector functions $\phi_{T,j}^L \in \mathcal{V}^{\mathrm{f}}(\omega_T^L) := \{v \in \mathcal{V}^{\mathrm{f}} \mid v|_{\Omega \setminus \omega_T^L} = 0\}$ by

$$a_h(\phi_{T,j}^L, w) = a_h(\lambda_{T,j}, w) \quad \text{for all } w \in \mathcal{V}^{\mathrm{f}}(\omega_T^L). \tag{3.3}$$

Further, we define the multiscale approximation space

$$\mathcal{V}_H^{ms,L} = \operatorname{span}\{\lambda_{T,j} - \phi_{T,j}^L \mid T \in \mathcal{T}_H, \ j = 1, \ldots, r\}.$$

The dG multiscale method seeks $u_H^{ms,L} \in \mathcal{V}_H^{ms,L}$ such that

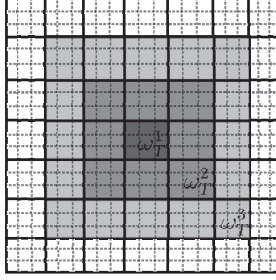$$a_h(u_H^{ms,L}, v) = F(v) \quad \text{for all } v \in \mathcal{V}_H^{ms,L}. \tag{3.4}$$

FIGURE 1. *Example of a one layer patch ω_T^1, two layer patch ω_T^2, and a three layer patch ω_T^3, on a quadrilateral mesh.*

Since $\mathcal{V}_H^{ms,L} \subset \mathcal{V}_h$, this method is a Galerkin method in the Hilbert space $\mathcal{V}_h$ (with scalar product a_h) and, hence, inherits well-posedness from the reference discretization (2.4).

Moreover, the proposed basis $\{\lambda_{T,j} - \phi_{T,j}^L \mid T \in \mathcal{T}_H, \ j = 1, \ldots, r\}$ is stable with respect to the fine scale parameter h, as we shall see in Lemma 7 below.

3.3. Compressed discontinuous Galerkin multiscale method. The basis functions in the above multiscale method have enlarged supports (element patches) when compared with standard dG methods (elements). We can decompose the corrector functions into its element contributions

$$\phi_{T,j}^L = \sum_{T' \in \mathcal{T}_H : T' \subset \omega_T^L} \phi_{T,j}^L \chi_{T'},$$

where $\chi_{T'}$ is the indicator function of the element $T' \in \mathcal{T}_H$.

This motivates the coarse approximation space

$$\mathcal{W}_H^{ms,L} = \text{span}\big(\{\lambda_{T,j} \mid T \in \mathcal{T}_H, \ j = 1, \ldots, r\}$$
$$\cup \{\phi_{T,j}^L \chi_{T'} \mid T, T' \in \mathcal{T}_H, \ T' \subset \omega_T^L, \ j = 1, \ldots, r\},$$

This space offers the advantage of a known basis with element-wise support which leads to improved (localized) connectivity in the corresponding stiffness matrix. This is at the expense of a slight increase in the dimension of the space

$$\dim(\mathcal{W}_H^{ms,L}) \approx L^d \dim(\mathcal{V}_H^{ms,L}).$$

The corresponding localized dG multiscale method seeks $w_H^{ms,L} \in \mathcal{W}_H^{ms,L}$ such that

$$a_h(w_H^{ms,L}, v) = F(v) \quad \text{for all } v \in \mathcal{W}_H^{ms,L}. \tag{3.5}$$

Since $\mathcal{V}_H^{ms,L} \subset \mathcal{W}_H^{ms,L} \subset \mathcal{V}_h$, Galerkin orthogonality yields

$$|||u_h - w_H^{ms,L}|||_h \leq |||u_h - u_H^{ms,L}|||_h, \tag{3.6}$$

i.e., the new localized version (3.5) is never worse than the previous multiscale approximation in terms of accuracy. However, it may lead to very ill-conditioned element

stiffness matrices (cf. Lemma 10 which shows that $\phi_{T,j}^L \xi_{T'}$ may be very small if the distance between T and T' relative to their sizes is large).

To circumvent ill-conditioning, one may choose a reduced local approximation space on the basis of a singular value decomposition. Since the dimension of the local approximation space is small (at most proportional to L^d), the cost for this additional preprocessing step is comparable with the cost for the solution of the local problems for the corrector functions.

To determine an acceptable level of truncation of the localized basis functions, we can use the the a posteriori error estimator contribution of the local problem from [8], which is an estimation of the local fine scale error. This procedure may additionally lead to large reduction of the dimension of the local approximation spaces.

4. Error analysis. We present an a priori error analysis for the proposed multiscale method (3.4). In view of (3.6), this analysis applies immediately to the modified versions presented in Section 3.3. The error analysis will be split into a number of steps. First, in Section 4.1, we present some properties of the coarse scale projection operator Π_H. In Section 4.2, an error bound for dG multiscale method u_H^{ms} from (3.2) (Theorem 8) is shown, whereby the corrected basis functions are solved globally. Results for the decay of the localized corrected basis function (Lemma 10 and Lemma 11) are shown, along with an error bound for the dG multiscale method $u_H^{ms,L}$ from (3.4) (Theorem 12) ,where the corrected basis functions are solved locally on element patches. Finally, in Section 4.3, we show an error bound given a quantity of interest (Theorem 14), leading to an error bound in L^2-norm (Corollary 15).

We shall make use of the following (semi)norms. The jump-seminorm and energy norms, associated with the coarse space $\mathcal{V}_H$, are defined by

$$| \bullet |_H^2 := \sum_{e \in \mathcal{E}_H(\Omega) \cup \mathcal{E}_H(\Gamma_D)} \frac{\sigma}{H_e} \|[\bullet]\|_{L^2(e)}^2,$$

$$||| \bullet |||_H := (\|A^{1/2}\nabla_H \bullet\|_{L^2(\Omega)}^2 + | \bullet |_H^2)^{1/2},$$

respectively, along with a localized version of the local jump and energy norms (2.2) and (2.3) on a patch $\omega \subseteq \Omega$, where ω is aligned with the mesh $\mathcal{T}_h$, given by

$$| \bullet |_{h,\omega}^2 := \sum_{\substack{e \in \mathcal{E}(\Omega) \cup \mathcal{E}(\Gamma_D): \\ e \cap \bar{\omega} \neq 0}} \frac{\sigma}{h_e} \|[\bullet]\|_{L^2(e)}^2,$$

$$||| \bullet |||_{h,\omega} := (\|A^{1/2}\nabla_h \bullet\|_{L^2(\omega)}^2 + | \bullet |_{h,\omega}^2)^{1/2}.$$

The shape-regularity assumptions $h_T \approx h_e$ for all $e \in \partial T : T \in \mathcal{T}_h$ and $H_T \approx H_e$ for all $T \in \partial T : T \in \mathcal{T}_H$ will also be used.

4.1. Properties of the coarse scale projection operator Π_H. The following lemma gives stability and approximation properties of the operator Π_H.

LEMMA 4. *For any $v \in \mathcal{V}_h$, the estimate*

$$H^{-1}\|v - \Pi_H v\|_{L^2(T)} \lesssim \alpha^{-1/2}|||v|||_{h,T},$$

is satisfied for all $T \in \mathcal{T}_H$. Moreover, it holds

$$\beta^{-1/2}|||\Pi_H v|||_H + \|H^{-1}(v - \Pi_H v)\|_{L^2(\Omega)} \lesssim \alpha^{-1/2}|||v|||_h.$$

Proof. Theorem 2.2 in [12], implies that for each $v \in \mathcal{V}_h$, there exists a bounded linear operator $\mathcal{I}_h^c : \mathcal{V}_h \to \mathcal{V}_h \cap H^1(\Omega)$ such that

$$\beta^{-1/2} \|A^{1/2} \nabla_H (v - \mathcal{I}_h^c v)\|_{L^2(\Omega)} + \|h^{-1}(v - \mathcal{I}_h^c v)\|_{L^2(\Omega)} \lesssim \alpha^{-1/2} |v|_h. \tag{4.1}$$

Split $v = v^c + v^d \in \mathcal{V}_h$ into a conforming, $v^c = \mathcal{I}_h^c v$, and non-conforming, $v^d = v - \mathcal{I}_h^c v$, part. We obtain

$$\begin{aligned} H^{-1} \|v - \Pi_H v\|_{L^2(T)} &\leq H^{-1}(\|v^c - \Pi_H v^c\|_{L^2(T)} + \|v^d - \Pi_H v^d\|_{L^2(T)}) \\ &\lesssim \|\nabla_h v\| + \|\nabla_h (v - v^c)\|_{L^2(T)} + H^{-1} \|v^d\|_{L^2(T)}) \\ &\lesssim \alpha^{-1/2} |||v|||_{h,T} \end{aligned} \tag{4.2}$$

using the triangle inequality, stability of the L^2-projection, and (4.1). Also,

$$\begin{aligned} |||\Pi_H v|||_H^2 &= \sum_{T \in \mathcal{T}_H} \|\sqrt{A} \nabla(\Pi_H v - \Pi_0(\mathcal{T}_H) v)\|_{L^2(T)}^2 + \sum_{e \in \Gamma} \frac{\sigma}{H} \|[v_c - \Pi_H v]\|_{L^2(e)}^2 \\ &\lesssim \sum_{T \in \mathcal{T}_H} \beta \left(\frac{1}{H^2} \|v - \Pi_0(\mathcal{T}_H) v\|_{L^2(T)}^2 + \frac{1}{H^2} \|v_c - \Pi_H v\|_{L^2(T)}^2 \right) \\ &\lesssim C_{\beta/\alpha}^2 |||v|||_h^2, \end{aligned}$$

using the triangle inequality, (4.1), and (4.2) which concludes the proof. $\square$

The operator Π_H is surjective. The next lemma shows that, given some $v_H \in \mathcal{V}_H$ in the image of Π_H there exists a H^1-conforming pre-image $v \in \Pi_H^{-1} v_H \subset \mathcal{V}_h$ with comparable support.

LEMMA 5. *For each $v_H \in \mathcal{V}_H$, there exists a $v \in \mathcal{V}_h \cap H^1(\Omega)$ such that $\Pi_H v = v_H$, $|||v|||_h \lesssim C_{\beta/\alpha} |||v_H|||_H$, and $supp(v) \subseteq supp(v_H)$.*

Proof. Using (4.1) but on space $\mathcal{V}_H$ gives, for each $v \in \mathcal{V}_H$, there exists a bounded linear operator $\mathcal{I}_H^c : \mathcal{V}_H \to \mathcal{V}_H \cap H^1(\Omega)$ such that

$$\beta^{-1/2} \|A^{1/2} \nabla_H (v - \mathcal{I}_H^c v)\|_{L^2(\Omega)} + \|H^{-1}(v - \mathcal{I}_H^c v)\|_{L^2(\Omega)} \lesssim \alpha^{-1/2} |v|_H. \tag{4.3}$$

We define

$$v := \mathcal{I}_H^c v_H + \sum_{T \in \mathcal{T}_H,\, j=1,\dots,r} (v_H(x_j) - \mathcal{I}_H^c v_H(x_j)) \, \theta_{T,j},$$

where $\theta_{T,j} \in \mathcal{V}_h \cap H_0^1(T)$ are bubble functions, supported on each element T, with $\Pi_H \theta_{T,j} = \lambda_{T,j}$ and $|||\theta_{T,j}|||_h^2 \lesssim \beta H^{d-2}$. Observe that $\text{supp}(v) \subseteq \text{supp}(v_H)$. The interpolation property follows from

$$\begin{aligned} \Pi_H v &= \mathcal{I}_H^c v_H + \Pi_H \sum_{T \in \mathcal{T}_H,\, j=1,\dots,r} (v_H(x_j) - \mathcal{I}_H^c v_H(x_j)) \, \theta_j, \\ &= \mathcal{I}_H^c v_H + v_H - \mathcal{I}_H^c v_H = v_H. \end{aligned}$$

To prove stability, we estimate $|||v|||_h$ as follows:

$$\begin{aligned} |||v|||_h^2 &\leq \|A^{1/2} \nabla \mathcal{I}_H^c v_H\|_{L^2(\Omega)}^2 + \sum_{T \in \mathcal{T}_H,\, j=1,\dots,r} |v_H(x_j) - \mathcal{I}_H^c v_H(x_j)|^2 \, |||\theta_j|||_h^2 \\ &\lesssim \|A^{1/2} \nabla_H \mathcal{I}_H^c v_H\|_{L^2(\Omega)}^2 + \beta \|H^{-1}(v_H - \mathcal{I}_H^c v_H)\|_{L^2(\Omega)}^2 \\ &\lesssim C_{\beta/\alpha}^2 |||v_H|||_H^2 \end{aligned}$$

using the inverse estimate $\|v\|_{L^\infty(T)} \leq H^{-d/2}\|v\|_{L^2(T)}$ for all $v \in \mathcal{V}_H$, and the estimate (4.3). □

REMARK 6. *Note that $\theta_{T,j} \in \mathcal{V}_h \cap H_0^1(T)$ for all $T \in \mathcal{T}_H$ (fulfilling the conditions in Lemma 5) can be constructed using two (or more) refinements of the coarse scale parameter H. We can let $\theta_{T,j} \in \mathcal{V}_{h'} \cap H_0^1(T)$ where $\mathcal{V}_{h'} \subset \mathcal{V}_h$ and $h \leq h' \leq 2^{-2}H$. This does not put a big restriction on h since the mesh $\mathcal{T}_h$ is assumed to be sufficiently fine to resolve the variation in the coefficient A, while the parameter H does not need to resolve A.*

The following lemma says that the corrected basis is stable with respect to the fine scale parameter h in the energy norm (2.3), this is not a trivial result since the basis function $\{\lambda_{T,j} | T \in \mathcal{T}_H,\ j = 1, \ldots, r\}$ are discontinuous.

LEMMA 7 (Stability of the corrected basis functions). *For all, $T \in \mathcal{T}_H,\ j = 1, \ldots, r$ and $L > 0 \in \mathbb{N}$, the estimate*

$$|||\lambda_{T,j} - \phi_{T,j}^L|||_h \lesssim C_{\beta/\alpha} |||\lambda_{T,j}|||_H,$$

is satisfied, independently of the fine scale parameter h.

Proof. For any $T \in \mathcal{T}_H,\ j = 1, \ldots, r$, by Lemma 5 there exists a b such that $v = \lambda_{T,j} - b \in \mathcal{V}_h^f(\omega_T^L)$, and $|||b|||_h \lesssim C_{\beta/\alpha}|||\lambda_{T,j}|||_H$. We have

$$|||\lambda_{T,j} - \phi_{T,j}^L|||_h^2 \lesssim a_h(\lambda_{T,j} - \phi_{T,j}^L, \lambda_{T,j} - \phi_{T,j}^L) = a_h(\lambda_{T,j} - \phi_{T,j}^L, \lambda_{T,j} - v),$$
$$\lesssim a_h(\lambda_{T,j} - \phi_{T,j}^L, b) \lesssim C_{\beta/\alpha}|||\lambda_{T,j} - \phi_{T,j}^L|||_h|||\lambda_{T,j}|||_H,$$

which concludes the proof. □

4.2. A priori estimates. The following theorem gives an error bound for the idealized dG multiscale method, whereby the correctors for the basis are solved globally.

THEOREM 8. *Let $u_h \in \mathcal{V}_h$ solve (2.4) and $u_H^{ms} \in \mathcal{V}_H^{ms}$ solve (3.4), then the estimate*

$$|||u_h - u_H^{ms}|||_h \leq C_1 \alpha^{-1/2} \|H(f - \Pi_H f)\|_{L^2(\Omega)},$$

is satisfied, where C_1 neither depends on the mesh (h or H) size nor the diffusion matrix A.

Proof. Let $e := u_h - u_H^{ms} = u_f \in \mathcal{V}^f$, then

$$|||e|||_h^2 \lesssim a_h(e, e) = (f, e)_{L^2(\Omega)} = (f - \Pi_H f, e - \Pi_H e)_{L^2(\Omega)}$$
$$\leq \|H(f - \Pi_H f)\|_{L^2(\Omega)}\|H^{-1}(e - \Pi_H e)\|_{L^2(\Omega)}^2$$
$$\lesssim \frac{1}{\sqrt{\alpha}}\|H(f - \Pi_H f)\|_{L^2(T)}|||e|||_h,$$

using Lemma 2, Lemma 1, Cauchy-Schwarz inequality, and Lemma 4, respectively. □

DEFINITION 9. *The cut off functions $\zeta_T^{d,D} \in P_0(\mathcal{T}_h)$ are defined by the conditions*

$$\zeta_T^{d,D}|_{\omega_T^d} = 1,$$
$$\zeta_T^{d,D}|_{\Omega \setminus \omega_T^D} = 0,$$
$$\|[\zeta_T^{d,D}]\|_{L^\infty(T)} \lesssim \frac{h_T}{(D-d)H_T} \quad \text{for all } T \in \mathcal{T}_H,$$

and that $\zeta_T^{d,D}$ is constant on the boundary $\partial(\omega_T^D \setminus \omega_T^d)$.

The next lemma shows the exponential decay in the corrected basis, which is a key result in the analysis.

LEMMA 10. *For all $T \in \mathcal{T}_H$, $j = 1, \ldots, r$, the estimate*

$$|||(\lambda_j - \phi_{T,j}) - (\lambda_j - \phi_{T,j}^L)|||_h = |||\phi_{T,j} - \phi_{T,j}^L|||_h \le C_3 \gamma^L |||\phi_{T,j} - \lambda|||_h,$$

is satisfied, with $C_3 = CC_{\beta/\alpha}^3$, $0 < \gamma < 1$ given by $\gamma := (\frac{C_2}{\ell})^{\frac{k-1}{2\ell}}$, $C_2 = C' C_{\beta/\alpha}^2$, and $L = k\ell$, $k, \ell \ge 2 \in \mathbb{N}$, noting that C and C' are positive constants that are independent of the mesh (h or H), of the patch size L, and of the diffusion matrix A.

Proof. Define $e := \phi_{T,j} - \phi_{T,j}^L = \phi_{T,j} - \phi_{T,j}^{\ell k}$. We have

$$|||e|||_h^2 \lesssim a_h(e, \phi_{T,j} - \phi_{T,j}^{\ell k}) = a_h(e, \phi_{T,j} - v) \lesssim |||e|||_h \cdot |||\phi_{T,j} - v|||_h, \qquad (4.4)$$

for $v \in \mathcal{V}_h^f(\omega_T^{\ell k})$. Let $\zeta := \zeta_T^{\ell k-1, \ell k}$; then by Lemma 5 there exists a b such that $v = \zeta\phi_{T,j} - b \in \mathcal{V}_h^f(\omega_T^{\ell k})$, $\Pi_H b = \Pi_H \zeta\phi_{T,j}$, $|||b|||_h \lesssim C_{\beta/\alpha} |||\Pi_H \zeta\phi_{T,j}|||_H$, and $\mathrm{supp}(b) \subseteq \mathrm{supp}(\Pi_H \zeta\phi_{T,j})$. Then, we have

$$\begin{aligned}
|||\phi_{T,j} - v|||_h &= |||\phi_{T,j} - (\zeta\phi_{T,j} - b)|||_h \\
&\le |||\phi_{T,j} - \zeta\phi_{T,j}|||_h + |||b|||_h \\
&\lesssim |||\phi_{T,j} - \zeta\phi_{T,j}|||_h + C_{\beta/\alpha} |||\Pi_H(\zeta\phi_{T,j} - \phi_{T,j})|||_H \\
&\lesssim C_{\beta/\alpha}^2 |||\phi_{T,j} - \zeta\phi_{T,j}|||_h.
\end{aligned} \qquad (4.5)$$

Furthermore, using the properties of ζ we have

$$\|\sqrt{A}\nabla_h(1-\zeta)\phi_{T,j}\|_{L^2(\Omega)} \le \|\sqrt{A}\nabla_h\phi_{T,j}\|_{L^2(\Omega\setminus\omega_T^{\ell k-1})}, \qquad (4.6)$$

and

$$\begin{aligned}
|(1-\zeta)\phi_{T,j}|_h^2 &= \sum_{e\in\mathcal{E}(\Omega)\cup\mathcal{E}(\Gamma_D)} \frac{\sigma}{h_e} \|[(1-\zeta)\phi_{T,j}]\|_{L^2(e)}^2 \\
&\le \sum_{e\in\mathcal{E}(\Omega)\cup\mathcal{E}(\Gamma_D)} \frac{\sigma}{h_e} \left(\|\{1-\zeta\}[\phi_{T,j}]\|_{L^2(e)}^2 + \|\{\phi_{T,j}\}[1-\zeta]\|_{L^2(e)}^2 \right) \\
&\le \sum_{\substack{e\in\mathcal{E}(\Omega)\cup\mathcal{E}(\Gamma_D): \\ e\cap\Omega\setminus\omega_T^{\ell k-1}\ne 0}} \left(\frac{\sigma}{h_e} \|[\phi_{T,j}]\|_{L^2(e)}^2 + \frac{\sigma h_T^2}{h_e H_T^2} \|\{\phi_{T,j}\}\|_{L^2(e)}^2 \right) \\
&\le \sum_{\substack{e\in\mathcal{E}(\Omega)\cup\mathcal{E}(\Gamma_D): \\ e\cap\Omega\setminus\omega_T^{\ell k-1}\ne 0}} \frac{\sigma}{h_e} \|[\phi_{T,j}]\|_{L^2(e)}^2 + \frac{\sigma}{H_T^2} \|\phi_{T,j} - \Pi_H\phi_{T,j}\|_{L^2(\Omega\setminus\omega_T^{\ell k-1})}^2 \\
&\lesssim C_{\beta/\alpha}^2 |||\phi_{T,j}|||_{h,\Omega\setminus\omega_T^{\ell k-1}},
\end{aligned} \qquad (4.7)$$

using a trace inequality and Lemma 4, respectively. Combining (4.4), (4.5), (4.6), and (4.7) yields

$$|||\phi_{T,j} - \zeta\phi_{T,j}|||_h \lesssim C_{\beta/\alpha}^3 |||\phi_{T,j}|||_{h,\Omega\setminus\omega_T^{\ell k-1}}. \qquad (4.8)$$

To simplify notation, let $m := \ell(k-1) - 1$ and $M := \ell k - 1$. For $\eta_T := 1 - \zeta_T^{m,M}$, we obtain

$$|||\phi_{T,j}|||_{h,\Omega\setminus\omega_T^M}^2 \le |||\eta_T\phi_{T,j}|||_h^2 \lesssim a_h(\eta_T\phi_{T,j}, \eta_T\phi_{T,j}), \qquad (4.9)$$

where

$$a_h(\eta_T\phi_{T,j}, \eta_T\phi_{T,j}) = (A\nabla_h\eta_T\phi_{T,j}, \nabla_h\eta_T\phi_{T,j})_{L^2(\Omega)}$$
$$+ \sum_{e\in\mathcal{E}(\Omega)\cup\mathcal{E}(\Gamma_D)} \left(-2(\{\nu\cdot A\nabla\eta_T\phi_{T,j}\}, [\eta_T\phi_{T,j}]) + \frac{\sigma}{h_e}([\eta_T\phi_{T,j}], [\eta_T\phi_{T,j}])\right).$$
(4.10)

For the first term on the right-hand side of (4.10), we have

$$(A\nabla_h\eta_T\phi_{T,j}, \nabla_h\eta_T\phi_{T,j})_{L^2(\Omega)} = (A\nabla_h\phi_{T,j}, \nabla_h\eta_T^2\phi_{T,j})_{L^2(\Omega)}, \qquad (4.11)$$

since η_T is constant on each element $T \in \mathcal{T}_h$; for the other terms we use (A.3) and (A.4) (with $v = \eta_T$, $w = \nu\cdot A\nabla\phi_{T,j}$ and $u = \phi_{T,j}$). We can, thus, arrive to

$$|||\phi_{T,j}|||^2_{h,\Omega\setminus\omega_T^M} \le a_h(\eta_T\phi_{T,j}, \eta_T\phi_{T,j}) = a_h(\phi_{T,j}, \eta_T^2\phi_{T,j})$$
$$+ \sum_{e\in\mathcal{E}(\Omega)} \big(1/2(\{\nu\cdot A\nabla\phi_{T,j}\}, [\eta_T]^2[\phi_{T,j}])_{L^2(e)} - 1/4([\nu\cdot A\nabla\phi_{T,j}], [\eta_T]^2\{\phi_{T,j}\})_{L^2(e)}$$
$$- \frac{\sigma}{4h_e}([\eta_T]^2, [\phi_{T,j}]^2)_{L^2(e)} + \frac{\sigma}{h_e}([\eta_T]^2, \{\phi_{T,j}\}^2)_{L^2(e)}\big),$$
(4.12)

using (4.9), (4.10), and (4.11). Note that,

$$\sum_{e\in\mathcal{E}(\Omega)} \big(1/2(\{\nu\cdot A\nabla\phi_{T,j}\}, [\eta_T]^2[\phi_{T,j}])_{L^2(e)} - 1/4([\nu\cdot A\nabla\phi_{T,j}], [\eta_T]^2\{\phi_{T,j}\})_{L^2(e)}$$
$$- \frac{\sigma}{4h_e}([\eta_T]^2, [\phi_{T,j}]^2)_{L^2(e)} + \frac{\sigma}{h_e}([\eta_T]^2, \{\phi_{T,j}\}^2)_{L^2(e)}\big)$$
$$\lesssim \sum_{\substack{e\in\mathcal{E}(\Omega):\\ e\cap\omega_T^M\setminus\omega_T^m\ne 0}} \frac{h_T^2}{\ell^2 H_T^2}\Big(\|\{\nu\cdot A\nabla\phi_{T,j}\}\|_{L^2(e)}\|[\phi_{T,j}]\|_{L^2(e)} + \|[\nu\cdot A\nabla\phi_{T,j}]\|_{L^2(e)}\|\{\phi_{T,j}\}\|_{L^2(e)}$$
$$+ \frac{\sigma}{h_e}\Big(\|[\phi_{T,j}]\|^2_{L^2(e)} + \|\{\phi_{T,j}\}\|^2_{L^2(e)}\Big)\Big)$$
$$\lesssim \sum_{\substack{e\in\mathcal{E}(\Omega):\\ e\cap\omega_T^M\setminus\omega_T^m\ne 0}} \big(\frac{h_T}{\ell^2 H_T^2}\|A\nabla\phi_{T,j}\|_{L^2(T^+\cup T^-)}\|\phi_{T,j}\|_{L^2(T^+\cup T^-)} + \frac{\sigma}{\ell^2 H_T^2}\|\phi_{T,j}\|^2_{L^2(T^+\cup T^-)}\big)$$
$$\lesssim \beta\ell^{-2}\|H_T^{-1}(\phi_{T,j} - \Pi_H\phi_{T,j})\|^2_{L^2(\omega_T^M\setminus\omega_T^m)} \le C^2_{\beta/\alpha}\ell^{-2}|||\phi_{T,j}|||^2_{h,\omega_T^M\setminus\omega_T^m}.$$
(4.13)

Now we bound the term

$$a_h(\phi_{T,j}, \eta_T^2\phi_{T,j}) = a_h(\phi_{T,j}, \eta_T^2\phi_{T,j} - b) + a_h(\phi_{T,j}, b) = a_h(\phi_{T,j}, b)$$
$$\lesssim |||\phi_{T,j}|||_{h,\omega_T^M\setminus\omega_T^m}|||b|||_{h,\omega_T^M\setminus\omega_T^m} \qquad (4.14)$$
$$\le C_{\beta/\alpha}|||\phi_{T,j}|||_{h,\omega_T^M\setminus\omega_T^m}|||\Pi_H\eta_T^2\phi_{T,j}|||_{H,\omega_T^M\setminus\omega_T^m}.$$

Furthermore, we have that

$$
\begin{aligned}
|||\Pi_H \eta_T^2 \phi_{T,j}|||_{H,\omega_T^M \setminus \omega_T^m}^2 &= |||\Pi_H (\eta_T^2 - \Pi_0(\mathcal{T}_H)\eta_T^2)\phi_{T,j}|||_{H,\omega_T^M \setminus \omega_T^m}^2 \\
&= \|\sqrt{A}\nabla_H \Pi_H(\eta_T^2 - \Pi_0(\mathcal{T}_H)\eta_T^2)\phi_{T,j}\|_{L^2(\omega_T^M \setminus \omega_T^m)}^2 \\
&\quad + \sum_{\substack{e \in \mathcal{E}(\Omega) \cup \mathcal{E}(\Gamma_D): \\ e \cap \omega_T^M \setminus \omega_T^m \neq 0}} \frac{\sigma}{H_e}\|[\Pi_H(\eta_T^2 - \Pi_0(\mathcal{T}_H)\eta_T^2)\phi_{T,j}]\|_{L^2(e)}^2 \\
&\lesssim \beta\|H_e^{-1}\Pi_H(\eta_T^2 - \Pi_0(\mathcal{T}_H)\eta_T^2)\phi_{T,j}\|_{L^2(\omega_T^M \setminus \omega_T^m)}^2 \\
&\lesssim \beta\|H_e^{-1}(\eta_T^2 - \Pi_0(\mathcal{T}_H)\eta_T^2)\|_{L^\infty(T)}\|\phi_{T,j}\|_{L^2(\omega_T^M \setminus \omega_T^m)}^2 \\
&\lesssim \beta\ell^{-2}\|H_e^{-1}(\phi_{T,j} - \Pi_H\phi_{T,j})\|_{L^2(\omega_T^M \setminus \omega_T^m)}^2 \\
&\lesssim C_{\beta/\alpha}^2 \ell^{-2}|||\phi_{T,j}|||_{h,\omega_T^M \setminus \omega_T^m}^2,
\end{aligned}
\tag{4.15}
$$

using a trace inequality, inverse inequality, and Lemma 4, respectively. Combining the inequalities (4.12), (4.13), (4.14), and (4.15) yields

$$
|||\phi_{T,j}|||_{h,\Omega \setminus \omega_T^M}^2 \leq \frac{C_2}{\ell}|||\phi_{T,j}|||_{h,\omega_T^M \setminus \omega_T^m}^2 \leq \frac{C_2}{\ell}|||\phi_{T,j}|||_{h,\Omega \setminus \omega_T^m}^2.
$$

where $C_2 = C'C_{\beta/\alpha}^2$. Substituting back to ℓ and k and using a cut off function with a slightly different argument, yields

$$
\begin{aligned}
|||\phi_{T,j}|||_{h,\Omega \setminus \omega_T^{\ell k-1}}^2 &\leq \frac{C_2}{\ell}|||\phi_{T,j}|||_{h,\Omega \setminus \omega_T^{\ell(k-1)-1}}^2 \leq (\frac{C_2}{\ell})^2|||\phi_{T,j}|||_{h,\Omega \setminus \omega_T^{\ell(k-2)-1}}^2 \\
&\leq \cdots \leq (\frac{C_2}{\ell})^{k-1}|||\phi_{T,j}|||_{h,\omega^\ell \setminus \omega_T^{\ell-1}}^2,
\end{aligned}
$$

which concludes the proof together with (4.8). □

LEMMA 11. *For all, $T \in \mathcal{T}_H$, $j = 1, \ldots, r$, the estimate*

$$
|||\sum_{T \in \mathcal{T}_H,\, j=1,\ldots,r} v_j(\phi_{T,j} - \phi_{T,j}^L)|||_h^2 \leq C_4 L^d \sum_{T \in \mathcal{T}_H,\, j=1,\ldots,r} |v_j|^2 |||\phi_{T,j} - \phi_{T,j}^L|||_h^2,
$$

is satisfied, with $C_4 = CC_{\beta/\alpha}^3$ and C positive constant independent of the mesh (h or H), of the patch size L, and of the diffusion matrix A.

Proof. Let $w = \sum_{T \in \mathcal{T}_H,\, j=1,\ldots,r} v_j(\phi_{T,j} - \phi_{T,j}^L)$, and note that

$$
\begin{aligned}
a_h(\phi_{T,j} - \lambda_{T,j}, w - \zeta_T w + b_T) &= 0, \\
a_h(\phi_{T,j}^L - \lambda_{T,j}, w - \zeta_T w + b_T) &= 0,
\end{aligned}
\tag{4.16}
$$

where $\zeta_T := \zeta_T^{L+1,L+2}$, using Lemma 5 and the property of the cut-off function. We

obtain

$$
\begin{aligned}
||| \sum_{T \in \mathcal{T}_H, \, j=1,\ldots,r} v_j (\phi_{T,j} - \phi_{T,j}^L) |||_h &\lesssim \sum_{T \in \mathcal{T}_H, \, j=1,\ldots,r} v_j a_h (\phi_{T,j} - \phi_{T,j}^L, w) \\
&= \sum_{T \in \mathcal{T}_H, \, j=1,\ldots,r} v_j a_h (\phi_{T,j} - \phi_{T,j}^L, \zeta_T w - b_T) \\
&\lesssim \sum_{T \in \mathcal{T}_H, \, j=1,\ldots,r} |v_j| \cdot |||\phi_{T,j} - \phi_{T,j}^L|||_h \left(|||\zeta_T w|||_h + |||b_T|||_h \right) \\
&\lesssim \sum_{T \in \mathcal{T}_H, \, j=1,\ldots,r} |v_j| \cdot |||\phi_{T,j} - \phi_{T,j}^L|||_h \left(|||\zeta_T w|||_h + C_{\beta/\alpha} |||\Pi_H \zeta_T w|||_H \right) \\
&\lesssim \sum_{T \in \mathcal{T}_H, \, j=1,\ldots,r} |v_j| \cdot |||\phi_{T,j} - \phi_{T,j}^L|||_h C_{\beta/\alpha}^2 |||\zeta_T w|||_h.
\end{aligned}
\tag{4.17}
$$

From (4.6) and (4.7), we have

$$
|||\zeta_T w|||_h = |||\zeta_T w|||_{h, \omega_T^{L+2}} \lesssim C_{\beta/\alpha} |||w|||_{h, \omega_T^{L+2}}.
\tag{4.18}
$$

Then, further estimation of (4.17) can be achieved using (4.18) and the discrete Cauchy-Schwarz inequality:

$$
\begin{aligned}
||| &\sum_{T \in \mathcal{T}_H, \, j=1,\ldots,r} v_j (\phi_{T,j} - \phi_{T,j}^L) |||_h \\
&\leq C_{\beta/\alpha}^3 \left(\sum_{T \in \mathcal{T}_H, \, j=1,\ldots,r} |v_j|^2 |||\phi_{T,j} - \phi_{T,j}^L|||_h^2 \right)^{1/2} \left(\sum_{T \in \mathcal{T}_H, \, j=1,\ldots,r} |||w|||_{h, \omega_T^{L+2}}^2 \right)^{1/2} \\
&\leq C_{\beta/\alpha}^3 L^{d/2} \cdot \left(\sum_{T \in \mathcal{T}_H, \, j=1,\ldots,r} |v_j|^2 |||\phi_{T,j} - \phi_{T,j}^L|||_h^2 \right)^{1/2} \cdot |||w|||_h.
\end{aligned}
$$

Dividing by w on both sides concludes the proof. □

The following theorem gives an error bound for the dG multiscale method.

THEOREM 12. *Let $u \in H_D^1(\Omega)$ solve (1.2) and $u_H^{ms,L} \in \mathcal{V}_H^{ms,L}$ solve (3.4). Then, the estimate*

$$
\begin{aligned}
|||u - u_H^{ms,L}|||_h \leq &|||u - u_h|||_h + C_1 \alpha^{-1/2} \|H(f - \Pi_H f)\|_{L^2(\Omega)} \\
&+ C_5 \|H^{-1}\|_{L^\infty(\Omega)} L^{d/2} \gamma^L \|f\|_{L^2(\Omega)},
\end{aligned}
$$

is satisfied, with $0 < \gamma < 1$, L from Lemma 10, C_1 from Theorem 8, $C_5 = C C_{\beta/\alpha}^2 C_4^{1/2} C_3$ where C_3 is from Lemma 10 and C_4 is from Lemma 11. C a positive constant independent of the mesh (h or H), of the patch size L, and of the diffusion matrix A.

REMARK 13. *To counteract the factor $\|H^{-1}\|_{L^\infty(\Omega)}$ in the error bound in Theorem 12, we can choose the localization parameter as $L = \lceil C \log(\|H^{-1}\|_{L^\infty(\Omega)}) \rceil$. On adaptively refined meshes it is recommended to choose $L = \lceil C \log(H^{-1}) \rceil$.*

Proof. We define $\tilde{u}_H^{ms,L} := \sum_{T \in \mathcal{T}_H, \, j=1,\ldots,r} u_{H,T}^{ms}(x_j) \phi_{T,j}^L$. Then, we obtain

$$
\begin{aligned}
|||u - u_H^{ms,L}|||_h &\leq |||u - \tilde{u}_H^{ms,L}|||_h \\
&\leq |||u - u_h|||_h + |||u_h - u_H^{ms}|||_h + |||u_H^{ms} - \tilde{u}_H^{ms,L}|||_h \\
&\leq |||u - u_h|||_h + |||u_h - u_H^{ms}|||_h + ||| \sum_{T \in \mathcal{T}_H, \, j=1,\ldots,r} u_{H,T}^{ms}(x_j)(\phi_{T,j} - \phi_{T,j}^L) |||_h.
\end{aligned}
\tag{4.19}
$$

Now, estimating the terms in (4.19), we have

$$|||u_h - u_H^{ms}|||_h \leq C_1 \alpha^{-1/2} \|H(f - \Pi_H f)\|_{L^2(\Omega)},$$

using Theorem 8, and

$$
\begin{aligned}
||| \sum_{T \in \mathcal{T}_H, \, j=1,\ldots,r} & u_{H,T}^{ms}(x_j)(\phi_{T,j} - \phi_{T,j}^L)|||_h^2 \\
&\leq C_4 L^d \sum_{T \in \mathcal{T}_H, \, j=1,\ldots,r} |u_{H,T}^{ms}(x_j)|^2 |||\phi_{T,j} - \phi_{T,j}^L|||_h^2. \\
&\leq C_4 C_3^2 L^d \gamma^{2L} \sum_{T \in \mathcal{T}_H, \, j=1,\ldots,r} |u_{H,T}^{ms}(x_j)|^2 |||\phi_{T,j} - \lambda_j|||_h^2,
\end{aligned}
\tag{4.20}
$$

using Lemma 11 and Lemma 10, respectively. Further estimation, using Lemma 7, yields

$$
\begin{aligned}
\sum_{T \in \mathcal{T}_H, \, j=1,\ldots,r} & |u_{H,T}^{ms}(x_j)|^2 |||\phi_{T,j} - \lambda_{T,j}|||_h^2 \\
&\lesssim C_{\beta/\alpha}^2 \sum_{T \in \mathcal{T}_H, \, j=1,\ldots,r} |u_{H,T}^{ms}(x_j)|^2 |||\lambda_{T,j}|||_H^2 \\
&\lesssim C_{\beta/\alpha}^2 \beta \sum_{T \in \mathcal{T}_H, \, j=1,\ldots,r} |u_{H,T}^{ms}(x_j)|^2 H_T^{-2} \|\lambda_{T,j}\|_{L^2(T)}^2 \\
&= C_{\beta/\alpha}^2 \beta \sum_{T \in \mathcal{T}_H, \, j=1,\ldots,r} \|H_T^{-1} u_{H,T}^{ms}(x_j)\lambda_{T,j}\|_{L^2(T)}^2 \\
&\lesssim C_{\beta/\alpha}^2 \beta \| \sum_{T \in \mathcal{T}_H, \, j=1,\ldots,r} H_T^{-1} u_{H,T}^{ms}(x_j)\lambda_{T,j}\|_{L^2(\Omega)}^2.
\end{aligned}
\tag{4.21}
$$

Furthermore, using a Poincare-Friedrich inequality for piecewise H^1 functions, we deduce

$$
\begin{aligned}
\| \sum_{T \in \mathcal{T}_H, \, j=1,\ldots,r} & H_T^{-1} u_{H,T}^{ms}(x_j)\lambda_{T,j}\|_{L^2(\Omega)}^2 \\
&\lesssim \| \sum_{T \in \mathcal{T}_H, \, j=1,\ldots,r} H_T^{-1} u_{H,T}^{ms}(x_j)\Pi_H(\lambda_{T,j} - \phi_{T,j})\|_{L^2(\Omega)}^2 \\
&\lesssim \alpha^{-1} |||H^{-1} u_H^{ms}|||_h^2 \\
&\lesssim \alpha^{-1} \|H^{-1}\|_{L^\infty(\Omega)}^2 \|f\|_{L^2(\Omega)}^2.
\end{aligned}
\tag{4.22}
$$

Combining (4.20), (4.21) and (4.22), we arrive to

$$|||u_H^{ms} - u_H^{ms,L}|||_h \lesssim C_{\beta/\alpha}^2 C_4^{1/2} C_3 \|H^{-1}\|_{L^\infty(\Omega)} L^{d/2} \gamma^L \|f\|_{L^2(\Omega)}.$$

□

4.3. Error in a quantity of interest. In engineering applications, we are often interested in a quantity of interest, usually a functional $g \in L^2(\Omega)$ of the solution. To this end, consider the dual reference solution (2.4): find $\phi_h \in \mathcal{V}_h$ such that

$$a_h(v, \phi_h) = g(v) \quad \text{for all } v \in \mathcal{V}_h, \tag{4.23}$$

and the dual multiscale solution (3.4): find $\phi_{H,h}^L \in \mathcal{V}_{H,h}^L$ such that

$$a_h(v, \phi_{H,h}^{ms,L}) = g(v) \quad \text{for all } v \in \mathcal{V}_{H,h}^L. \tag{4.24}$$

THEOREM 14. *Let $u \in H_D^1(\Omega)$ solve (1.2), $u_H^{ms,L} \in \mathcal{V}_H^{ms,L}$ solve (3.4), and let $g \in L^2(\Omega)$ be the quantity of interest. Then, the estimate*

$$|g(u) - g(u_{H,h}^L)| \lesssim |g(u) - g(u_h)| + |||u_h - u_H^{ms,L}|||_h |||\phi_h - \phi_H^{ms,L}|||_h,$$

is satisfied.

Proof. From (4.23) and (4.24), we obtain the Galerkin orthogonality

$$a_h(v, \phi_h - \phi_H^{ms,L}) = 0 \quad \text{for all } v \in \mathcal{V}_H^{ms,L}. \tag{4.25}$$

Using the triangle inequality, we have

$$|g(u) - g(u_H^{ms,L})| \le |g(u) - g(u_h)| + |g(u_h) - g(u_H^{ms,L})|.$$

Finally, observing that

$$\begin{aligned} |g(u_h - u_{h,H}^L)| &= |a_h(u_h - u_{h,H}^L, \phi_h)| \\ &= |a_h(u_h - u_{h,H}^L, \phi_h - \phi_{H,h}^L)| \\ &\lesssim |||u_h - u_{h,H}^L|||_h |||\phi_h - \phi_{H,h}^L|||_h, \end{aligned}$$

using (4.25), concludes the proof. □

COROLLARY 15. *For $g(v) = (u_h - u_{H,h}^L, v)_{L^2(\Omega)}$, the following L^2-norm error estimates hold:*

$$\|u - u_{H,h}^L\|_{L^2(\Omega)} \lesssim \|u - u_h\|_{L^2(\Omega)} + |||u_h - u_H^{ms,L}|||_h^{1/2} |||\phi_h - \phi_H^{ms,L}|||_h^{1/2},$$

and

$$\|u - u_{H,h}^L\|_{L^2(\Omega)} \lesssim \|u - u_h\|_{L^2(\Omega)} + H|||u_h - u_H^{ms,L}|||_h, \tag{4.26}$$

for $L = \lceil C \log(H^{-1}) \rceil$ with C sufficiently large positive constant independent of the mesh parameters.

REMARK 16. *As expected, if we are interested in a smoother functional, a higher convergence rate is obtained for $|g(u_h - u_H^{ms,L})|$. For example, given the forcing function for the primal problem $f \in H^m(\mathcal{T}_H)$, a quantity of interest $g \in H^n(\mathcal{T}_H)$ (with $H^0(\mathcal{T}_H)$ denoting the standard $L^2(\Omega)$ space), and choosing $L = \lceil C \log(H^{-1}) \rceil$ with large enough C, gives*

$$|g(u - u_H^{ms,L})| \lesssim |g(u) - g(u_h)| + H^{2+m+n} \Big(\sum_{T \in \mathcal{T}_H} |f|_{H^m(T)} \Big) \Big(\sum_{T \in \mathcal{T}_H} |g|_{H^n(T)} \Big).$$

5. Numerical Experiments. Let Ω where be an L-shaped domain (constructed by removing the lower right quadrant in the unit square) and let the forcing function be $f = 1 + \cos(2\pi x)\cos(2\pi y)$ for $(x, y) \in \Omega$. The boundary Γ is divided into the Neumann boundary $\Gamma_N := \Gamma \cap (\{(x, y) : y = 0\} \cup \{(x, y) : x = 1\})$ and the Dirichlet boundary $\Gamma_D = \Gamma \setminus \Gamma_N$. We shall consider three different permeabilities: constant $A_1 = 1$, $A_2 = A_2(x)$, which is piecewise constant with periodic values of 1 and 0.01

(a) $\beta/\alpha = 10^2$ (b) $\beta/\alpha \approx 4 \cdot 10^6$
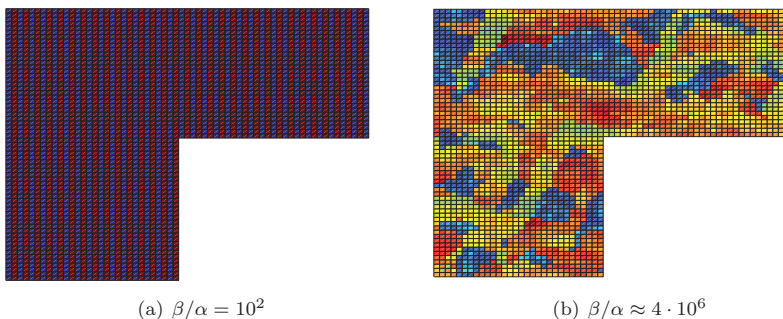
FIGURE 2. *The permeability structure of A_2 (a) and A_3 (b) in log scale.*

with respect to a Cartesian grid of width 2^{-6} in the x-direction, and $A_3 = A_3(x, y)$ which piecewise constant with respect to a Cartesian grid of width 2^{-6} both in the x- and y-directions and has a maximum ratio $\beta/\alpha = 4 \cdot 10^6$. The data for A_3 are taken from layer 64 in the SPE benchmark problem, see http://www.spe.org/web/csp/. The permeabilities A_2 and A_3 are illustrated in Figure 2. For the periodic problem many of the corrected basis functions will be identical. For instance, all the local corrected basis in the interior are solved on identical patches, thereby reducing the computational effort considerably. In the extreme case of a problem with periodic coefficients on a unit hypercube, with period boundary conditions, the correctors $\phi_{T,j}$, $j = 1, \ldots, r$, will be identical for all $T \in \mathcal{T}_H$.

Consider the uniform (coarse) quadrilateral mesh $\mathcal{T}_H$ with size $H = 2^{-i}$, $i = 1, \ldots, 6$. The convergence rate $-p/2$ corresponds to $\mathcal{O}(H^p)$ since the number degrees of freedom $\approx H^{-2}$. The corrector functions (3.3) are solved on a subgrid of a (fine) quadrilateral mesh $\mathcal{T}_h$ with mesh size 2^{-8}. The mesh $\mathcal{T}_h$ will also act as a reference grid for which we shall compute a reference solution $u_h \in \mathcal{V}_h$ (2.4) on. Note that the mesh $\mathcal{T}_h$ is chosen so that it resolves the fine scale features for A_i, $i = 1, 2, 3$, hence we assume that the solution u_h is sufficiently accurate.

5.1. Localization parameter. If $f \in H^m(\mathcal{T}_H)$ we have the bound

$$||H(f - \Pi_H f))||_{L^2(\Omega)} \lesssim \sum_{T \in \mathcal{T}_H} H^{k+1} |f|_{H^k(T)}, \tag{5.1}$$

where $k = 0$ for $m = 0$, $k = 1$ for $m = 1$, and $k = 2$ for $m > 1$. Hence, to balance the error in between the terms on the right-hand side of the estimate in Theorem 12, different constant C has to be used for the localization parameter, $L = \lceil C \log(H^{-1}) \rceil$, depending on the element-wise regularity of the forcing function f on $\mathcal{T}_H$. Figure 3 shows the relative error in the energy norm $|||u_h - u_H^{ms,L}|||_h / |||u_h|||_h$ and Figure 4 the relative error in the L^2-norm $||u_h - u_H^{ms,L}||_{L^2(\Omega)} / ||u_h||_{L^2(\Omega)}$ between u_h and $u_H^{ms,L}$ against the number of degrees of freedom $N_{\text{dof}} \approx O(H^{-2})$, using different constants $C = 1, 3/2, 2, 5/2$. With the chose $C = 5/2$, the errors due to the localization can be neglected compared to the errors from the forcing function, both for the energy- and for the L^2-norm. For $f \notin H^1(\mathcal{T}_h)$, $C = 3/2$ is sufficient since (5.1) gives linear convergence. In the following numerical experiments we shall use $C = 2$, since this value seems to balance the error sufficiently. Note that the numerical overhead increases
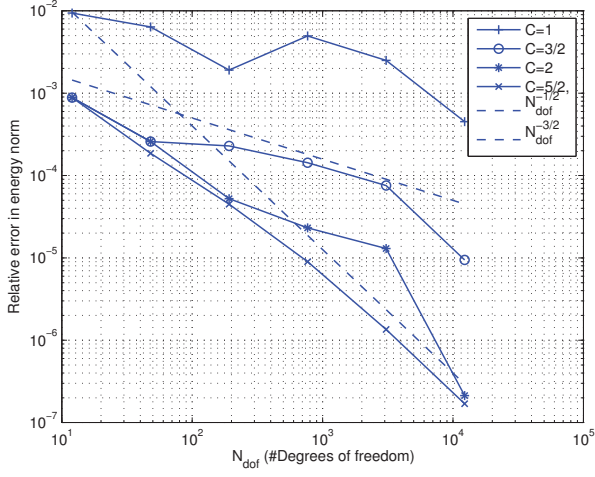
FIGURE 3. *Diffusion coefficient $A_1 = 1$. Relative energy-norm error against N_{dof}, for different values of C for the localisation parameter L.*
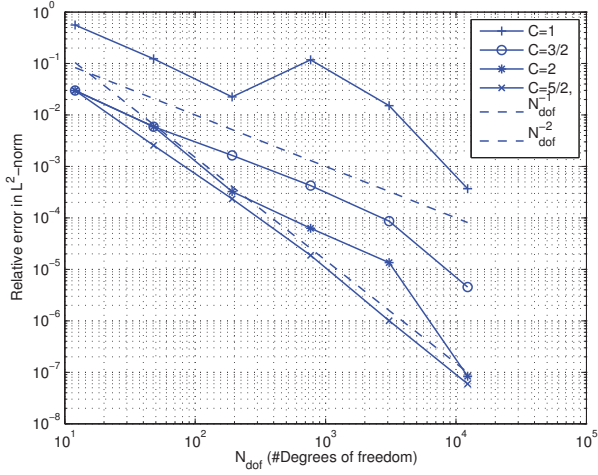
FIGURE 4. *Diffusion coefficient $A_1 = 1$. Relative L^2-norm error against N_{dof}, for different values of C for the localisation parameter L.*

with C as the sizes of the patches $\omega_T^L \ T \in \mathcal{T}_H$, increases with $L = \lceil C \log(H^{-1}) \rceil$. This results in both increased computational effort to compute the corrector functions and reduced sparseness in the coarse scale stiffness matrix.

5.2. Energy-norm convergence. Let the localization parameter be $L = \lceil 2 \log(H^{-1}) \rceil$. Figure 5 shows the relative error in the energy norm plotted against the number of degrees of freedom. The different permeabilities A_i, $i = 1, 2, 3$, and

the singularity arising from the L-shaped domain do not appear to have a substantial impact on the convergence rate, which is about $3/2$, as expected. We note in passing that using standard dG on the coarse mesh only admits poor convergence behaviour for A_2 and for A_3. This is to be expected, since standard dG on the coarse mesh does not resolve the fine scale features.

FIGURE 5. *Relative energy-norm error against N_{dof}, for $C = 2$ in the localisation parameter L for the the diffusion coefficients A_1, A_2, and A_3.*

5.3. L^2-norm convergence. Again, set $L = \lceil 2 \log(H^{-1}) \rceil$. Figure 6 and Figure 7, shows the relative L^2-norm error again the number of degrees of freedom between, u_h and $u_{H,h}^L$ and between u_h and $\Pi_H u_{H,h}^L$, viz., $\|u_h - \Pi_H u_H^{ms,L}\|_{L^2(\Omega)} / \|u_h\|_{L^2(\Omega)}$, respectively. In Figure 6 we see that the L^2-norm error between u_h and $u_H^{ms,L}$ converges at a faster rate than in the energy norm (convergence rate -2 compared to $-3/2$, respectively,) as expected from (4.26). In Figure 7 only the coarse part of $u_H^{ms,L}$ is used (i.e. $\Pi_H u_H^{ms,L}$); nevertheless it appears to have a faster convergence rate than $-1/2$, except for the case of the permeability A_3.

REFERENCES

[1] D. N. Arnold, *An interior penalty finite element method with discontinuous elements*, SIAM J. Numer. Anal. **19** (1982), no. 4, 742–760.
[2] I. Babuška, G. Caloz, and J. E. Osborn, *Special finite element methods for a class of second order elliptic problems with rough coefficients*, SIAM J. Numer. Anal. **31** (1994), no. 4, 945–981.
[3] I. Babuška and R. Lipton, *The penetration function and its application to microscale problems*, Multiscale Model. Simul. **9** (2011), no. 1, 373–406.
[4] I. Babuška and J. E. Osborn, *Generalized finite element methods: their performance and their relation to mixed methods*, SIAM J. Numer. Anal. **20** (1983), no. 3, 510–536.
[5] L. Berlyand and H. Owhadi, *Flux norm approach to finite dimensional homogenization approximations with non-separated scales and high contrast*, Arch. Ration. Mech. Anal. **198** (2010), no. 2, 677–721.
[6] F. Brezzi, L.P. Franca, T.J.R. Hughes, and A. Russo, $b = \int g$, Comput. Methods Appl. Mech. Engrg. **145** (1997), 329–339.

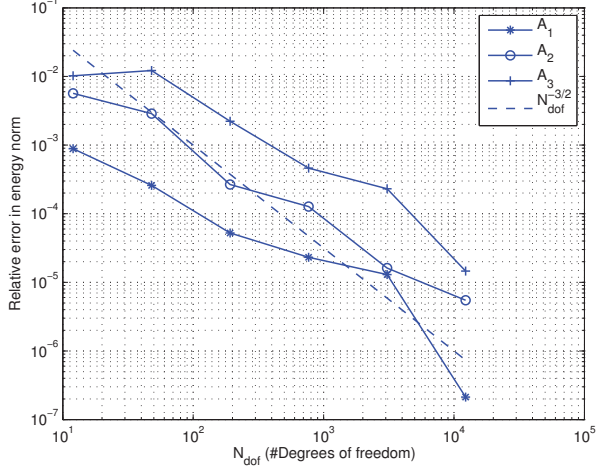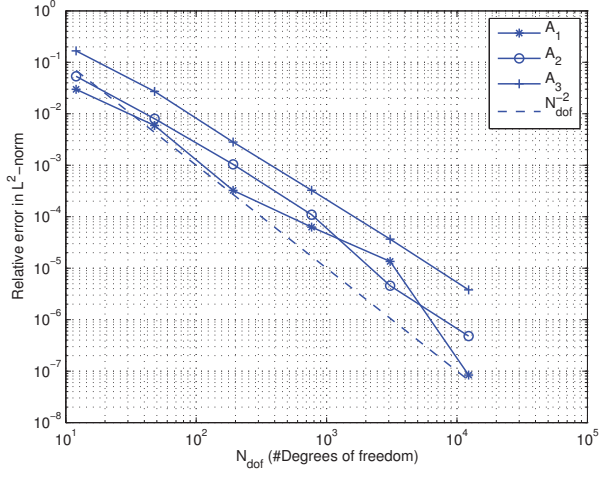FIGURE 6. *Relative L^2-norm error against N_{dof}, for $C = 2$ in the localisation parameter L for the the diffusion coefficients A_1, A_2, and A_3.*
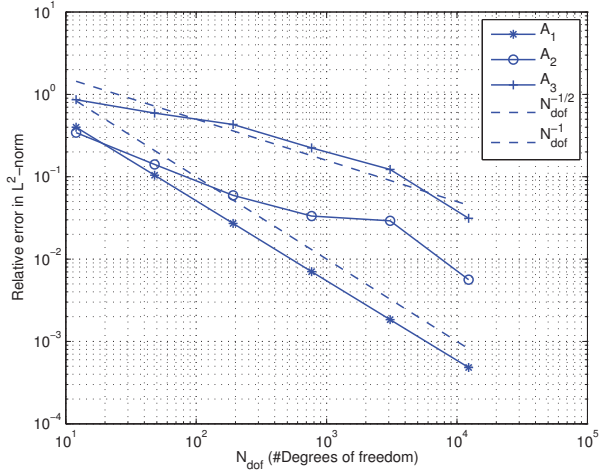
FIGURE 7. *Relative L^2-norm error against N_{dof}, for $C = 2$ in the localisation parameter L for the the diffusion coefficients A_1, A_2, and A_3.*

[7] J. Douglas and T. Dupont, *Interior penalty procedures for elliptic and parabolic Galerkin methods*, Computing methods in applied sciences (Second Internat. Sympos., Versailles, 1975), Springer, Berlin, 1976, pp. 207–216. Lecture Notes in Phys., Vol. 58. MR 0440955 (55 #13823)

[8] D. Elfverson, E. Georgoulis, and A. Målqvist, *An adaptive discontinuous galerkin multiscale method for elliptic problems*, Submitted for publication (2012).

[9] T. Y. Hou and X.-H. Wu, *A multiscale finite element method for elliptic problems in composite materials and porous media*, J. Comput. Phys. **134** (1997), no. 1, 169–189.

[10] P. Houston, D. Schötzau, and T. P. Wihler, *Energy norm a posteriori error estimation of hp-adaptive discontinuous Galerkin methods for elliptic problems*, Math. Models Methods Appl. Sci. **17** (2007), no. 1, 33–62. MR 2290408 (2008a:65216)

[11] T. J. R. Hughes, G. R. Feijóo, L. Mazzei, and J.-B. Quincy, *The variational multiscale method— a paradigm for computational mechanics*, Comput. Methods Appl. Mech. Engrg. **166** (1998), no. 1-2, 3–24.

[12] O. Karakashian and F. Pascal, *A posteriori error estimates for a discontinuous Galerkin approximation of second-order elliptic problems*, SIAM J. Numer. Anal. **41** (2003), 2374–2399.

[13] M. G. Larson and A. Målqvist, *Adaptive variational multiscale methods based on a posteriori error estimation: Energy norm estimates for elliptic problems*, Computer Methods in Applied Mechanics and Engineering **196** (2007), no. 21-24, 2313–2324.

[14] A. Målqvist and D. Peterseim, *Localization of elliptic multiscale problems*, Submitted for publication in Math. Comp., in revision, available as preprint arXiv:1110.0692 (2011).

[15] A. Målqvist, *Multiscale methods for elliptic problems*, Multiscale Modeling & Simulation **9** (2011), no. 3, 1064–1086.

[16] H. Owhadi and L. Zhang, *Localized bases for finite-dimensional homogenization approximations with nonseparated scales and high contrast*, Multiscale Modeling & Simulation **9** (2011), no. 4, 1373–1398.

Appendix A. Equalities for averages and jump operators. We derive equalities for averages and jump operators across interfaces where the functions v and w have discontinuities. Using $[vw] = \{v\}[w] + [v]\{w\}$ and $\{v\}\{w\} = \{vw\} - 1/4[v][w]$, we have

$$
\begin{aligned}
\{vw\}[vu] =& \{w\}\{v\}[vu] + 1/4[v][w][vu] \\
=& \{w\}[v^2u] - \{w\}[v]\{vu\} + 1/4[v][w][vu] \\
=& \{w\}[v^2u] - [v]\{w\}\{v\}\{u\} - 1/4[v]^2\{w\}[u] \\
& + 1/4[v]^2[w]\{u\} + 1/4[v]\{v\}[w][u]
\end{aligned}
\tag{A.1}
$$

and

$$
\begin{aligned}
\{vw\}[vu] =& \{v\}\{vw\}[u] + \{vw\}[v]\{u\} \\
=& \{v^2w\}[u] - 1/4[v][vw][u] + \{vw\}[v]\{u\} \\
=& \{v^2w\}[u] - 1/4[v]^2\{w\}[u] - 1/4[v]\{v\}[w][u] \\
& + [v]\{v\}\{w\}\{u\} + 1/4[v]^2[w]\{u\}
\end{aligned}
\tag{A.2}
$$

Combining (A.1) and (A.2) we obtain

$$
2\{vw\}[vu] = \{w\}[v^2u] + \{v^2w\}[u] + 1/2[v]^2[w]\{u\} - 1/2[v]^2\{w\}[u]
\tag{A.3}
$$

Also,

$$
\begin{aligned}
[vu][vu] =& [u]\{v\}[vu] + [v]\{u\}[vu] \\
=& [u][v^2u] - [v][u]\{vu\} + [v]\{u\}[vu] \\
=& [u][v^2u]) - [v][u]\{v\}\{u\} - 1/4[v][u][v][u] \\
& + [v]\{u\}[v]\{u\} + [v]\{u\}\{v\}[u] \\
=& [u][v^2u] - 1/4[v]^2[u]^2 + [v]^2\{u\}^2
\end{aligned}
\tag{A.4}
$$

Paper IV

Discontinuous Galerkin multiscale methods for convection dominated problems

Daniel Elfverson[†‡]   Axel Målqvist[†§]

May 2, 2013

Abstract

We propose an extension of the discontinuous Galerkin multiscale method, presented in [11], to convection dominated problems with rough, heterogeneous, and highly varying coefficients. The properties of the multiscale method and the discontinuous Galerkin method allows us to better cope with multiscale features as well as boundary layers in the solution. In the proposed method the trail and test spaces are spanned by a corrected basis calculated on localized patches of size $\mathcal{O}(H \log(H^{-1}))$, where H is the mesh size. We prove convergence rates independent of the variation in the coefficients and present numerical experiments which verify the analytical findings.

1 Introduction

In this paper we consider numerical approximation of convection dominated problems with rough, heterogeneous, and highly varying coefficients, without assumption on scale separation or periodicity. This class of problems, normally refereed to as multiscale problem, are know to be very computational demanding and arise in many different areas of the engineering sciences, e.g., porous media flow and in composite materials. More precisely, we consider the following convection-diffusion-reaction equation: find the weak solution $u \in H_0^1$ such that

$$\begin{aligned}
-\nabla \cdot A\nabla u + \mathbf{b} \cdot \nabla u + cu &= f \quad \text{in } \Omega, \\
u &= 0 \quad \text{on } \Gamma,
\end{aligned} \tag{1.1}$$

with multiscale coefficients $A, \mathbf{b}, c$, which will be specified later.

There are two key issues which make classical conforming finite element methods perform badly for these kind of problems.

- First, the multiscale features of the coefficient need to be resolved by the finite element mesh.

- Second, strong convection leads to boundary layers in the solution which also need to be resolved.

To overcome the lack of performance using classical finite element methods many different so called multiscale methods have been proposed. Some important contributions are: the multiscale finite element method (MsFEM) [14, 4, 10, 9]), the heterogeneous multiscale method (HMM) [7, 8]), and the variational multiscale method (VMS) [16, 17, 22, 25, 26, 23]). Common to all mentioned approaches is that fine scale problems are solved on localized patches and the result is used to construct a different basis or a modified coarse scale operator. The analysis for most of these methods rely strongly on scale separation or periodicity. Recently there was a leap forward in the analysis of multiscale methods. In [26] a new technique for proving convergence for a class of multiscale methods without any assumptions on scale separation or periodicity, was proposed. The method proposed in [26] uses a trail and test space spanned by a corrected basis function computed on patches of size $\mathcal{O}(H \log(H^{-1}))$. Textbook convergence with respect the mesh size H was proven. This technique was furthered generalized to a class of non-conforming multiscale methods based on the discontinuous Galerkin multiscale method in [11].

There is a vast literature on numerical methods for convection dominated problems. Two such examples are, the streamline diffusion/Petrov Galerkin (SUPG) method [19, 15] and Galerkin least square method (GLS) [18]. There has also been a lot of work on discontinuous Galerkin (dG) methods, we refer to [27, 24, 2, 20] for some early work and to [5, 13, 28, 6] and references therein for recent development and a literature review. DG methods exhibit attractive properties for convection dominated problems, e.g., they have enhanced stability properties, good conservation property of the state variable, and the use of complex and/or irregular meshes are admissible. DG multiscale methods has also been considered, see e.g. [1, 29].

To better coop with convection dominated multiscale problems we extend the discontinuous Galerkin multiscale method in [11] to convection dominated problems, in the sense that the convective term is included when calculating the corrected basis. For problems with weak convection it is not necessary to include the convective part, see e.g. [12].

The outline of this paper is as follows. In section 2 the discrete setting and underlying dG method is presented. In section 3 the multiscale decomposition and the dG multiscale method and the corresponding convergence result are stated. The proofs for the theoretical results are given in Section 4. Finally, in Section 5 numerical experiments are presented.

2   Preliminaries

In this section we present some notations and properties frequently used in the paper. Throughout this paper standard notations of Lebesgue and Sobolev spaces are used.

2.1 Setting

Let $\Omega \subset \mathbb{R}^d$ be a polygonal domain with Lipschitz boundary Γ. We assume that: the diffusion coefficients, $A \in L^\infty(\Omega, \mathbb{R}_{sym}^{d \times d})$, has uniform spectral bounds $0 < \alpha, \beta < \infty$, defined by

$$0 < \alpha := \operatorname*{ess\,inf}_{x \in \Omega} \inf_{v \in \mathbb{R}^d \setminus \{0\}} \frac{(A(x)v) \cdot v}{v \cdot v} \leq \operatorname*{ess\,sup}_{x \in \Omega} \sup_{v \in \mathbb{R}^d \setminus \{0\}} \frac{(A(x)v) \cdot v}{v \cdot v} =: \beta < \infty, \quad (2.1)$$

the convective, $\mathbf{b} \in [W_\infty^1(\Omega)]^d$, and reactive, $c \in L^\infty(\Omega)$, coefficient fulfill the condition

$$(c_0(x))^2 = c(x) - \frac{1}{2} \nabla \cdot \mathbf{b}(x) \geq \mu_0 \text{ a.e. } x \in \Omega, \quad (2.2)$$

where $\mu_0 \in \mathbb{R} > 0$ is constant. Finally we assume $f \in L^2(\Omega)$.

In the rest of the paper we will consider two different meshes, one coarse and one fine with mesh function h and H, respectively. Let $\mathcal{T}_k$, for $k = \{h, H\}$, denote a shape-regular subdivision of Ω into (closed) regular simplexes or into quadrilaterals/hexahedra ($d = 2/d = 3$), given a mesh function $k : \mathcal{T}_k \to \mathbb{R}$ defined as $k := \operatorname{diam}(T) \in P_0(\mathcal{T}_k)$ for all $T \in \mathcal{T}_k$. Also, let $\nabla_k v$ denote the $\mathcal{T}_k$-broken gradient defined as $(\nabla v)|_T = \nabla v|_T$ for all $T \in \mathcal{T}_k$. For simplicity we will also assume that $\mathcal{T}_k$ is conforming in the sense that no hanging nodes are allowed, but the analysis can easily be extend to non-conforming meshes with a finite number of hanging nodes on each edge. Let $\mathcal{E}_k$ denote the set of edges in $\mathcal{T}_k$, where $\mathcal{E}_k(\Omega)$ is the set of interior edges and $\mathcal{E}_k(\Gamma)$ is the set of boundary edges, such that $\mathcal{E}_k = \mathcal{E}_k(\Omega) \cup \mathcal{E}_k(\Gamma)$. Let $\hat{T}$ be the reference simplex or (hyper)cube. We define $\mathcal{P}_p(\hat{T})$ to be the space of polynomials of degree less than or equal to p if $\hat{T}$ is a simplex, or the space of polynomials of degree less than or equal to p, in each variable, if $\hat{T}$ is a (hyper)cube. The space of discontinuous piecewise polynomial function is defined by

$$P_p(\mathcal{T}_k) := \{v : \Omega \to \mathbb{R} \mid \forall T \in \mathcal{T}_k, v|_T \circ F_T \in \mathcal{P}_p(\hat{T})\}, \quad (2.3)$$

where $F_T : \hat{T} \to T$, $T \in \mathcal{T}_k$ is a family of element maps. Also, let $\Pi_p(\mathcal{T}_k) : L^2(\Omega) \to P_p(\mathcal{T}_k)$ denote the L^2-projection onto $P_p(\mathcal{T}_k)$. Let T^+ and T^- be two adjacent elements in $\mathcal{T}_k$ sharing an edge $e = T^+ \cap T^- \in \mathcal{E}_k(\Omega)$, and let ν_e be the outer normal pointing from T^- to T^+, and for $e \in \mathcal{E}_k(\Gamma)$ let ν_e be outward unit normal of Ω. For any $v \in P_p(\mathcal{T}_k)$ we denote the value on edge $e \in \mathcal{E}(\Omega)$ as $v^\pm = v|_{e \cap T^\pm}$. The jump and average of $v \in P_p(\mathcal{T}_k)$ is defined as, $[v] = v^- - v^+$ and $\{v\} = (v^- + v^+)/2$ respectively for $e \in \mathcal{E}_k(\Omega)$, and $[v] = \{v\} = v|_e$ for $e \in \mathcal{E}_k(\Gamma)$.

Let $0 \leq C < \infty$ denote any generic constant that neither depends on the mesh size or the variables A, $\mathbf{b}$, and c; then $a \lesssim b$ abbreviates the inequality $a \leq Cb$.

2.2 Discontinuous Galerkin discretization

For simplicity let the bilinear form $a_k(\cdot,\cdot) : \mathcal{V}_k \times \mathcal{V}_k \to \mathbb{R}$, given any mesh function $k : \Omega \to P_0(\mathcal{T}_k)$, be split into two parts

$$a_k(u,v) := a_k^{\mathrm{d}}(u,v) + a_k^{\mathrm{c\text{-}r}}(u,v), \tag{2.4}$$

where $a_k^{\mathrm{d}}(\cdot,\cdot)$ represents the diffusion part and $a_k^{\mathrm{c\text{-}r}}(\cdot,\cdot)$ represents the convection-reaction part. The diffusion part is approximated using a symmetric interior penalty method, i.e.,

$$
\begin{aligned}
a_k^{\mathrm{d}}(u,v) := (A\nabla_k u, \nabla_k v)_{L^2(\Omega)} + \sum_{e\in\mathcal{E}_k} \Big(\frac{\sigma_e}{h_e}([u],[v])_{L^2(e)} \\
- (\{\nu_e \cdot A\nabla u\},[v])_{L^2(e)} - (\{\nu_e \cdot A\nabla v\},[u]_{L^2(e)}) \Big),
\end{aligned} \tag{2.5}
$$

where σ_e is a constant, depending on the diffusion, large enough to make $a_k^{\mathrm{d}}(\cdot,\cdot)$ coercive. The convection-reaction part is approximated by

$$
\begin{aligned}
a_k^{\mathrm{c\text{-}r}}(u,v) := (\mathbf{b}\cdot\nabla_k u + cu, v)_{L^2(\Omega)} + \sum_{e\in\mathcal{E}_k} (b_e[u],[v])_{L^2(e)} \\
- \sum_{e\in\mathcal{E}_k(\Omega)} (\nu_e\cdot\mathbf{b}\{u\},[v])_{L^2(e)} - \sum_{e\in\mathcal{E}_k(\Gamma)} \frac{1}{2}((\nu_e\cdot\mathbf{b})u,v)_{L^2(e)},
\end{aligned} \tag{2.6}
$$

or equivalently

$$
\begin{aligned}
a_k^{\mathrm{c\text{-}r}}(u,v) := ((c-\nabla\cdot\mathbf{b})u,v)_{L^2(\Omega)} - (u,\mathbf{b}\cdot\nabla_k v)_{L^2(T)} \\
+ \sum_{e\in\mathcal{E}_k} (b_e[u],[v])_{L^2(e)} + \sum_{e\in\mathcal{E}_k(\Omega)} (\nu_e\cdot\mathbf{b}\{u\},[v])_{L^2(e)} \\
+ \sum_{e\in\mathcal{E}_k(\Gamma)} \frac{1}{2}((\nu_e\cdot\mathbf{b})u,v)_{L^2(e)},
\end{aligned} \tag{2.7}
$$

where upwind is imposed choosing the stabilization term as $b_e = |\mathbf{b}\cdot\nu_e|/2$, see e.g. [3]. The energy norm on $\mathcal{V}_k$ is given by

$$
\begin{aligned}
|||v|||_{k,d}^2 = \|A^{1/2}\nabla_k v\|_{L^2}^2 + \sum_{e\in\mathcal{E}_k} \frac{\sigma_e}{k}\|[v]\|_{L^2(e)}^2, \\
|||v|||_{k,\mathrm{c\text{-}r}}^2 = \|c_o v\|_{L^2(\Omega)}^2 + \sum_{e\in\mathcal{E}_k} \|b_e^{1/2}[v]\|_{L^2(e)}^2, \\
|||v|||_k^2 = |||v|||_{k,d}^2 + |||v|||_{k,\mathrm{c\text{-}r}}^2.
\end{aligned} \tag{2.8}
$$

From Theorem 2.2 in [21] we have that for each $v \in \mathcal{V}_k$, there exist an averaging operator $\mathcal{I}_k^c : \mathcal{V}_k \to \mathcal{V}_k \cap H^1(\Omega)$ with the following property

$$\beta^{-1/2}\|A^{1/2}\nabla_k(v-\mathcal{I}_k^c v)\|_{L^2(\Omega)} + \|k^{-1}(v-\mathcal{I}_k^c v)\|_{L^2(\Omega)} \lesssim \alpha^{-1/2}|||v|||_k. \tag{2.9}$$

3 Multiscale method

In this section we present the multiscale decomposition, the multiscale methods, and the main convergence results.

3.1 Multiscale decomposition

In order to do the multiscale decomposition the problem is divided into a coarse and a fine scale. To this end, let $\mathcal{T}_H$ and $\mathcal{T}_h$, with the respective mesh function H and h, denote the two different subdivisions, where $\mathcal{T}_h$ is constructed using one or more (possible adaptive) refinements of $\mathcal{T}_H$.

The aim of this section is to construct a coarse generalized finite element space based on $\mathcal{T}_H$, which takes the fine scale behavior of the data into account. That is, we assume that the solution given by: find $u_h \in \mathcal{V}_h := P_1(\mathcal{T}_h)$ such that

$$a_h(u_h, v) = F(v) \quad \text{for all } v \in \mathcal{V}_h, \tag{3.1}$$

gives a sufficiently good approximation of the weak solution u to (1.1). However, u_h never has to be computed in practice, it only acts as a reference solution. We introduce a coarse projection operator $\Pi_H := \Pi_1(\mathcal{T}_H)$ and let the fine scale space be defined by the kernel of Π_H, i.e.,

$$\mathcal{V}^{\mathrm{f}} := \{v \in \mathcal{V}_h \mid \Pi_H v = 0\} \subset \mathcal{V}_h. \tag{3.2}$$

The next step is to split any $v \in \mathcal{V}_h$ into some coarse part based on $\mathcal{T}_H$, such that the fine scale reminder in the space $\mathcal{V}^{\mathrm{f}}$ is sufficiently small. The naive way to this splitting is to use a L^2-orthogonal split. Then the coarse space is defined by $\mathcal{V}_H := \Pi_H \mathcal{V}_h = P_1(\mathcal{T}_H)$ and is the standard dG space on the coarse scale. A given basis of $\mathcal{V}_H$ is the element-wise Lagrange basis functions $\{\lambda_{T,j} \mid T \in \mathcal{T}_H, j = 1, \ldots, r\}$ where $r = (1 + d)$ for simplexes or $r = 2^d$ for quadrilaterals/hexahedra. The space $\mathcal{V}_H$ is known to give poor approximation properties if $\mathcal{T}_H$ does not resolve the variable coefficients in (1.1). We will use another choice, see [26, 11], based on $a_h(\cdot, \cdot)$, to construct a space of corrected basis functions. To this end, we define a fine scale projection operator $\mathfrak{F} : \mathcal{V}_h \to \mathcal{V}^{\mathrm{f}}$ by

$$a_h(\mathfrak{F}v, w) = a_h(v, w) \quad \text{for all } v \in \mathcal{V}^{\mathrm{f}}, \tag{3.3}$$

and let the corrected coarse space be defined as

$$\mathcal{V}_H^{ms} := (1 - \mathfrak{F})\mathcal{V}_H. \tag{3.4}$$

The correctors for the coarse basis are computed as follows: find $\phi_{T,j} \in \mathcal{V}^{\mathrm{f}}$ such that

$$a_h(\phi_{T,j}, v) = a_h(\lambda_{T,j}, v) \quad \text{for all } v \in \mathcal{V}^{\mathrm{f}}. \tag{3.5}$$

That is, the space of corrected basis functions is defined by $\mathcal{V}_H^{ms} := \{\lambda_{T,j} - \phi_{T,j} \mid T \in \mathcal{T}_H, j = 1, \ldots, r\}$. Note that, $\dim(\mathcal{V}_H^{ms}) = \dim(\mathcal{V}_H)$. From (3.4) we have that any $v_h \in \mathcal{V}_h$ can be decomposed into a coarse, $v_H^{ms} \in \mathcal{V}_H^{ms}$, and a fine, $v^f \in \mathcal{V}^{\mathrm{f}}$, scale contribution, i.e., $v_h = v_H^{ms} + v^f$.

3.2 Methods and convergence results

In this section the main results in [11] is extended to convection dominated problem. For the convenience of the reader a short recap of the different constants used in the error estimate are stated below:

- $C_{\beta/\alpha} = \beta/\alpha$, where α and β is the lower respectively upper spectral bound of the diffusion matrix A defined in (2.1),

- $C_s = \left(C_{\beta/\alpha}^2 + \|c_0\|_{L^\infty(\Omega)}^2 \mu_0^{-2} + \|H\mathbf{b}\|_{L^\infty(\Omega)} \alpha^{-1} \right)^{1/2}$, appear in Lemma 7 which proves stability estimate in energy norm for Π_H and c_0, μ_0 are defined in (2.2),

- $C_b = C_{\beta/\alpha} + \|c_0\|_{L^\infty(\Omega)} \mu_0^{-1}$, appear in Lemma 8,

- $C_c = (1 + \|H\mathbf{b}\|_{L^\infty(\Omega)} \alpha^{-1})$, appears in Lemma 9 which shows continuity of the bilinear form on $\mathcal{V}^{\mathrm{f}} \times \mathcal{V}_h$,

- $C_\zeta = \left(C_{\beta/\alpha}^2 + \|h\mathbf{b}\|_{L^\infty(\Omega)} \alpha^{-1} \right)^{1/2}$, appears in Lemma 11 using the stability property of the cut off function from Definition 10.

- $C_\phi = (1 + \|H\mathbf{b}\|_{L^\infty(\Omega)} \alpha^{-1/2} + \|Hc\|_{L^\infty(\Omega)} \mu_0^{-1})$, appears in Lemma 13 using stability of the corrected basis functions.

3.2.1 Ideal discontinuous Galerkin multiscale method

An ideal multiscale method seeks $u_H^{ms} \in \mathcal{V}_H^{ms}$ such that

$$a_h(u_H^{ms}, v) = F(v) \quad \text{for all } v \in \mathcal{V}_H^{ms}. \tag{3.6}$$

Note that, to seek a solution in the space $\mathcal{V}_H^{ms}$, a variational problem has to be solved on the whole domain, Ω, for each local basis function, which is not feasible for real computations. The following theorem shows the convergence of the ideal multiscale method.

Theorem 1. *Let $u_h \in \mathcal{V}_h$ be the to solution to (3.1), and $u_H^{ms} \in \mathcal{V}_H^{ms}$ be the to solution (3.6), then*

$$|||u_h - u_H^{ms}||| \lesssim C_1 ||H(f - \Pi_H f)||_{L^2(\Omega)} \tag{3.7}$$

holds, where $C_1 = CC_c \alpha^{-1/2}$ and C is generic constant which do not depend on the mesh size or the problem data.

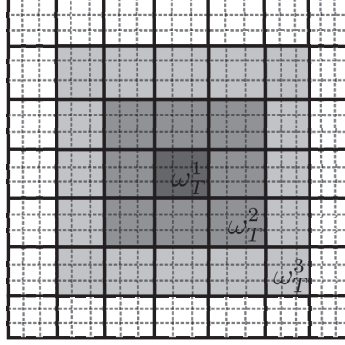*Proof.* The proof is found in Section 4. ☐

Figure 1: Example of a patch with size 1, ω_T^1, size 2 ω_T^2, and size ω_T^3, centered around element T.

3.2.2 Discontinuous Galerkin multiscale method

The fast decay of the corrected basis functions (Lemma 3), motivates us to solve the corrector functions on localized patches. This introduces a localization error, but choosing the patch size as $\mathcal{O}(H \log(H^{-1}))$ (as seen in Theorem 4) the localization error has the same convergence rate as the ideal multiscale method in Theorem 1. The corrector functions are solved on element patches, defined as follows.

Definition 2. For all $T \in \mathcal{T}_H$, let ω_T^L be a patch centered around element T and of size L, defined as,

$$
\begin{aligned}
\omega_T^1 &:= \mathrm{int}(T), \\
\omega_T^L &:= \mathrm{int}(\cup\{T' \in T_H \mid T \cap \bar{\omega}_T^{L-1} \neq 0\}), \quad L = 1, 2, \ldots.
\end{aligned}
\tag{3.8}
$$

See Figure 1 for an illustration.

The localized corrector functions are calculated as follows: for all $\{T \in \mathcal{T}_H, j = 1, \ldots, r\}$ find $\phi_{T,j}^L \in \mathcal{V}^f(\omega_T^L) = \{v \in \mathcal{V}^f \mid v|_{\Omega \setminus \omega_T^L} = 0\}$ such that

$$
a_h(\phi_{T,j}^L, v) = a_h(\lambda_{T,j}, v), \quad \text{for all } v \in \mathcal{V}^f(\omega_T^L).
\tag{3.9}
$$

The decay of the corrected basis function is given in the following lemma.

Lemma 3. For all $T \in \mathcal{T}_H$, $j = 1, \ldots, r$ where $\phi_{T,j}$ is the solution to (3.5) and $\phi_{T,j}^L$ is the solution to (3.9), the following estimate

$$
\left|\left|\left|\phi_{T,j} - \phi_{T,j}^L\right|\right|\right|_h \leq C_2 \gamma^L |||\lambda_{T,j} - \phi_{T,j}^L|||_{\mathrm{h}}
\tag{3.10}
$$

holds, where $L = \ell k$ is the size of the patch, $0 < \gamma = (\ell^{-1} C_3)^{\frac{k-1}{2\ell k}} < 1$, $C_2 = CC_c C_\zeta(1 + C_b C_s)$, $C_3 = C'(C_{\beta/\alpha}^2 + \|H\mathbf{b}\|_{L^\infty(\Omega)} \alpha^{-1} + C_c C_b \|\mathbf{b}\|_{L^\infty(\Omega)} \mu_0^{-1})$, and C, C' are generic constants neither depending on the mesh size, the size of the patches, or the problem data.

7

Proof. The proof is found in Section 4. □

The space of localized corrected basis function is defined by $\mathcal{V}_H^{ms,L} := \{\phi_{T,j}^L - \lambda_{T,j} \mid T \in \mathcal{T}_H, r = 1, \ldots, r\}$. The dG multiscale method now reads: find $u_H^{ms,L} \in \mathcal{V}_H^{ms,L}$ such that

$$a_h(u_H^{ms,L}, v) = F(v) \quad \text{for all } v \in \mathcal{V}_H^{ms,L}. \tag{3.11}$$

An error bound for the dG multiscale method using a localized corrected basis is given in Theorem 4. Also, note that it is only the first term $|||u - u_h|||_h$ in Theorem 4 that depends on the regularity of u.

Theorem 4. *Let $u_h \in \mathcal{V}_h$ be to solution to (3.1), and $u_H^{ms,L} \in \mathcal{V}_H^{ms,L}$ be to solution (3.11), then*

$$\begin{aligned}
|||u - u_H^{ms,L}|||_h \leq & |||u - u_h|||_h + C_1 \|H(f - \Pi_H f)\|_{L^2(\Omega)} \\
& + C_5 \|H^{-1}\|_{L^\infty(\Omega)} L^{d/2} \gamma^L \|f\|_{L^2(\Omega)}
\end{aligned} \tag{3.12}$$

holds, where L is the size of the patches, C_1 is a constant defined in Theorem 1, $0 < \gamma < 1$ and $C_5 = C_4^{1/2} C_2 C_\phi \alpha^{-1/2}$, where C_4 is defined in Lemma 12, and C_2 and γ are defined in Lemma 3.

Proof. The proof is found in Section 4. □

Remark 5. Theorem 4 is simplified to,

$$|||u - u_H^{ms,L}|||_h \leq |||u - u_h|||_h + C_1 \|H\|_{L^\infty(\Omega)}. \tag{3.13}$$

given that the patch size is chosen as $L = \lceil C \log(H^{-1}) \rceil$ with an appropriate C and $\|f\|_{L^2} = 1$.

Remark 6. For $|||u_h - u_H^{ms,L}|||_h$ to decay as $\mathcal{O}(H)$, it is sufficient that size of A and $\mathbf{b}$ fulfill the following relation, $\mathcal{O}(\beta) = \mathcal{O}(\|H\mathbf{b}\|_{L^\infty(\Omega)})$. If the convective part was omitted in the calculation of the corrected basis functions, using the same relation between the size of A and $\mathbf{b}$, the decay of $|||u_h - u_H^{ms,L}|||_h$ would be $\mathcal{O}(1)$, see [12].

4   Proofs from Section 3

Before proving the the main results, Theorem 1, Lemma 3, and Theorem 4, we state a some definitions and technical lemmas which will be necessary in the proofs.

4.1   Some technical lemmas

The following inequalities will frequently be used in the error analysis.

Lemma 7. *For any $v \in \mathcal{V}_h$ and $T \in \mathcal{T}_H$, the approximation property*

$$H|_T^{-1}\|v - \Pi_H v\|_{L^2(T)} \lesssim \alpha^{-1/2}|||v|||_{h,T}, \tag{4.1}$$

and stability estimate

$$|||\Pi_H v|||_H \lesssim C_s|||v|||_{\mathrm{h}}, \tag{4.2}$$

is satisfied, with

$$C_s = \left(C_{\beta/\alpha}^2 + \frac{\|c_0\|_{L^\infty(\Omega)}^2}{\mu_0^2} + \frac{\|H\mathbf{b}\|_{L^\infty(\Omega)}}{\alpha}\right)^{1/2}. \tag{4.3}$$

Proof. Using the same procedure as Lemma 4 in [11], the lemma follows. ∎

Lemma 8. *For each $v_H \in \mathcal{V}_H$, there exist a $v \in \mathcal{V}_h \cap H^1$ such that $\Pi_H v = v_H$, $\|v\|_{L^2(\Omega)} \lesssim \|v_H\|_{L^2(\Omega)}$, $|||v|||_{\mathrm{h}} \lesssim C_b|||v_H|||_H$, $\mathrm{supp}(v) \subset \mathrm{supp}(v_H)$, and $C_b := C_{\beta/\alpha} + \|c_0\|_{L^\infty(\Omega)}\mu_0^{-1}$.*

Proof. Using the same procedure as Lemma 5 in [11], the lemma follows. ∎

Continuity of the dG bilinear form for convection-reaction problems are usually done on a orthogonal subset of $\mathcal{V}_h$. Since the space $\mathcal{V}^{\mathrm{f}}$ is an orthogonal subset of $\mathcal{V}_h$ we derive the following lemma.

Lemma 9 (Continuity in $(\mathcal{V}^{\mathrm{f}} \times \mathcal{V}_h)$ and $(\mathcal{V}_h \times \mathcal{V}^{\mathrm{f}})$). *For all, $(u,v) \in \mathcal{V}^{\mathrm{f}} \times \mathcal{V}_h$, it holds*

$$a(v,w) \lesssim C_c|||v|||_{\mathrm{h}}|||w|||_{\mathrm{h}} \tag{4.4}$$

where

$$C_c = 1 + \|H\mathbf{b}\|_{L^\infty(\Omega)}\alpha^{-1/2}. \tag{4.5}$$

Proof. Since a_h^d is continuous in $(\mathcal{V}_h \times \mathcal{V}_h)$ continuity in $(\mathcal{V}^{\mathrm{f}} \times \mathcal{V}_h)$ follows from $\mathcal{V}^{\mathrm{f}} \subset \mathcal{V}_h$. For the convective part $a_h^{\mathrm{c\text{-}r}}$, we have

$$
\begin{aligned}
a^{\mathrm{c\text{-}r}}(v,w) = &\sum_{T \in \mathcal{T}_h} \left(((c - \nabla \cdot \mathbf{b})v, w)_{L^2(T)} - (v, \mathbf{b} \cdot \nabla w)_{L^2(T)}\right) \\
&+ \sum_{e \in \mathcal{E}_k} (b_e[v], [w])_{L^2(e)} + \sum_{e \in \mathcal{E}_k(\Omega)} (\nu_e \cdot \{\mathbf{b}v\}, [w])_{L^2(e)} \\
&+ \sum_{e \in \mathcal{E}_k(\Gamma)} ((\nu_e \cdot \mathbf{b})v, w)_{L^2(e)} \\
\lesssim &\sum_{T \in \mathcal{T}_h} \left(\|c_0 v\|_{L^2(T)}\|c_0 w\|_{L^2(T)} + \|\|\mathbf{b}\|_{L^\infty(T)}v\|_{L^2(T)}\|\nabla w\|_{L^2(T)}\right) \\
&+ \sum_{e \in \mathcal{E}_k} \left(\|\|\mathbf{b}\|_{L^\infty(e)}v\|_{L^2(T^+ \cap T^-)}h^{-1/2}\|[w]\|_{L^2(e)}\right).
\end{aligned}
\tag{4.6}
$$

Using a discrete Cauchy-Schwartz inequality and summing over the coarse elements, we have

$$
\begin{aligned}
a^{\text{c-r}}(v, w) &\lesssim |||v|||_{\text{h}} |||w|||_{\text{h}} + \alpha^{-1/2} \|H\mathbf{b}\|_{L^\infty(\Omega)} \|H^{-1}(v - \Pi_H v)\|_{L^2(\Omega)} |||w|||_{\text{h}}, \\
&\lesssim (1 + \|H\mathbf{b}\|_{L^\infty(\Omega)} \alpha^{-1/2}) |||v|||_{\text{h}} |||w|||_{\text{h}},
\end{aligned}
\tag{4.7}
$$

which concludes the proof for $(\mathcal{V}^{\text{f}} \times \mathcal{V}_h)$. A similar argument gives the proof of $(\mathcal{V}_h \times \mathcal{V}^{\text{f}})$. $\qquad\square$

In the proof Lemma 3, which proves the decay of the corrected basis function, the following cut off function will be used.

Definition 10. The function $\zeta^{d,D} \in P_o(\mathcal{T}_h)$, for $D > d$, is a cut off function fulfilling the following condition

$$
\begin{aligned}
\zeta_T^{d,D}|_{\omega_T^d} &= 1, \\
\zeta_T^{d,D}|_{\Omega \setminus \omega_T^D} &= 0, \\
\|[\zeta_T^{d,D}]\|_{L^\infty(\mathcal{E}_h(T))} &\lesssim \frac{\|h\|_{L^\infty(T)}}{(D - d)H|_T},
\end{aligned}
\tag{4.8}
$$

and $\|[\zeta^{d,D}]\|_{L^\infty(\partial(\omega_T^D \setminus \omega_T^d))} = 0$, for all $T \in \mathcal{T}_H$.

For the cut off function defined in Definition 10, we have the following stability condition.

Lemma 11. For any $v \in \mathcal{V}_h$ and $\zeta_T^{d,D}$ from Definition 10, the estimate,

$$
|||\zeta_T^{d,D} v|||_{\text{h}} \lesssim C_\zeta |||v|||_{h, \omega_T^D},
\tag{4.9}
$$

holds, where $C_\zeta = (C_{\beta/\alpha}^2 + \|h\mathbf{b}\|_{L^\infty(\Omega)})^{1/2}$.

Proof. Let us use the following for the diffusion part in [11],

$$
|||(1 - \zeta_T^{d,D})v|||_{\text{h,d}} \lesssim C_{\beta/\alpha} |||v|||_{h, \Omega \setminus \omega_T^{L-1}}
\tag{4.10}
$$

and focus on the convection-reaction part, where $e = S^+ \cap S^- \in \mathcal{E}_h$

$$|||(1 - \zeta_T^{d,D})v|||_{h,\text{c-r}}^2$$

$$\leq \|c_0 v\|_{L^2(\Omega \setminus \omega_T^{L-1})}^2 + \sum_{e \in \mathcal{E}_h} \|b_e^{1/2}[(1 - \zeta_T^{d,D})v]\|_{L^2(e)}^2$$

$$\leq \|c_0 v\|_{L^2(\Omega \setminus \omega_T^{L-1})}^2$$

$$+ \sum_{\substack{e \in \mathcal{E}_h: \\ e \cap \omega_T^{L-1} \neq 0}} \left(\|b_e^{1/2}[v]\|_{L^2(e)}^2 + \frac{\|h\|_{L^\infty(T)}^2}{\|H\|_{L^\infty(S^+ \cup S^-)}^2} \|b_e^{1/2}\{v\}\|_{L^2(e)}^2 \right) \quad (4.11)$$

$$\lesssim |||v|||_{h,\Omega \setminus \omega^{L-1}}^2 + \sum_{\substack{T \in \mathcal{T}_H: \\ e \cap \omega_T^{L-1} \neq 0}} \frac{\|h\mathbf{b}\|_{L^\infty(T)}}{\|H\|_{L^\infty(S^+ \cup S^-)}^2} \|v - \Pi_H v\|_{L^2(T)}^2$$

$$\leq |||v|||_{h,\Omega \setminus \omega^{L-1}}^2 + \frac{\|h\mathbf{b}\|_{L^\infty(\Omega)}}{\alpha} |||v|||_{h,\Omega \setminus \omega^{L-1}}^2,$$

using $[vw] = \{v\}[w] + \{w\}[v]$, the triangle inequality, and a trace inequality. The proof is concluded using (4.10) and (4.11). $\qquad \square$

The following lemmas will be necessary in order to prove Theorem 4.

Lemma 12. *The following estimate,*

$$||| \sum_{T \in \mathcal{T}_H, j=1,\ldots,r} v_j(\phi_{T,j} - \phi_{T,j}^L) |||_h^2 \leq C_4 L^d \sum_{T \in \mathcal{T}_H, j=1,\ldots,r} |v_j|^2 |||\phi_{T,j} - \phi_{T,j}^L|||_h^2,$$

$$(4.12)$$

holds, where $C_4 = C C_c^2 C_\zeta^2 (1 + C_b C_s)^2$ and C is a generic constant neither depending on the mesh size, the size of the patches, or the problem data.

Proof. Defining $\eta_T := \zeta_T^{L,L+1}$ and let $w \in \mathcal{V}^{\text{f}}$. From Lemma 8 there exist a b_T such that $\Pi_H b_T = \Pi_H(\eta_T w)$ such that $|||b_T|||_h \lesssim C_b |||\Pi_H(\eta_T w)|||_H$. We have the following relation

$$a_h(\phi_{T,j} - \phi_{T,j}^L, w - \eta_T w + b_T) = 0, \quad (4.13)$$

since $w - \eta_T w + b_T \in \mathcal{V}^{\text{f}}$ with no support in ω_T^L. Let $w = \sum_{T \in \mathcal{T}_H, j=1,\ldots,r} v_j(\phi_{T,j} - \phi_{T,j}^L)$, we obtain

$$|||w|||_h^2 \lesssim a_h(w, w)$$

$$= \sum_{T \in \mathcal{T}_H, j=1,\ldots,r} v_j a_h(\phi_{T,j} - \phi_{T,j}^L, w)$$

$$= \sum_{T \in \mathcal{T}_H, j=1,\ldots,r} v_j a_h(\phi_{T,j} - \phi_{T,j}^L, \zeta_T w - b_T) \quad (4.14)$$

$$= C_c \sum_{T \in \mathcal{T}_H, j=1,\ldots,r} |v_j| |||\phi_{T,j} - \phi_{T,j}^L|||_h \left(|||\zeta_T w|||_h + |||b_T|||_h \right).$$

11

Furthermore, using Lemma 8, Lemma 7, and Lemma 11, we have

$$|||b|||_{\mathrm{h}} \lesssim C_b |||\Pi_H \zeta_T w|||_H \lesssim C_b C_s |||\zeta_T \phi_h|||_{\mathrm{h}} \lesssim C_b C_s C_\zeta |||w|||_{h,\omega_T^{L+1}} \qquad (4.15)$$

and obtain,

$$|||w|||_{\mathrm{h}}^2 \lesssim C_c C_\zeta (1 + C_b C_s) \sum_{T \in \mathcal{T}_H, \, j=1,\ldots,r} |v_j| |||\phi_{T,j} - \phi_{T,j}^L|||_{\mathrm{h}} |||w|||_{h,\omega_T^{L+1}} \qquad (4.16)$$

using (4.14), (4.15), and (4.17). Also, note that

$$\sum_{T \in \mathcal{T}_H, \, j=1,\ldots,r} |||w|||_{h,\omega_T^{L+1}}^2 \lesssim L^d |||w|||_{\mathrm{h}}^2. \qquad (4.17)$$

and using a Cauchy-Schwartz inequality for the sum, concludes the proof with $C_4 = C C_c^2 C_\zeta^2 (1 + C_b C_s)^2$. Where C is a generic constant hidden in '$\lesssim$'. $\qquad \square$

Lemma 13 (Stability of the corrected basis function). *For all $T \in \mathcal{T}_H$, $j = 1,\ldots,r$, the following estimate*

$$|||\phi_{T,h} - \lambda_{T,j}|||_{\mathrm{h}} \leq C_\phi \|H^{-1}\lambda_{T,j}\|_{L^2(\Omega)} \qquad (4.18)$$

holds, where $C_\phi = C(1 + \|H\mathbf{b}\|_{L^\infty(\Omega)} \alpha^{-1/2} + \|Hc\|_{L^\infty(\Omega)} \mu_0^{-1})$ and C is generic constant neither depending on the mesh size or the problem data.

Proof. Let $v = \lambda_{T,j} - b_T \in \mathcal{V}^{\mathrm{f}}$, where $b_T \in H_0^1(T)$ and $\Pi_H b_{T,j} = \lambda_{T,j}$ from Lemma 8. We have

$$
\begin{aligned}
|||\phi_{T,h} - \lambda_{T,j}|||_{\mathrm{h}}^2 &\lesssim a_h(\phi_{T,h} - \lambda_{T,j}, \phi_{T,h} - \lambda_{T,j}) \\
&= a_h(\phi_{T,h} - \lambda_{T,j}, v - \lambda_{T,j}) = a_h(\phi_{T,h} - \lambda_{T,j}, b_{T,j}) \\
&= a_h^d(\phi_{T,h} - \lambda_{T,j}, b) + a_h^{\mathrm{c\text{-}r}}(\phi_{T,h} - \lambda_{T,j}, b_{T,j}) \\
&= a_h^d(\phi_{T,h} - \lambda_{T,j}, b) + (\mathbf{b} \cdot \nabla_h(\phi_{T,h} - \lambda_{T,j}) + c(\phi_{T,h} - \lambda_{T,j}), b_{T,j})_{L^2(\Omega)}
\end{aligned}
\qquad (4.19)
$$

Using that the diffusion part in (4.19) of the bilinear form is continuous in $(\mathcal{V}_h \times \mathcal{V}_h)$, Lemma 8, and a inverse inequality, we have

$$
\begin{aligned}
a_h^d(\phi_{T,h} - \lambda_{T,j}, b_{T,j}) &\lesssim |||\phi_{T,h} - \lambda_{T,j}|||_{\mathrm{h}} |||b_{T,j}|||_{\mathrm{h}} \\
&\lesssim C_b |||\phi_{T,h} - \lambda_{T,j}|||_{\mathrm{h}} |||\lambda_{T,j}|||_H \\
&\lesssim C_b \beta^{1/2} |||\phi_{T,h} - \lambda_{T,j}|||_{\mathrm{h}} \|H^{-1}\lambda_{T,j}\|_{L^2(T)}.
\end{aligned}
\qquad (4.20)
$$

For the convection-reaction part in (4.19), we have

$$
\begin{aligned}
&(\mathbf{b} \cdot \nabla_h(\phi_{T,h} - \lambda_{T,j}) + c(\phi_{T,h} - \lambda_{T,j}), b_{T,j})_{L^2(\Omega)} \\
&\lesssim \left(\|\mathbf{b} \cdot \nabla_h(\phi_{T,h} - \lambda_{T,j})\|_{L^2(\Omega)} + \|c(\phi_{T,h} - \lambda_{T,j})\|_{L^2(\Omega)} \right) \|b_{T,j}\|_{L^2(\Omega)} \\
&\lesssim \left(\|H\mathbf{b}\|_{L^\infty(\Omega)} \|\nabla_h(\phi_{T,h} - \lambda_{T,j})\|_{L^2(\Omega)} \right. \\
&\quad \left. + \|Hc\|_{L^\infty(\Omega)} \mu_0^{-1} \|c_0(\phi_{T,h} - \lambda_{T,j})\|_{L^2(\Omega)} \right) \|H^{-1}\lambda_{T,j}\|_{L^2(\Omega)}.
\end{aligned}
\qquad (4.21)
$$

We obtain

$$|||\phi_{T,h} - \lambda_{T,j}|||_{\mathrm{h}} \leq C_\phi \|H^{-1}\lambda_{T,j}\|_{L^2(\Omega)}. \qquad (4.22)$$

where $C_\phi = C(1 + \|H\mathbf{b}\|_{L^\infty(\Omega)} \alpha^{-1/2} + \|Hc\|_{L^\infty(\Omega)} \mu_0^{-1})$ and C is generic constant hidden in '$\lesssim$'. $\qquad \square$

4.2 Proof of main results

We are now ready prove, Theorem 1, Lemma 3, and Theorem 4.

Proof of Theorem 1. Let us decompose u_h into a coarse contribution, $v_H^{ms} \in \mathcal{V}_H^{ms}$, and a fine scale remainder, $v^f \in \mathcal{V}^f$, i.e., $u_h = v_H^{ms} + v^f$. For v^f we have

$$
\begin{aligned}
|||v^f|||_{\mathrm{h}}^2 &\lesssim a_h(v^f, v^f) = a_h(u_h, v^f) = (f, v^f)_{L^2(\Omega)} \\
&= (f - \Pi_H f, v^f - \Pi_H v^f)_{L^2(\Omega)} \\
&\le \|H(f - \Pi_H f)\|_{L^2(\Omega)} \|H^{-1}(v^f - \Pi_H v^f)\|_{L^2(\Omega)} \\
&\le \alpha^{-1/2} \|H(f - \Pi_H f)\|_{L^2(\Omega)} |||v^f|||_{\mathrm{h}}.
\end{aligned}
\tag{4.23}
$$

Using continuity, we have

$$
\begin{aligned}
|||u_h - u_H^{ms}|||_{\mathrm{h}}^2 &\lesssim a_h(u_h - u_H^{ms}, u_h - u_H^{ms}) = a_h(u_h - u_H^{ms}, u_h - v_H^{ms}) \\
&\lesssim C_c |||u_h - u_H^{ms}|||_{\mathrm{h}} |||u_h - v_H^{ms}|||_{\mathrm{h}}
\end{aligned}
\tag{4.24}
$$

which concludes the proof together with (4.23). $\qquad\square$

Proof of Lemma 3. Define $e := \phi_{T,j} - \phi_{T,j}^L$ where $\phi_{T,j} \in \mathcal{V}^f$ and $\phi_{T,j}^L \in \mathcal{V}^f(\omega_T^L)$. We have

$$
\begin{aligned}
|||e|||_h^2 &\lesssim a_h(e, \phi_{T,j} - \phi_{T,j}^L) = a_h(e, \phi_{T,j} - v) \\
&\lesssim C_c |||e|||_{\mathrm{h}} |||\phi_{T,j} - v|||_{\mathrm{h}}.
\end{aligned}
\tag{4.25}
$$

Furthermore from Lemma 8, there exist a $v = \zeta_T^{L-1,L} \phi_{T,j} - b_T \in \mathcal{V}^f(\omega_T^L)$ such that $\Pi_H b_T = \Pi_H(\zeta_T^{L-1,L} \phi_{T,j})$ and $|||b_T|||_{\mathrm{h}} \lesssim C_b |||\Pi_H(\zeta_T^{L-1,L} \phi_{T,j})|||_H$, we have

$$
|||e|||_h \lesssim C_c \left(|||(1 - \zeta_T^{L-1,L}) \phi_{T,j}|||_{\mathrm{h}} + |||b_T|||_{\mathrm{h}} \right),
\tag{4.26}
$$

where

$$
\begin{aligned}
|||b_T|||_{\mathrm{h}} &\lesssim C_b |||\Pi_H \zeta_T^{L-1,L} \phi_{T,j}|||_H = C_b |||\Pi_H(1 - \zeta_T^{L-1,L}) \phi_{T,j}|||_H \\
&\lesssim C_b C_s |||(1 - \zeta_T^{L-1,L}) \phi_{T,j}|||_{\mathrm{h}} \lesssim C_b C_s C_\zeta |||\phi_{T,j}|||_{\mathrm{h}, \Omega \setminus \omega_T^{L-1}}.
\end{aligned}
\tag{4.27}
$$

using Lemma 8, Lemma 7, and Lemma 11. We obtain,

$$
|||e|||_h \lesssim C_2 |||\phi_{T,j}|||_{h, \Omega \setminus \omega_T^{L-1}},
\tag{4.28}
$$

where $C_2 = CC_c C_\zeta(1 + C_b C_s)$ from (4.26) and (4.27). Where C is the generic constant hidden in '$\lesssim$'.

The next step in the proof is to construct a recursive relation which will be used to prove the decay in the correctors. To this end, let $\ell k = L - 1$, and define another the cut off function, $\eta_T^m := (1 - \zeta^{\ell(k-m), \ell(k-m+1)})$ and the patch $\tilde{\omega}_T^m := \omega_T^{\ell(k-m+1)}$, for $m = 1, \ldots, k - 1$. Note that $\tilde{\omega}_T^{m+1} \subset \tilde{\omega}_T^m$. We have

$$
|||\phi_{T,j}|||_{h, \Omega \setminus \bar{\omega}_T^m} \le |||\eta_T^m \phi_{T,j}|||_{\mathrm{h}} \lesssim a_h(\eta_T^m \phi_{T,j}, \eta_T^m \phi_{T,j})
\tag{4.29}
$$

13

So shorten the proof we refer to the following inequality

$$a^{\mathrm{d}}(\eta_T^m \phi_{T,j}, \eta_T^m \phi_{T,j}) \lesssim a^{\mathrm{d}}(\phi_{T,j}, (\eta_T^m)^2 \phi_{T,j} - b_T) + \frac{C_{\beta/\alpha}^2}{\ell} |||\phi_{T,j}|||_{h, \omega_T^m \setminus \bar{\omega}_T^{m+1}}^2.$$
(4.30)

where $(\eta_T^m)^2 \phi_{T,j} - b_T \in \mathcal{V}^{\mathrm{f}}$, in the proof of Lemma 10 in [11]. We focus on the term convection-reaction term, i.e.,

$$a^{\mathrm{c\text{-}r}}(\eta_T^m \phi_{T,j}, \eta_T^m \phi_{T,j})$$

$$= \sum_{\substack{S \in \mathcal{T}_h: \\ S \cap (\Omega \setminus \tilde{\omega}_T^{m+1}) \neq 0}} ((\gamma - \nabla \cdot \mathbf{b}) \eta_T^m \phi_{T,j}, \eta_T^m \phi_{T,j})_{L^2(S)} - (\eta_T^m \phi_{T,j}, \mathbf{b} \cdot \nabla \eta_T^m \phi_{T,j})_{L^2(S)}$$

$$+ \sum_{\substack{e \in \mathcal{E}_h: \\ e \cap (\Omega \setminus \tilde{\omega}_T^{m+1}) \neq 0}} (b_e [\eta_T^m \phi_{T,j}], [\eta_T^m \phi_{T,j}])_{L^2(e)}$$

$$+ \sum_{\substack{e \in \mathcal{E}_h(\Omega): \\ e \cap (\Omega \setminus \tilde{\omega}_T^{m+1}) \neq 0}} ((\nu_e \cdot \{\mathbf{b} \eta_T^m \phi_{T,j}\}, [\eta_T^m \phi_{T,j}])_{L^2(e)}$$

$$+ \sum_{\substack{e \in \mathcal{E}_h(\Gamma): \\ e \cap (\Omega \setminus \tilde{\omega}_T^{m+1}) \neq 0}} \frac{1}{2} ((\nu_e \cdot \mathbf{b}) \eta_T^m \phi_{T,j}, \eta_T^m \phi_{T,j})_{L^2(e)}$$
(4.31)

Since the cut of function is piecewise constant it follows that

$$((\gamma - \nabla \cdot \mathbf{b}) \eta_T^m \phi_{T,j}, \eta_T^m \phi_{T,j})_{L^2(S)} - (\eta_T^m \phi_{T,j}, \mathbf{b} \cdot \nabla \eta_T^m \phi_{T,j})_{L^2(S)}$$
$$= (\gamma - \nabla \cdot \mathbf{b}) \phi_{T,j}, (\eta_T^m)^2 \phi_{T,j})_{L^2(S)} - (\phi_{T,j}, \mathbf{b} \cdot \nabla (\eta_T^m)^2 \phi_{T,j})_{L^2(S)}$$
(4.32)

for all $S \in \mathcal{T}_h$. Using the following equalities from (Appendix A in [11])

$$\{vw\}[vw] = \{w\}[v^2 w] - [v]\{w\}\{v\}\{w\} + 1/4[v]\{v\}[w][w]$$
$$[vw][vw] = [w][v^2 w] - 1/4[v]^2[w]^2 + [v]^2\{w\}^2$$
(4.33)

and (4.32), we obtain

$$a^{\mathrm{c\text{-}r}}(\eta_T^m \phi_{T,j}, \eta_T^m \phi_{T,j}) = a^{\mathrm{c\text{-}r}}(\phi_{T,j}, (\eta_T^m)^2 \phi_{T,j})$$

$$+ \sum_{\substack{e \in \mathcal{E}_h(\Omega): \\ e \cap (\tilde{\omega}_T^m \setminus \tilde{\omega}_T^m) \neq 0}} \Big(- (\nu_e \cdot \mathbf{b} [\eta_T^m] \{\phi_{T,j}\}, \{\eta_T^m\}\{\phi\})_{L^2(e)}$$
(4.34)

$$+ 1/4 (\nu_e \cdot \mathbf{b} [\eta_T^m] \{\phi_{T,j}\}, \{\eta_T^m\}[\phi_{T,j}])_{L^2(e)}$$

$$- 1/4 (b_e [\eta_T^m]^2, [\phi_{T,j}]^2)_{L^2(e)} + (b_e [\eta_T^m]^2, \{\phi_{T,j}^2\})_{L^2(e)} \Big)$$

Next we bound the terms in (4.34) in two steps, first the sum over the edges, and then the bilinear form. The sum over the edges terms can be bounded by using that $\|[\eta_T^m]\|_{L^\infty(T)} \lesssim \|h\|_{L^\infty(T)}/H|_T$, $\|\{\eta_T^m\}\|_{L^\infty(\Omega)} \lesssim 1$, $\|h\|_{L^\infty(T)}/H|_T \ell < 1$,

14

and a trace inequality. Let $e = S^+ \cap S^- \in \mathcal{E}_h$, we obtain

$$
\sum_{\substack{e \in \mathcal{E}_h(\Omega): \\ e \cap (\tilde{\omega}_T^m \setminus \tilde{\omega}_T^m) \neq 0}} \frac{\|\mathbf{b}\|_{L^\infty(S^+ \cup S^-)}}{\|H\|_{L^\infty(S^+ \cap S^-)} \ell} \left(\|h^{1/2}\{\phi_{T,j}\}\|_{L^2(e)} \|h^{1/2}\{\phi\}\|_{L^2(e)} + \right.
$$

$$
\|h^{1/2}\{\phi_{T,j}\}\|_{L^2(e)} \|h^{1/2}[\phi_{T,j}]\|_{L^2(e)} + \|h^{1/2}[\phi_{T,j}]\|_{L^2(e)}^2
$$

$$
\left. + \|h^{1/2}\{\phi_{T,j}\}\|_{L^2(e)}^2 \right)
$$

$$
\lesssim \sum_{\substack{e \in \mathcal{E}_H(\Omega): \\ e \cap (\tilde{\omega}_T^m \setminus \tilde{\omega}_T^m) \neq 0}} \frac{\|\mathbf{b}\|_{L^\infty(T^+ \cup T^-)}}{\ell} \|H^{-1}\phi_{T,j}\|_{L^2(T^+ \cup T^-)}^2 \tag{4.35}
$$

$$
\lesssim \sum_{\substack{T \in \mathcal{T}_H: \\ T \cap (\tilde{\omega}_T^m \setminus \tilde{\omega}_T^m) \neq 0}} \frac{\|\mathbf{b}\|_{L^\infty(T)}}{\ell} \|H^{-1}(\phi_{T,j} - \Pi_H \phi_{T,j})\|_{L^2(T)}^2
$$

$$
\lesssim \frac{\|H\mathbf{b}\|_{L^\infty(\Omega)}}{\ell \alpha} \|\|\phi_{T,j}\|\|_{h,(\tilde{\omega}_T^m \setminus \tilde{\omega}_T^{m+1})}^2
$$

For the bilinear form, using Lemma 8 there exist a b_T with support in $\tilde{\omega}_T^m \setminus \tilde{\omega}_T^{m+1}$, such that $(\eta_T^m)^2 \phi_{T,j} - b_T \in \mathcal{V}^{\mathrm{f}}$ and $\|\|b_T\|\|_{\mathrm{h}} \lesssim C_b \|\|\Pi_H((\eta_T^m)^2 \phi_{T,j})\|\|_H$. We have

$$
\begin{aligned}
a^{\mathrm{c\text{-}r}}(\phi_{T,j}, (\eta_T^m)^2 \phi_{T,j}) &= a^{\mathrm{c\text{-}r}}(\phi_{T,j}, (\eta_T^m)^2 \phi_{T,j} - b_T) + a^{\mathrm{c\text{-}r}}(\phi_{T,j}, b_T) \\
&\lesssim a^{\mathrm{c\text{-}r}}(\phi_{T,j}, (\eta_T^m)^2 \phi_{T,j} - b_T) \\
&\quad + C_c \|\|\phi_{T,j}\|\|_{\mathrm{a},h,\tilde{\omega}_T^m \setminus \tilde{\omega}_T^{m+1}} \|c_0 b_T\|_{L^2(\tilde{\omega}_T^m \setminus \tilde{\omega}_T^{m+1})} \\
&\quad + C_c \|\|\phi_{T,j}\|\|_{\mathrm{a},h,\tilde{\omega}_T^m \setminus \tilde{\omega}_T^{m+1}} \|c_0 b_T\|_{L^2(\tilde{\omega}_T^m \setminus \tilde{\omega}_T^{m+1})}
\end{aligned} \tag{4.36}
$$

which can be further estimated, using Lemma 7. For all $T \in \mathcal{T}_H$ the operator Π_H is stable in the $L^2(T)$-norm, we have

$$
\begin{aligned}
&\|b_T\|_{L^2(\tilde{\omega}_T^m \setminus \tilde{\omega}_T^{m+1})} \\
&\lesssim C_b \|Hc_0\|_{L^\infty(\tilde{\omega}_T^m \setminus \tilde{\omega}_T^{m+1})} \|H^{-1}\Pi_H((\eta_T^m)^2 \phi_{T,j})\|_{L^2(\tilde{\omega}_T^m \setminus \tilde{\omega}_T^{m+1})} \\
&= C_b \|\Pi_H(((\eta_T^m)^2 - \Pi_0(\eta_T^m)^2)H^{-1}\phi_{T,j})\|_{L^2(\tilde{\omega}_T^m \setminus \tilde{\omega}_T^{m+1})} \\
&\leq C_b \|(\eta_T^m)^2 - \Pi_0(\eta_T^m)^2\|_{L^\infty(\tilde{\omega}_T^m \setminus \tilde{\omega}_T^{m+1})} \|H^{-1}\phi_{T,j}\|_{L^2(\tilde{\omega}_T^m \setminus \tilde{\omega}_T^{m+1})} \\
&\lesssim H C_b \ell^{-1} \mu_0^{-1} \|\|\phi_{T,j}\|\|_{h,\tilde{\omega}_T^m \setminus \tilde{\omega}_T^{m+1}}.
\end{aligned} \tag{4.37}
$$

using Lemma 8 and that $\Pi_H \phi = 0$. We obtain

$$
\begin{aligned}
&\|\|\phi_{T,j}\|\|_{h,\Omega \setminus \omega_T^m}^2 \\
&\lesssim \left(a^{\mathrm{d}}(\phi_{T,j}, (\eta_T^m)^2 \phi_{T,j} - \tilde{b}) + a^{\mathrm{c\text{-}r}}(\phi_{T,j}, (\eta_T^m)^2 \phi_{T,j} - \tilde{b}) \right) \\
&\quad + (C_{\beta/\alpha}^2 + \|H\mathbf{b}\|_{L^\infty(\Omega)} \alpha^{-1} + C_c C_b \|c_0 \mu_0^{-1}\|_{L^\infty(\Omega)} \ell^{-1} \|\|\phi_{T,j}\|\|_{h,\omega_T^m \setminus \omega_T^{m+1}}^2 \\
&= C_3 \ell^{-1} \|\|\phi_{T,j}\|\|_{h,\omega_T^m \setminus \omega_T^m}^2 \leq C_3 \ell^{-1} \|\|\phi_{T,j}\|\|_{h,\Omega \setminus \omega_T^{m+1}}^2,
\end{aligned} \tag{4.38}
$$

15

where $C_3 = C'(C_{\beta/\alpha}^2 + \|H\mathbf{b}\|_{L^\infty(\Omega)}\alpha^{-1} + C_c C_b\|c_0\|_{L^\infty(\Omega)}\mu_0^{-1})$, using (4.30), (4.36), and (4.37). Where C' is the generic constant hidden in '$\lesssim$'. Implying that

$$|||\phi_{T,j}|||_{h,\Omega\setminus\omega_T^m} \lesssim C_3\ell^{-1}|||\phi_{T,j}|||_{h,\Omega\setminus\omega_T^{m+1}}, \quad \text{for any } m = 1,2,\ldots,k-1. \quad (4.39)$$

Using (4.39) recursively, we have

$$|||\phi_{T,j}|||_{h,\Omega\setminus\tilde{\omega}_T^1}^2 \lesssim (C_3\ell^{-1})^{k-1}|||\phi_{T,j}|||_{h,\Omega\setminus\tilde{\omega}_T^k}^2 = (C_3\ell^{-1})^{k-1}|||\phi_{T,j} - \lambda_{T,j}|||_{h,\Omega}^2 \quad (4.40)$$

Equation (4.28) together with (4.39), gives

$$|||\phi_{T,j} - \phi_h^L|||_h \leq C_2(C_3\ell^{-1})^{\frac{k-1}{2}}|||\phi_{T,j} - \lambda_{T,j}|||_h. \quad (4.41)$$

which concludes the proof is concluded. $\square$

Proof of Theorem 4. Using the triangle inequality, we have

$$|||u - u_H^{ms,L}|||_h \leq |||u - u_h|||_h + |||u_h - u_H^{ms,L}|||_h. \quad (4.42)$$

Note that, $u_h \in \mathcal{V}_h$, can be decomposed into a coarse, $v_H^{ms} \in \mathcal{V}_H^{ms}$, and a fine, $v^f \in \mathcal{V}^f$, scale contribution, i.e., $u_h = v_H^{ms} + u^f$. Also, let $v_H^{ms,L} \in \mathcal{V}_H^{ms,L}$ be chosen such that $\Pi_H v_H^{ms,L} = \Pi_H v_H^{ms}$. We have

$$\begin{aligned}
|||u_h - u_H^{ms,L}|||_h &\lesssim a_h(u_h - u_H^{ms,L}, u_h - u_H^{ms,L}) \\
&= a_h(u_h - u_H^{ms,L}, u_h - v_H^{ms,L}) \\
&\lesssim C_c|||u_h - u_H^{ms,L}|||_h|||u_h - v_H^{ms,L}|||_h,
\end{aligned} \quad (4.43)$$

and obtain

$$\begin{aligned}
|||u - u_H^{ms,L}|||_h \leq &|||u - u_h|||_h \\
&+ C_c\left(|||u_h - v_H^{ms}|||_h + |||v_H^{ms} - v_H^{ms,L}|||_h\right).
\end{aligned} \quad (4.44)$$

The first term in (4.44) implies that the reference mesh need to be sufficiently fine to get a sufficient approximation. The second term is approximated using using (4.23), i.e.

$$|||u_h - v_H^{ms}|||_h \lesssim \alpha^{-1/2}\|H(1 - \Pi_H)f\|_{L^2(\Omega)}, \quad (4.45)$$

and for the last term in we have,

$$\begin{aligned}
|||v_H^{ms} - v_H^{ms,L}|||_h^2 &= ||| \sum_{T\in\mathcal{T}_H,\, j=1,\ldots,r} v_{H,T}^{ms}(x_j)(\phi_{T,h} - \phi_{T,j}^L)|||_h^2 \\
&\lesssim C_4 L^d \sum_{T\in\mathcal{T}_H,\, j=1,\ldots,r} |v_{H,T}^{ms}(x_j)|^2|||\phi_{T,h} - \phi_{T,j}^L|||_h^2 \\
&\lesssim C_4 C_2^2 L^d \gamma^{2L} \sum_{T\in\mathcal{T}_H,\, j=1,\ldots,r} |v_{H,T}^{ms}(x_j)|^2|||\phi_{T,h} - \lambda_{T,j}|||_h^2
\end{aligned} \quad (4.46)$$

16

using Lemma 12 and Lemma 3.

We obtain, using Lemma 13, that

$$
\begin{aligned}
&\sum_{T \in \mathcal{T}_H,\, j=1,\dots,r} |v_{H,T}^{ms}(x_j)|^2 |||\phi_{T,h} - \lambda_{T,j}|||_{\mathrm{h}}^2 \\
&\leq C_\phi^2 \sum_{T \in \mathcal{T}_H,\, j=1,\dots,r} |v_{H,T}^{ms}(x_j)|^2 \|H^{-1}\lambda_{T,j}\|_{L^2(T)}^2 \\
&= C_\phi^2 \sum_{T \in \mathcal{T}_H,\, j=1,\dots,r} \|H^{-1}v_{H,T}^{ms}(x_j)\lambda_{T,j}\|_{L^2(\Omega)}^2 \\
&\lesssim C_\phi^2 \| \sum_{T \in \mathcal{T}_H,\, j=1,\dots,r} H^{-1}v_{H,T}^{ms}(x_j)\lambda_{T,j}\|_{L^2(\Omega)}^2 \\
&= C_\phi^2 \| \sum_{T \in \mathcal{T}_H,\, j=1,\dots,r} H^{-1}v_{H,T}^{ms}(x_j)\Pi_H(\lambda_{T,j} - \phi_{T,j})\|_{L^2(\Omega)}^2 \\
&\leq C_\phi^2 \| \sum_{T \in \mathcal{T}_H,\, j=1,\dots,r} H^{-1}v_{H,T}^{ms}(x_j)(\lambda_{T,j} - \phi_{T,j})\|_{L^2(\Omega)}^2 \\
&\leq C_\phi^2 \|H^{-1}v_H^{ms}\|_{L^2(\Omega)}^2 \\
&\leq C_\phi^2 \left(\|H^{-1}u_h\|_{L^2(\Omega)} + \|H^{-1}u^f\|_{L^2(\Omega)} \right)^2 \\
&\leq C_\phi^2 \left(\|H^{-1}\|_{L^\infty(\Omega)} |||u_h|||_{\mathrm{h}} + \alpha^{-1/2} |||u^f|||_{\mathrm{h}} \right)^2 .
\end{aligned}
\tag{4.47}
$$

Using (4.23), we have

$$
\begin{aligned}
&\sum_{T \in \mathcal{T}_H,\, j=1,\dots,r} |v_{H,T}^{ms}(x_j)|^2 |||\phi_{T,h} - \lambda_{T,j}|||_{\mathrm{h}}^2 \\
&\lesssim C_\phi^2 \left(\|H^{-1}\|_{L^\infty(\Omega)} \|f\|_{L^2(\Omega)} + \alpha^{-1}\|H(1 - \Pi_H)f\|_{L^2(\Omega)} \right)^2 \\
&\lesssim C_\phi^2 \left(\|H^{-1}\|_{L^\infty(\Omega)}^2 \|f\|_{L^2(\Omega)}^2 + \alpha^{-1}\|Hf(1 - \Pi_H f)\|^2 \right).
\end{aligned}
\tag{4.48}
$$

which concludes the proof. $\qquad\square$

5 Numerical experiment

We consider the domain $\Omega = [0,1] \times [0,1]$ and the forcing function $f = 1 + \cos(2\pi x)\cos(2\pi y)$. The localization parameter, which determine the size of the patches, is chosen as $L = \lceil 2\log(H^{-1})\rceil$, i.e., the size of the patches are $2H\log(H^{-1})$. Consider a coarse quadrilateral mesh, $\mathcal{T}_H$, of size $H = 2^{-i}$, $i = 2,3,4,5$. The corrector functions are solved on sub-grids of the quadrilateral mesh, $\mathcal{T}_h$, where $h = 2^{-7}$. We consider three different permeabilities: $A_1 = 1$, $A_2 = A_2(y)$ which is piecewise constant with respect to a Cartesian grid of width 2^{-6} in y-direction taking the values 1 or 0.01, and $A_3 = A_3(x,y)$ which is piecewise constant with respect to a Cartesian grid of width 2^{-6} both in the x- and y-directions, bounded below by $\alpha = 0.05$ and has a maximum ratio $\beta/\alpha = 4 \cdot 10^5$. The permeability A_3 is taken from the 31 layer in the SPE benchmark
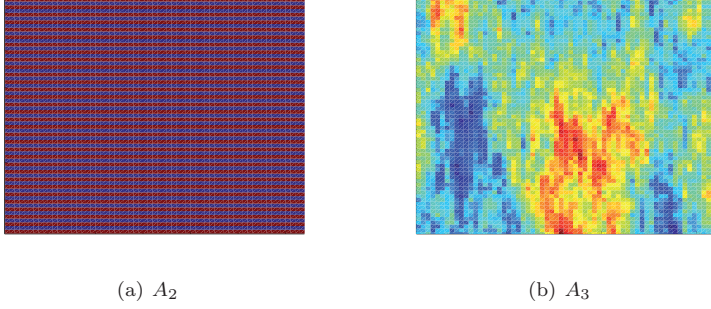
(a) A_2 (b) A_3

Figure 2: The diffusion coefficients A_2 and A_3 in log scale.

problem, see `http:www.spe.org/web/csp/`. The diffusion coefficients A_2 and A_3 are illustrated in Figure 2. For the convection term we consider: $\mathbf{b} = [C, 0]$, for different values of C.

To investigate how the error in relative energy-norm, $|||u_h - u_H^{ms,L}|||/|||u_h|||$, depends on the magnitude of the convection we consider: A_1 and $\mathbf{b} = [C, 0]$ with $C = \{32, 64, 128\}$. Figure 3 shows the convergence in energy-norm as a function of the coarse mesh size H for the different values of C.
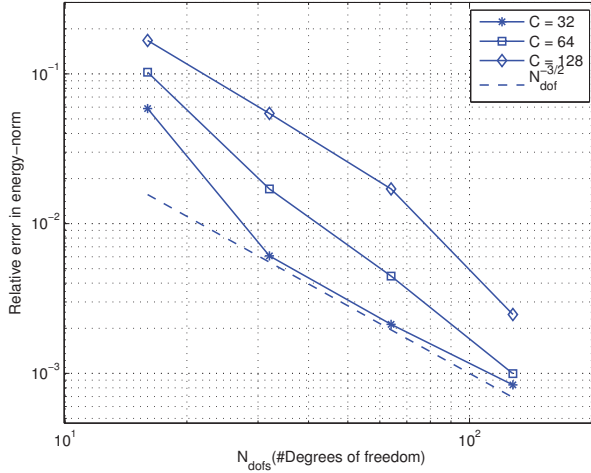

Figure 3: The number degrees of freedom (N_{dof}) vs. the relative error in energy-norm, for different sizes of the convection term, C.

Also, to see the effect of heterogeneous diffusion of the error in the relative energy-norm, $|||u_h - u_H^{ms,L}|||/|||u_h|||$, we consider: Figure 4 which shows the

18

error in relative energy-norm using A_2 and $\mathbf{b} = [1, 0]$ and Figure 5 which shows the error in relative energy-norm using A_3 and $\mathbf{b} = [512, 0]$.
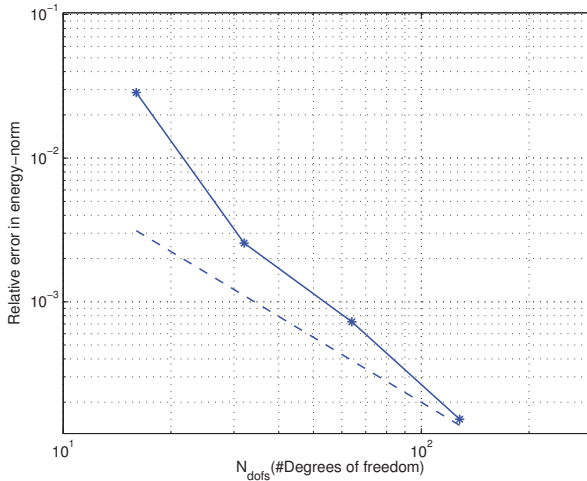

Figure 4: The number degrees of freedom (N_{dof}) vs. the relative error in energy-norm, using a high contrast diffusion coefficients A_2 and $\mathbf{b} = [1, 0]$. The dotted line corresponds to $N_{dof}^{-3/2}$.

We conclude that H^3 convergence of the dG multiscale method to a reference solution in the relative energy-norm, $|||u_h - u_H^{ms,L}|||/|||u_h|||$, is obtained, independent of the variation in the coefficients or regularity of the underlying solution.

References

[1] A. Abdulle. Multiscale method based on discontinuous Galerkin methods for homogenization problems. *C. R. Math. Acad. Sci. Paris*, 346:97–102, 2008.

[2] G. A. Baker. Finite element methods for elliptic equations using nonconforming elements. *Math. Comp.*, 31:45–59, 1977.

[3] F. Brezzi, L. D. Marini, and E. Süli. Discontinuous Galerkin methods for first-order hyperbolic problems. *Mathematical Models and Methods in Applied Sciences*, 14:1893–1903, 2004.

[4] J. Chu, Y. Efendiev, V. Ginting, and T. Y. Hou. Flow based oversampling technique for multiscale finite element methods. *Advances in Water Resources*, 31:599–608, 2008.
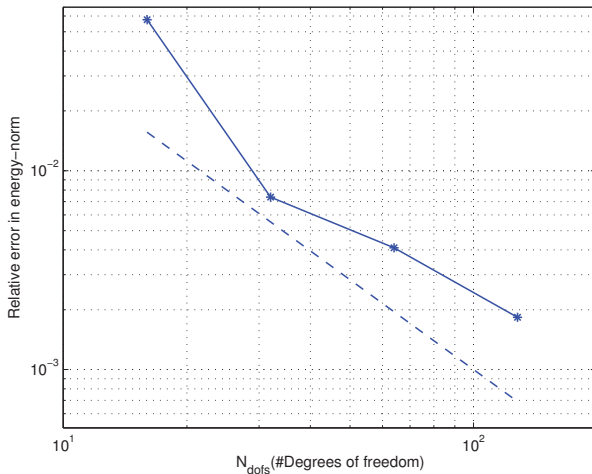
Figure 5: The number degrees of freedom (N_{dof}) vs. the relative error in energy-norm, using a high contrast diffusion coefficients A_3 and $\mathbf{b} = [512, 0]$. The dotted line corresponds to $N_{dof}^{-3/2}$.

[5] B. Cockburn, G. E. Karniadakis, and C-W. Shu, editors. *Discontinuous Galerkin methods*, volume 11 of *Lecture Notes in Computational Science and Engineering*. Springer-Verlag, Berlin, 2000.

[6] D. A. Di Pietro and A. Ern. *Mathematical aspects of discontinuous Galerkin methods*, volume 69 of *Mathématiques & Applications (Berlin) [Mathematics & Applications]*. Springer, Heidelberg, 2012.

[7] W. E and B. Engquist. The heterogeneous multiscale methods. *Commun. Math. Sci.*, 1:87–132, 2003.

[8] W. E and B. Engquist. Multiscale modeling and computation. *Notices Amer. Math. Soc.*, 1:1062–1070, 2003.

[9] Y. Efendiev and T. Y. Hou. *Multiscale finite element methods*, volume 4 of *Surveys and Tutorials in the Applied Mathematical Sciences*. Springer, New York, 2009. Theory and applications.

[10] Y. R. Efendiev, T. Y. Hou, and X.-H. Wu. Convergence of a nonconforming multiscale finite element method. *SIAM J. Numer. Anal.*, 37:888–910, 2000.

[11] D. Elfverson, E. Georgoulis, A. Målqvist, and D. Peterseim. Convergence of a discontinuous Galerkin multicale method. *Submitted for publication, available as preprint arXiv:1211.5524*, 2012.

[12] P. Henning, A. Målqvist, and D. Peterseim. A rigorous multiscale method for semi-linear elliptic problems. *Submitted for publication, available as preprint arXiv:1211.3551*, 2012.

[13] J. S. Hesthaven and T. Warburton. *Nodal discontinuous Galerkin methods*, volume 54 of *Texts in Applied Mathematics*. Springer, New York, 2008.

[14] T. Y. Hou and X.-H. Wu. A multiscale finite element method for elliptic problems in composite materials and porous media. *J. Comput. Phys.*, 134:169–189, 1997.

[15] M. Hughes, T. Mallet and A. Mizukami. A new finite element formulation for computational fluid dynamics. II. Beyond SUPG. *Comput. Methods Appl. Mech. Engrg.*, 54:341–355, 1986.

[16] T. Hughes. Multiscale phenomena: Green's functions, the Dirichlet-to-Neumann formulation, subgrid scale models, bubbles and the origins of stabilized methods. *Computer Methods in Applied Mechanics and Engineering*, 127:387–401, 1995.

[17] T. Hughes, G. Feijóo, L. Mazzei, and J.-B. Quincy. The variational multi-scale method—a paradigm for computational mechanics. *Comput. Methods Appl. Mech. Engrg.*, 166:3–24, 1998.

[18] T. Hughes, L. P. Franca, and G. Hulbert. A new finite element formulation for computational fluid dynamics. VIII. The Galerkin/least-squares method for advective-diffusive equations. *Comput. Methods Appl. Mech. Engrg.*, 73:173–189, 1989.

[19] C. Johnson and U. Nävert. An analysis of some finite element methods for advection-diffusion problems. In *Analytical and numerical approaches to asymptotic problems in analysis (Proc. Conf., Univ. Nijmegen, Nijmegen, 1980)*, volume 47 of *North-Holland Math. Stud.*, pages 99–116. North-Holland, Amsterdam, 1981.

[20] C. Johnson and J. Pitkäranta. An analysis of the discontinuous Galerkin method for a scalar hyperbolic equation. *Math. Comp.*, 46:1–26, 1986.

[21] O. Karakashian and F. Pascal. A posteriori error estimates for a discontinuous Galerkin approximation of second-order elliptic problems. *SIAM J. Numer. Anal.*, 41:2374–2399, June 2003.

[22] M. G. Larson and A. Målqvist. Adaptive variational multiscale methods based on a posteriori error estimation: energy norm estimates for elliptic problems. *Comput. Methods Appl. Mech. Engrg.*, 196:2313–2324, 2007.

[23] Mats G. Larson and Axel Målqvist. An adaptive variational multiscale method for convection-diffusion problems. *Comm. Numer. Methods Engrg.*, 25:65–79, 2009.

[24] P. Lesaint and P.-A. Raviart. On a finite element method for solving the neutron transport equation. In *Mathematical aspects of finite elements in partial differential equations (Proc. Sympos., Math. Res. Center, Univ. Wisconsin, Madison, Wis., 1974)*, pages 89–123. Publication No. 33. Math. Res. Center, Univ. of Wisconsin-Madison, Academic Press, New York, 1974.

[25] A. Målqvist. Multiscale methods for elliptic problems. *Multiscale Modeling & Simulation*, 9:1064–1086, 2011.

[26] A. Målqvist and D. Peterseim. Localization of elliptic multiscale problems. *Submitted for publication in Math. Comp., in revision, available as preprint arXiv:1110.0692*, 2011.

[27] W. H. Reed and T. R. Hill. Triangular mesh methods for the neutron transport equation. Technical report, Los Alamos Scientific Laboratory, 1973.

[28] B. Rivière. *Discontinuous Galerkin methods for solving elliptic and parabolic equations*, volume 35 of *Frontiers in Applied Mathematics*. Society for Industrial and Applied Mathematics (SIAM), Philadelphia, PA, 2008. Theory and implementation.

[29] Robert Söderlund. *Finite element methods for multiscale/multiphysics problems*. PhD thesis, Umeå University, Department of Mathematics and Mathematical Statistics, 2011.

Recent licentiate theses from the Department of Information Technology

2013-002   Marcus Holm: *Scientific Computing on Hybrid Architectures*

2013-001   Olov Rosén: *Parallelization of Stochastic Estimation Algorithms on Multicore Computational Platforms*

2012-009   Andreas Sembrant: *Efficient Techniques for Detecting and Exploiting Runtime Phases*

2012-008   Palle Raabjerg: *Extending Psi-calculi and their Formal Proofs*

2012-007   Margarida Martins da Silva: *System Identification and Control for General Anesthesia based on Parsimonious Wiener Models*

2012-006   Martin Tillenius: *Leveraging Multicore Processors for Scientific Computing*

2012-005   Egi Hidayat: *On Identification of Endocrine Systems*

2012-004   Soma Tayamon: *Nonlinear System Identification with Applications to Selective Catalytic Reduction Systems*

2012-003   Magnus Gustafsson: *Towards an Adaptive Solver for High-Dimensional PDE Problems on Clusters of Multicore Processors*

2012-002   Fredrik Bjurefors: *Measurements in Opportunistic Networks*

2012-001   Gunnika Isaksson-Lutteman: *Future Train Traffic Control – Development and deployment of new principles and systems in train traffic control*

2011-006   Anette Löfström: *Intranet Use as a Leadership Strategy*

UPPSALA
UNIVERSITET

Department of Information Technology, Uppsala University, Sweden